In presenting the dissertation as a partial fulfillment of the requirements for an advanced degree from the Georgia Institute of Technology, I agree that the Library of the Institute shall make it available for inspection and circulation in accordance with its regulations governing materials of this type. I agree that permission to copy from, or to publish from, this dissertation may be granted by the professor under whose direction it was written, or, in his absence, by the Dean of the Graduate Division when such copying or publication is solely for scholarly purposes and does not involve potential financial gain. It is understood that any copying from, or publication of, this dissertation which involves potential financial gain will not be allowed without written permission.

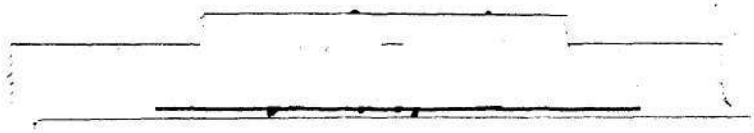

7/25/68

PHASE EQUILIBRIA IN THE HELIUM-CARBON DIOXIDE, -ARGON, -METHANE, -NITROGEN, AND -OXYGEN SYSTEMS

A THESIS

Presented to

The Faculty of the Graduate Division

by

Ker Fah Liu

In Partial Fulfillment

of the Requirements for the Degree

Doctor of Philosophy in the School of Chemical Engineering

Georgia Institute of Technology

July, 1969

PHASE EQUILIBRIA IN THE HELIUM-CARBON DIOXIDE,

-ARGON, -METHANE, -NITROGEN, AND -OXYGEN SYSTEMS

Approved:

Date approved by Chairman: 10/24/69

ACKNOWLEDGMENTS

I wish to thank Dr. W. T. Ziegler, my thesis advisor, for his patient and understanding guidance in the laboratory and in the classroom. He generated my interest in phase equilibria, pointed out this particular problem, and helped constantly during the course of this work. He taught me the experimental techniques and attitudes necessary to initiate and carry out a research project. I also wish to thank him for making possible the financial support received by me throughout the period of this work.

My fellow students also contributed with a helping hand or a responsive mind to this work. In particular, I wish to thank Dr. J. C. Mullins for helping with the learning of the operation of the apparatus, and with the computer programs. To Dr. B. S. Kirk who built the equipment and who, together with Dr. Mullins, developed many of the computer programs, I am also indebted. Others I wish to thank are Mr. Richard J. Holt, Dr. D. W. Yarborough, Mr. James D. Garber, and Mr. George Nelson Brown, Jr.

I wish to thank Dr. Frederick Bellinger of the Engineering Experiment Station and Dr. Homer V. Grubb of the School of Chemical Engineering of the Georgia Institute of Technology, for providing funds for this work. I also am indebted to the Standard Oil Company of California for their Chemical Engineering Fellowship for 1966-67. I am grateful to the Rich Electronic Computer Center for the use of their facilities and for providing part-time employment.

Finally, I wish to thank Dr. H. A. McGee, Jr., and Dr. W. M. Newton for serving on the Reading Committee.

TABLE OF CONTENTS

TABLE OF CONTENTS (continued)

LIST OF TABLES

LIST OF TABLES (continued)

LIST OF TABLES (continued)

LIST OF FIGURES

LIST OF FIGURES (Continued)

NOMENCLATURE

a	=	Used as a constant in Equation (IV-5)
B	=	Second virial coefficient; see Equation (IV-6)
B_K	=	Second virial coefficient calculated from classical Kihara core model (6-12); see Equation (IV-23)
B^*_{CL}	=	Reduced classical second virial coefficient from LJCL (6-12) intermolecular potential function (also written $B^*_{CL}(T^*)$; see Equation (IV-15)
B^*_I, B^*_{II}, B^*_{III}	=	First, second, and third reduced translational quantum corrections for the second virial coefficient from LJCL (6-12) intermolecular potential function; see Equation (IV-29) and Equation (IV-30)
B^*_o	=	Reduced translational quantum second virial coefficient for an ideal gas; see Equation (IV-33)
b	=	Used as a constant in Equation (IV-5)
b_o	=	Volumetric parameter in LJCL (6-12) intermolecular potential function; see Equation (IV-13)
$b_s^{(j)}$	=	Coefficients for series representation of F_s; see Equation (IV-25)
C	=	Third virial coefficient; see Equation (IV-6)
C_j	=	Weighting factors in least-squares fit; see Table 16
C^*_{CL}	=	Reduced classical third virial coefficient from LJCL (6-12) intermolecular potential function (also written $C^*_{CL}(T^*)$); see Equation (IV-18)
c	=	Used as a constant in Equation (IV-5)
e	=	Energy parameter in LJCL (6-12) intermolecular potential function; see Equation (IV-10)
e/k	=	Energy parameter in LJCL (6-12) intermolecular potential function; units are ^oK
F_1, F_2, F_3	=	Reduced functions for second virial coefficient from Kihara core model (6-12); see Equation (IV-24)

g	=	Free energy of 1 mole of gas
h	=	Used as peak height on chromatogram
j	=	Summation index integer
KIH	=	Kihara core model (6-12), see p. 33
KIHQ	=	Kihara core model with quadrupole, see p. 36
k	=	Boltzmann constant = 1.380308×10^{-16} erg/^{o}K molecule
LJCL	=	Lennard-Jones classical model, see p. 31
LJCLA	=	Lennard-Jones classical model with $(e/k)_{12}$ adjusted, see p. 37
ℓn	=	Natural (base e) logarithm
log	=	Common (base 10) logarithm
M	=	Molecular weight
M_o	=	Core parameter in Kihara core model
m	=	Mass of molecule, M/N_A
N_A	=	Avogadro's number 6.0238×10^{23} molecules/gm mole
n	=	Number of gm moles
P	=	Total absolute pressure
P_c	=	Critical pressure
P_R	=	P/P_c
p_{01}	=	Vapor pressure of component 1
R	=	Gas constant = 0.0820574 liter-atm/gm mole-^{o}K
r	=	Intermolecular distance measured between centers of molecules
S_o	=	Core parameter in Kihara core model
s	=	Summation index integer; also dummy variable in Equation (IV-24) and attenuation factor on chromatograph (see Appendix C)
T	=	Temperature (^{o}K)

T^* = kT/e

U_o/k = Energy parameter in Kihara core model (6-12); units are ^oK

U = Intermolecular potential energy

V = Total volume of gas

V^∞ = Molal volume of gas at pressure sufficiently low to behave ideally

V_m = Molal volume of gas mixture

V_1 = Molal volume of component 1 gas

V_2 = Molal volume of component 2 gas

$\bar{V}_i$ = Partial molal volume of component i

V_o = Core parameter in Kihara core model

V_{01} = Molal volume of component 1 gas at its vapor pressure, p_{01}

v = Molal volume of condensed phase

x = Mole fraction in condensed phase; also independent variable in general least-squares fit

y = Mole fraction in gas phase; also independent variable in general least-squares fit

Z = Compressibility factor, PV/nRT; also (U_o/kT) in Kihara core model

Greek Letters

α_{ij} = Coefficients in least-squares fit; see Table 16

α = Defined by Equation (V-2)

β = Defined by Equation (V-3)

Γ = Gamma function Equation (IV-16)

γ_1' = Activity coefficient of component 1 in liquid solutions referred to the pure liquid component at the system pressure and temperature

Λ^* = Translational quantum mechanical parameter; see Equation (IV-28)

ρ = Used as shortest distance between molecular cores in Kihara core model

ρ_o = Shortest distance between molecular cores at minimum potential energy. Parameter in Kihara core model

σ = Length parameter in LJCL (6-12) intermolecular potential; see Equation (IV-10)

ϕ = Enhancement Factor = Py_1/p_{01}

μ = Chemical potential

Subscripts

1 = Carbon dioxide, argon, methane, nitrogen, or oxygen

01 = Gas at its normal vapor pressure

2 = Helium

m = Gas mixture

max = Maximum value of variable in data set

i, j, k = 1, 2, or m

Superscripts

V = Vapor phase

L = Liquid phase

^{o} = Ideal gas state at 1 atmosphere and temperature T

SUMMARY

This work is a continuation of the experimental and theoretical investigation started in this laboratory by Kirk[45,46] and Mullins.[64,66] It is concerned with phase equilibria in binary systems in which one component is below its critical temperature, while the other component is above its critical temperature. The experimental part deals with the measurement of the gas-phase equilibrium compositions for the helium-carbon dioxide system (with the solid phase assumed to be the pure condensed component) at varying pressures up to 120 atmospheres along different isotherms. The theoretical study examines various thermodynamic models used to describe the behavior of the gas phase.

It is the purpose of this work to extend the experimental data and to examine the combination rules used in some of the theoretical models for expressing gas mixture behavior. The experimental apparatus has been described by Kirk[45] and Kirk and Ziegler.[46] It is a single-pass flow type apparatus suitable for operation from liquid nitrogen temperatures to room temperature and for pressures up to 140 atmospheres. Using this apparatus the solid-vapor equilibrium for the helium-carbon dioxide has been measured at 181.05, 190.03, and 199.95°K and at pressures up to 120 atmospheres. The equilibrium gas-phase composition in the liquid-vapor region at 220.31°K has been measured at pressures between 80 and 140 atmospheres. The vapor phase composition measured here and expressed as the Enhancement Factor ϕ ($\phi = Py_1/p_{01}$) agrees well with the results of other investigators. The 190.03°K isotherm was compared with the results

of Ewald[23] at 190°K, while the 220.31°K isotherm was compared with the results of Barrick et al.[4] at 219.9°K. The temperature measured in this work is estimated to be accurate to within ±0.05°K, the pressure measurements are estimated to be accurate to within ±1/2 per cent, and the composition is estimated to be accurate to within ±3 per cent of the carbon dioxide analysis.

The equilibria data obtained in this work and the available phase equilibria data for the helium-carbon dioxide,[4,23] -argon,[56,64,66,86] -methane,[25,28,31,41,87] -nitrogen,[8,18,20,24,42,80] and -oxygen[5,86] systems have been used to test theoretical models for the gas phase. The virial equation of state up to the third virial coefficient was used to describe the gas phase. The two theoretical models tested for the calculation of the virial coefficients were the Lennard-Jones (6-12) and Kihara core models. The second virial coefficient was calculated using both models, while the third virial coefficient was calculated with the Lennard-Jones (6-12) model only. The solid phase was assumed to be pure and incompressible. The liquid phase was assumed to be an ideal solution.

The procedure described by Mullins[64] was used to obtain the interaction second virial coefficient, B_{12}, from the phase equilibria data. The resulting B_{12} values were compared and combined with available data for the systems. The B_{12} obtained here are in the lower temperature regions where very few data exist. However, taken in conjunction with the available high-temperature data they appear to be valid values. The values of B_{12} obtained here are estimated to be accurate in general to within ±3 cc/gm-mole. Smooth values of B_{12} versus temperature were obtained graphically. It was shown that the theoretical B_{12} values were

generally lower (with the Kihara core model values lower than those of the Lennard-Jones (6-12) model), than the experimental values for B_{12}.

The smooth values for the interaction second virial coefficient were used to test the combination rules for the parameters of the Lennard-Jones (6-12) model. These combination rules are as follows. The energy parameter $(e/k)_{12}$ is obtained from $(e/k)_1$ and $(e/k)_2$ by the geometric average. The volume parameter $(b_o)_{12}$ is obtained from $(b_o)_1$ and $(b_o)_2$ by the Lorentz average. With the exception of the helium-oxygen system these combination rules and similar ones for the Kihara core model were not adequate for correctly predicting B_{12}. To obtain a measure of the departures from these combination rules, $(e/k)_{12}$ and $(b_o)_{12}$ were derived from a least-squares fit of the Lennard-Jones (6-12) potential function to the smooth B_{12} data. Three cases were considered:

(i) Both $(e/k)_{12}$ and $(b_o)_{12}$ allowed to vary to fit the B_{12} data

(ii) With $(e/k)_{12}$ fixed by the geometric average, $(b_o)_{12}$ allowed to vary to fit the B_{12} data

(iii) With $(b_o)_{12}$ fixed by the Lorentz average, $(e/k)_{12}$ allowed to vary to fit the B_{12} data.

As might be expected, case (i) resulted in the closest fit of the B_{12} data. The closeness of the fit for case (ii) was not within the error of the B_{12} data, and thus the fit was not acceptable. While the closeness of fit for case (iii) was not as close as that for case (i) it was within the error of the B_{12} data, and hence acceptable. From the preceding results it is concluded that the correct prediction of B_{12} depends more on the correct prediction of $(e/k)_{12}$ than on $(b_o)_{12}$. The major failing of the combination rules for the Lennard-Jones (6-12)

model is in the geometric average rule for the energy parameter. Although nor similarly demonstrated, this conclusion is applicable also to the combination rules for the Kihara core model which are the same rules. Thus Mullins,[64] and Hiza and Duncan[30] have shown that adjustments in the energy parameter for the Kihara core model will result in a better representation of B_{12} with that model.

The main results of this work are:

(1) The extension of the experimental phase-equilibria in the helium-carbon dioxide system into the vapor-solid region. Confirmation of the existing data at the lower temperature end of the vapor-liquid region for the helium-carbon dioxide system.

(2) The extraction of the interaction second virial coefficient from the experimental phase equilibria data for the helium-carbon dioxide, -argon, -methane, -nitrogen, and -oxygen systems. The B_{12} data so obtained are in temperature regions where very few data exist. They have been combined with existing higher temperature B_{12} data for the above systems to yield a set of smooth B_{12} versus temperature values.

(3) The combination rules for the parameters to the Lennard-Jones (6-12) and Kihara core models have been shown to be inadequate for correctly predicting B_{12} in the helium systems considered here. The geometric average rule for the energy parameter in these two models appears to be mainly at fault.

(4) Theoretical Enhancement Factor calculations have been made for the helium systems considered in this work. Although (with the exception of the helium-oxygen system) the calculated Enhancement Factors do not agree very well with the experimental values, they have use in semi-quantitative considerations.

CHAPTER I

INTRODUCTION

Background and Statement of Problem

The study of phase equilibria is of particular interest to the chemical engineer. In most chemical processes there is a step or steps requiring the separation of a mixture to recover one or more desired products. The separation is usually carried out by means such as distillation, extraction, adsorption, or crystallization. All these operations are based on the principles of phase equilibria. The design of the equipment is usually based on a combination of experimental data and application of theory. Such an approach conserves part of the efforts needed to gather extensive experimental data, while providing some data to demonstrate the validity of the theoretical model being applied. With the computational barrier removed by the electronic computer, it has become much easier than previously possible to "experiment" with mathematical models. This facility, rather than deemphasizing experimentation, has actually placed greater emphasis on obtaining accurate data from which better models could be built. The advantage is that once a viable model has been obtained, the phenomenon can be studied via its model. Thus, a phase equilibrium model which will accurately predict the phase compositions in a given system at desired temperature and pressure conditions would be easier to use than to do the necessary experiments. The ability to calculate phase equilibria has been and still is one of the prime interests and concerns

of chemical engineering. This work is a small part of the overall efforts to extend the experimental data, and to the building and testing of theoretical models of phase equilibria.

The methods and equations for the calculation of phase equilibria are set down by thermodynamics. Thermodynamics requires that at equilibrium at a fixed temperature and pressure the chemical potential of a component in every phase must be equal. For a pure substance in phase equilibrium with itself only its equation of state is needed to compute its chemical potential. To compute the chemical potential of a component in a multicomponent system, an equation of state for the mixture is needed, in addition to the equations of state for the pure components. Equations of state for pure substances are better known than those for mixtures, which being composition-dependent, require much more effort to measure. In practice, an equation of state for a mixture is approximated from the equations of state for the pure components. The approximation is done by means of mixing rules for the parameters of the equations of state for the pure components. The advantage of such an approach is that phase equilibria of mixtures of any combinations of components could be studied, if the appropriate equation of state for the pure components and mixing rules thereof are known. This is usually the starting point for phase equilibria calculations in multicomponent systems.

This work is an experimental and theoretical study of vapor-liquid and vapor-solid equilibria in a special class of binary systems. These binary systems are studied at conditions such that one component is below its critical temperature while the other component is above

its critical temperature. Of specific interest here are the cryogenic systems such as the hydrogen-methane, helium-nitrogen, helium-methane, helium-argon, and other similar compressed gas-condensed gas systems. The helium systems, for instance, are of interest in the helium purification process in which gases other than helium are removed by condensation. While the theory developed is not limited to these low temperature levels, some important simplifying assumptions can be made for the treatment of the helium systems. The major assumptions are that the liquid phase is an ideal solution and that the solid phase is pure. These assumptions are based on the fact that liquid-vapor equilibria in such systems are characterized by low concentration (usually less than 10 mole %) of the compressed-gas component in the liquid. The concentration of the condensed component in the gas phase is also small, usually only several mole per cent. However, the partial pressure of the condensed component is usually greater than its vapor pressure at that temperature, giving rise to the term Enhancement Factor. The Enhancement Factor, ϕ, is defined as Py_1/p_{01}, where P is the total pressure of system, y_1 is the mole fraction of component 1 (the condensed component) in the gas phase, and p_{01} is the vapor pressure of component 1 at the system temperature. For the systems of interest here ϕ is always greater than one. The gas phase non-ideality in these systems is studied by means of theoretical calculations of the Enhancement Factor.

The theoretical and experimental investigation of phase equilibria in cryogenic systems has been of continuing interest to this laboratory. This work forms part of that interest. The systems which have been experimentally and theoretically studied in this laboratory are

hydrogen-methane by Kirk,[45] and helium-argon and hydrogen-argon by Mullins.[64] Some similar systems which have been studied by workers in other laboratories are helium-nitrogen,[8,18,20,24,42,80] helium-oxygen,[5,86] helium-argon,[56,64,66,86] helium-methane,[25,28,31,41,87] helium-carbon dioxide,[4,23] helium-ethane,[30] helium-ethylene,[30] and others.

The phase equilibria apparatus of this laboratory is a single-pass flow type apparatus designed and built by Kirk.[45] It is suitable for liquid-vapor or solid-vapor equilibria studies from liquid nitrogen temperatures to room temperatures. A brief description of the apparatus is given in the following chapter. Detailed descriptions are presented by Kirk,[45] and Kirk and Ziegler.[46] Other types of apparatus used by other laboratories are the static type and the vapor-recirculation type. The merits of each type of apparatus have been discussed by Kirk.

The theoretical investigation of the cryogenic systems has made use of various equations of state to predict the vapor phase composition. Kirk et al.,[47] Kirk,[45] and Mullins[64] have made calculations using empirical equations of state (Beattie-Bridgeman, Benedict-Webb-Rubin) and the theoretical virial equation of state. In the application of the virial equation of state they considered theoretical models and empirical correlations for calculating the virial coefficients. Again, such calculations are not unique to this laboratory but are also done by other laboratories. Some of the workers who are or have been interested in such calculations are Dokoupil,[20] Smith, Sonntag, and Van Wylen,[89] Barrick et al.,[4] Prausnitz et al.,[76] Prausnitz and Chueh,[75] Chiu and Canfield,[11] and Hiza and Duncan.[30]

This work is the study of a small group of binary systems which

have one common component. In this case, helium is the common compressed gas component. The aim of such a study is a better understanding of the interaction between dissimilar molecules. A satisfactory model of the gas phase should, of course, represent the pure component properties as well as those of the mixture. The model selected here is the theoretically based virial equation of state. The virial equation has some drawbacks as well as merits. Some of the limitations of the virial equation are that it cannot be applied over a wide range of temperature and pressure without the complication of the higher virial coefficients, and that its main usefulness is in the gas phase, whereas empirical equations such as the Benedict-Webb-Rubin equation can cover both the gas and liquid phases. However, it has several desirable features. The virial coefficients are a measure of interactions between the molecules in the gas phase. Thus, the second and third virial coefficients are characteristic of the two- and three-body interactions. The inclusion or truncation of the number of virial coefficients in the equation allows easy variations in the degree of complexity. The virial coefficients can be calculated from an assumed form of the intermolecular potential function. When the virial equation is used for a gas mixture, the interaction virial coefficients give a measure of the interaction between dissimilar molecules. Hence, the virial equation is most suitable when trying to study intermolecular interactions.

In the application of the virial equation to phase equilibria calculations, Kirk,[45] Mullins,[64] and Hiza and Duncan[30] point out that the usual combination rules did not correctly predict the interaction second virial coefficient. By arbitrarily adjusting the energy

parameter of the Kihara core model, Mullins was able to represent the B_{12} for the helium-argon system with that model. While the approach taken by Hiza and Duncan (see Chapter V) is different, they also show that the geometric combination rule for the Kihara core model is not valid. Chueh and Prausnitz[13] in working with the Redlich-Kwong equation have found the usual combination rules for it to be inadequate. Thus in both the theoretical virial equation and the empirical Redlich equation the basic failing of combination rules appear. Chueh and Prausnitz[13] used the idea of a correction factor to the usual combination rules and have derived a set of these factors for use with the critical temperature for the Redlich-Kwong equation for a large group of systems. Hiza and Duncan also used this idea with respect to the energy parameter of the Kihara core model. Such an approach is also used in this work. Although Hiza and Duncan were able to obtain a correlation between their correction factor with the ionization potential, Chueh and Prausnitz did not report any correlation for their correction factor. While the correction factor concept is useful, it remains to be shown whether any fundamental significance can be attached to it.

Selection of Systems for Study

The selection of a class of systems to study was dependent on several considerations: the systems had to be such that the necessary assumptions would apply; enough experimental data are available for checking the theoretical results; theoretical parameters and other complementary data are available for making the calculations. The helium-condensable gas systems appeared to best meet the above

requirements. Phase equilibria of the helium-argon and hydrogen-argon systems have been shown by Mullins to be treatable with the necessary assumptions. Since the other helium systems did not appear to be greatly different, the same assumptions could reasonably be applied to them. Phase equilibria data exist for the helium-carbon dioxide,[4,23*] -argon,[56,64,66,86] -methane,[25,28,31,41,87] -nitrogen,[8,18,20,24,42,80] -oxygen,[5,86] and -hydrogen[88] systems.

---

* A final survey of the literature yielded two up-to-date papers related to this work. One is by Sneed, Sonntag, and Van-Wylen (Journal of Chemical Physics 49, No. 5, 2410-14 (1968)) on the liquid-vapor equilibrium in the helium-hydrogen system up to 100 atmospheres. The other is by Iomtev, Morozov, and Chumak (Russian Journal of Physical Chemistry 42 (8), 1089-91 (1968), which is the English translation of the original Russian article in Zhurnal Fizicheskoi Khimii 42 (8), 2069-71 (1968)) on the solid-vapor equilibrium in the helium-carbon dioxide system. The helium-hydrogen system is not of immediate concern. The work of Iomtev et al. is of interest here. They attempted to measure the solubility of helium in solid carbon dioxide, and estimated from their results that the solubility was less than 10^{-3} mole fraction between 77 and 195°K and at pressures up to 120 atmospheres. Thus, the assumption of a pure solid phase in the helium-carbon dioxide system, and in the other helium systems considered here appears to be a good one. Iomtev et al. also measured the solubility of solid carbon dioxide in helium at 160, 170, 180, and 190°K and up to 100 atmospheres. Their data overlap the data of this work above 180°K. Below 180°K their data are the only available set. At 190°K and below 50 atmospheres their data (in terms of the Enhancement Factor) are in very good agreement with this work and that of Ewald[23]. However, at 190°K and 83.3 atmospheres Iomtev et al.'s point is about 6% smaller than those of this work and Ewald's. At 190°K and 100 atmospheres Ewald is about 5% higher, while Iomtev et al. are about 4% lower than this work. Iomtev et al.'s 180°K isotherm is lower by about 3% than the 181°K isotherm of this work. Their results confirm the small Enhancement Factor and its insensitivity to temperature in the helium-carbon dioxide system. An interesting point is that their data seem to suggest that at some point between 180 and 190°K the Enhancement Factor increases with increasing temperature above that point, while below that point the Enhancement Factor decreases with increasing temperature, which is the usual trend in similar systems. Because of the small magnitude and the ill-defined temperature dependence of the Enhancement Factor in the helium-carbon dioxide system this observation is not conclusive. (con't.)

While this work was in progress, phase equilibria data for the helium-neon,[27,49] and helium-propane[83] systems became available. Very recently, after the completion of this work, data for the helium-ethane[30] and helium-ethylene[30] systems became available. The helium-carbon dioxide, -argon, -methane, -nitrogen, and -oxygen systems were selected as being a representative set of this class of systems. The helium-hydrogen system is a special one in that both components are light quantum gases, and hence, it is different from the others. The helium-neon system again is more akin to the helium-hydrogen system. The helium-propane, helium-ethane, and helium-ethylene systems deserve attention since, like carbon dioxide, propane, ethane, and ethylene introduce molecules that are more complicated than the others into the study. The selected systems are of practical interest since the condensable components are possible contaminants in the purification of helium. Study of this phase equilibria with helium is of practical use in the design of cryogenic equipment. A disadvantage from a theoretical point is that the Enhancement Factor is rather small (generally less than 3) in the helium systems. This makes it difficult to resolve the different contributions to the Enhancement Factor.

---

*(con't.) The helium-carbon dioxide data of Iomtev et al. are in the low temperature region, while the data of Barrick et al.[4] are in the high temperature region. The data of this work fall in between the two sets of data and in the region of overlap agree well with both sets. Thus the data obtained here fill the gap and serve to check and complete the range of data for the helium-carbon dioxide system.

The objectives of this work are summarized below:

(1) To determine the vapor-phase composition in the vapor-solid region for the helium-carbon dioxide system. To confirm the available vapor-liquid equilibrium data at the lowest isotherm for the helium-carbon dioxide system.

(2) To extract the interaction second virial coefficient from the available phase equilibria data for the helium-carbon dioxide, -argon, -methane, -nitrogen, and -oxygen systems. To combine the B_{12} so obtained with the available B_{12} data for these systems and obtain a set of smooth B_{12} versus temperature values. At the present time, the B_{12} data in the lower temperature regions (where the phase equilibria data for these systems lie) are very few. Hence the B_{12} data obtained in this work would be an extension of the existing data, which are in the higher temperature regions.

(3) To examine the combination rules used in the Lennard-Jones (6-12) and Kihara core models.

(4) To improve the theoretical methods for the calculation of the Enhancement Factor.

CHAPTER II

EXPERIMENTAL APPARATUS

General Description of Apparatus

A schematic diagram of the apparatus used to determine the phase-equilibria in the helium-carbon dioxide system is shown in Figure 1. The apparatus has been described in detail by Kirk[45] and also by Kirk and Ziegler.[46] It will be briefly described here as it related to the helium-carbon dioxide system.

The heart of the apparatus is a single-pass flow-type equilibrium cell. The cell is in a copper-block cryostat, which is insulated with an evacuated powder insulation. Refrigeration is provided by liquid nitrogen contained in a reservoir suspended beneath the copper block. An annular space packed with copper wool is between the cell and the copper block. A capillary tube extends from the bottom of the reservoir to this annular space. The liquid nitrogen is injected into the space through this capillary. The pressure in the reservoir is maintained slightly above that of the vent exit by means of a differential pressure regulator. A throttling valve in the vent line controls the rate of evaporation of the liquid nitrogen.

Temperature is controlled by balancing a slight excess of refrigeration with heat from an electric heater wrapped on the copper block. The energy input to this heater is controlled by an automatic controller.

The temperature of the cell is measured with a platinum resistance

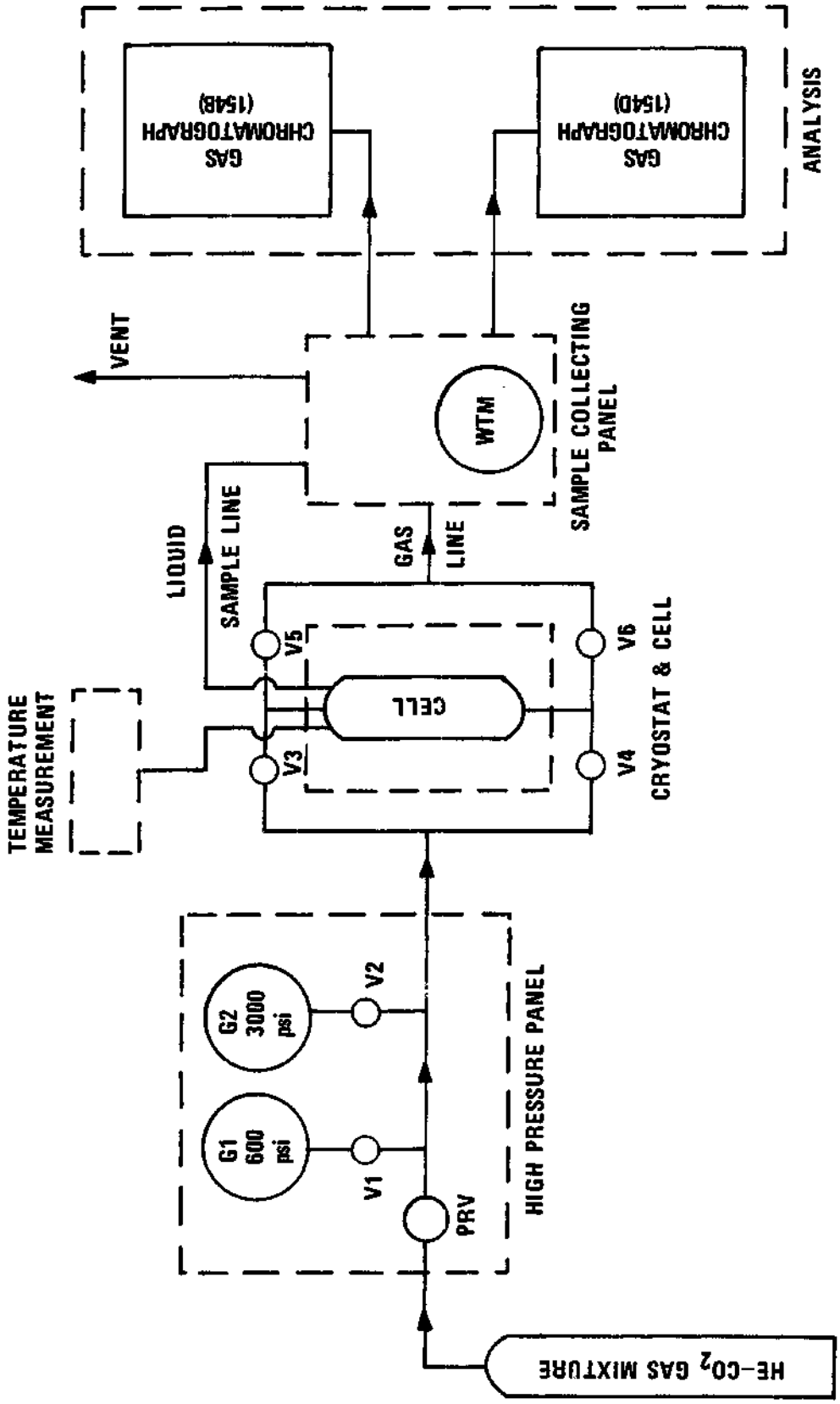

Figure 1. Schematic Diagram of Phase Equilibrium Apparatus.

thermometer located in a well at the top shoulder of the cell. The thermometer has been calibrated by the National Bureau of Standards on the International Practical Kelvin Scale above 90.18°K. The assigned ice-point is 273.15°K. Below 90.18°K the NBS-1955 Scale is used. The cell is also instrumented with thermopiles and difference couples for monitoring temperature and temperature differences at various points in it.

The high-pressure panel is used for the regulation and measurement of the pressure in the system, and for directing the flow path of the gas. Pressure is regulated with the pressure regulating valve, PRV, which is capable of regulating pressure from 0 to 4500 psi outlet pressure. Pressure gauges G1 (0-600 psi) and G2 (0-3000 psi) are used to measure the pressure. They have been calibrated by Kirk against a dead-weight gauge. Needle valves V1 and V2 can isolate these gauges from the system. A rough uncalibrated gauge, not shown, is also available on the panel. A gauge-protector, set for 450 psi cut-off, protects G1 from inadvertent excess pressures. Needle valves V3, V4, V5, and V6 control the direction of the gas flow through the equilibrium cell are also located on the high-pressure panel.

The sample collection panel provides facilities for the collection of the exit gas from the equilibrium cell. The flow rate of the exit gas can be measured with a wet-test meter, WTM. Two burettes are provided for the collection of samples from the gas and liquid sample lines from the equilibrium cell. Appropriate connections allow the collected samples to be introduced into the analysis section of the apparatus.

The analysis section consists of two gas chromatographs: a Perkin-

Elmer Model 154B and a Model 154D. In the vapor-liquid region the gas and liquid phase samples vary greatly in composition. The availability of the two chromatographs allows the instruments to be calibrated separately for the analysis of the minor component using the major component as the carrier gas. Thus, the 154B is usually calibrated for the analysis of the gas sample and 154D calibrated for the liquid sample. The outputs of the chromatographs are recorded on strip-chart recorders.

Experimental Procedure

The first step in starting up the apparatus is the evacuation of the powder insulation for the cryostat. A good vacuum is necessary for stable temperature control. With a mechanical pump an acceptable vacuum of less than 75 microns could be attained at room temperature. The next step is the cool-down of the cryostat. The equilibrium cell is flushed by flowing helium gas through it. This insures that no condensables are left in the system to plug up or contaminate the cell when the cryostat is cooled. The vent for the vaporized liquid nitrogen and the differential pressure regulator on the liquid-nitrogen reservoir are both opened. Liquid nitrogen is introduced into the reservoir through a filling line at the top of the cryostat. The reservoir has a capacity of 2 liters. With the reservoir filled the filling line and the differential pressure regulator are closed. The over-pressure in the reservoir injects liquid nitrogen via the capillary tube into the annular space between the copper block and the equilibrium cell. The evaporation of the nitrogen cools the block and the cell. To allow for a fast rate of cool-down the throttle valve on the vent line is opened

wide. As the cryostat cools down the vacuum in the insulation space improves and eventually reaches about 50 microns. The cool-down from room temperature to liquid nitrogen temperature takes about six hours and uses about 3 to 4 liters of liquid nitrogen. Once the cryostat is at liquid nitrogen temperature or at approximately the desired temperature, the refrigeration rate is reduced by means of the throttle valve in the vent line. The refrigeration rate is adjusted so that in addition to overcoming the heat leak into the cryostat, it provides a slight cooling. The slight cooling is finely balanced by means of the heat supplied through the automatic temperature controller. This procedure results in a temperature control of about $\pm 0.05^{\circ}K$ in the cryostat. At steady operating conditions a filling of the reservoir provides sufficient liquid nitrogen for about 20 hours.

After the temperature of the cryostat has been established at the desired point the next step is the introduction of the components into the equilibrium cell. The procedure up to this point is similar whether operating in the solid-vapor or liquid-vapor region.

When making measurements in the solid-vapor region the cell is pressurized with helium to the highest pressure to be run. The temperature is balanced roughly at the desired level. The helium-carbon dioxide gas mixture is allowed to flow through the cell. This mixture has been prepared beforehand with a carbon dioxide concentration somewhat larger than the equilibrium concentration expected at the planned temperature of the run. Too large an excess of carbon dioxide causes plugging and is to be avoided. The gas flow is from the top to the bottom of the cell. This is done with valves V3 and V6 open, while valves V4 and V5 are closed.

The condensation of carbon dioxide on the packing in the upper part of the cell and the flow of gas through the cell slightly raises the temperature of the cell. The power to the cryostat heater is slightly lowered to obtain a balance in the temperature. A judicious application of heat to the inlet line to the cell insures that the carbon dioxide will not prematurely condense out in the line and cause plugging. Heat is also applied to the exit line so that once the gas comes out of the cell no further condensation can take place. The use of these heaters results in a temperature gradient along the cell of about $0.08^{\circ}K$, with the top of the cell at a higher temperature than the bottom.

Plugging may occur at the inlet to the cell. This is first indicated by a rapid rise in the temperature of the cell due to the depletion of its contents. The pressure in the cell also drops. The pressure drop is detected by closing a valve at the outlet of the pressure regulating valve and quickly opening V4. The pressure gauge will indicate a sudden pressure drop. Plugging can be eliminated by appropriate adjustment of the electrical heaters referred to above.

With the cell operating satisfactorily, the exit gas from the cell passes to the sample collection panel. Here its flow rate is measured with the wet test meter and samples of it are collected at regular intervals. The isolated samples are then analyzed on the 154B chromatograph. Gas samples can also be taken through the liquid sample line. The liquid sample line extends to approximately the middle of the cell. When analysis of consecutive samples differs by less than 3 per cent, it is taken as an indication that equilibrium has been reached. Meanwhile, the resistance of the platinum resistance thermometer has

been measured on a Mueller G-2 bridge and the thermocouples on the cell have been measured with a K-2 Leeds and Northrup potentiometer. The pressure has also been measured on the pressure gauges. The measurement of composition, temperature, and pressure constitute an equilibrium point on the isotherm. The next point on the isotherm is established by reducing the pressure and again establishing equilibrium. Measurement of a point on an isotherm in the solid-vapor region takes between 1-1/4 to 1-1/2 hours.

In the liquid-vapor region pure carbon dioxide is first condensed in the cell. With liquid carbon dioxide in the cell the helium gas flow is from the bottom of the cell to the top. This is done by closing valves V3 and V6, and opening valves V4 and V5. The helium thus bubbles through the liquid carbon dioxide. Only four gas phase points were run on the 220^{o}K isotherm in the liquid-vapor region. These points were used as a check with the data of Barrick, et al.[4] No liquid samples were taken because the chromatograph was not calibrated for the analysis.

The results of the experiments are presented in Chapter III. The treatment of the experimental data are given in Appendices C and D.

CHAPTER III

EXPERIMENTAL RESULTS AND DISCUSSION

Experimental Results

The experimental results obtained for the helium-carbon dioxide system are presented in Figures 2 through 5. The detailed results are given in Appendix D. The vapor-phase composition is in the form of the Enhancement Factor, ϕ, which is plotted against the total pressure, P. The points represent the average values, while the length of the vertical lines indicate the scatter of the experimental data. The smooth curves were drawn in by eye and restricted to intersect the abscissa at the value of P equal to the vapor pressure of carbon dioxide at that particular temperature.

Figure 2 shows the Enhancement Factor versus total pressure curve at 181.05°K. Figure 3 shows the 190.03°K isotherm and also the data of Ewald[23] at 190°K. Figure 4 shows the 199.95°K isotherm. All the preceding are isotherms in the solid-vapor region. The 220.31°K isotherm in the liquid-vapor region is shown in Figure 5. Also plotted in Figure 5 are the data of Barrick et al.[4] at 219.9°K.

Discussion of Results

It is clear from Figures 2 through 5 that the Enhancement Factor in helium-carbon dioxide system is not much greater than one. This is generally true in the five helium systems considered here. In the solid-vapor region and for pressures up to 120 atmospheres, the

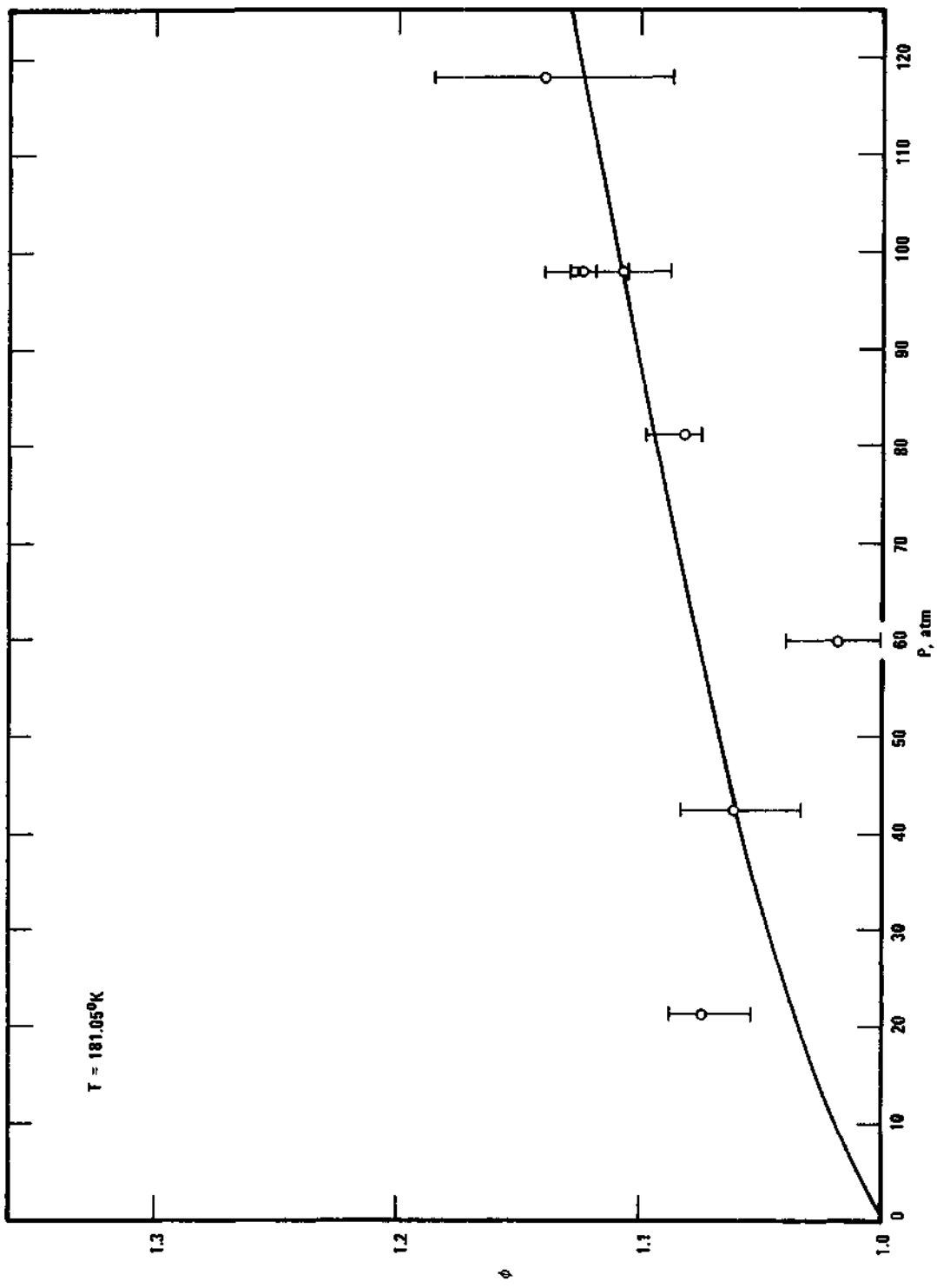

Figure 2. Experimental Enhancement Factor of Carbon Dioxide in Helium 181.05°K.

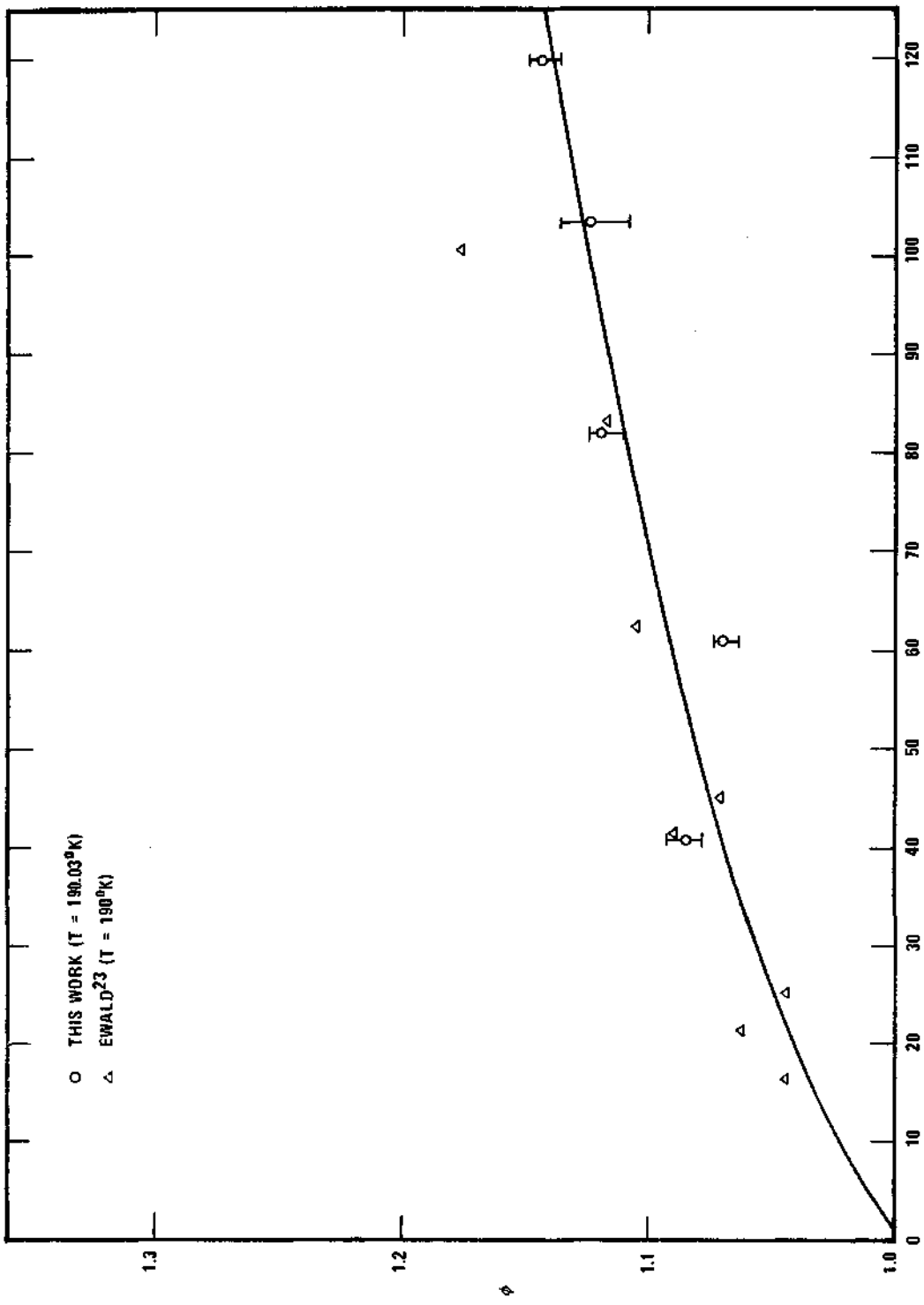

Figure 3. Experimental Enhancement Factor of Carbon Dioxide in Helium 190.03°K.

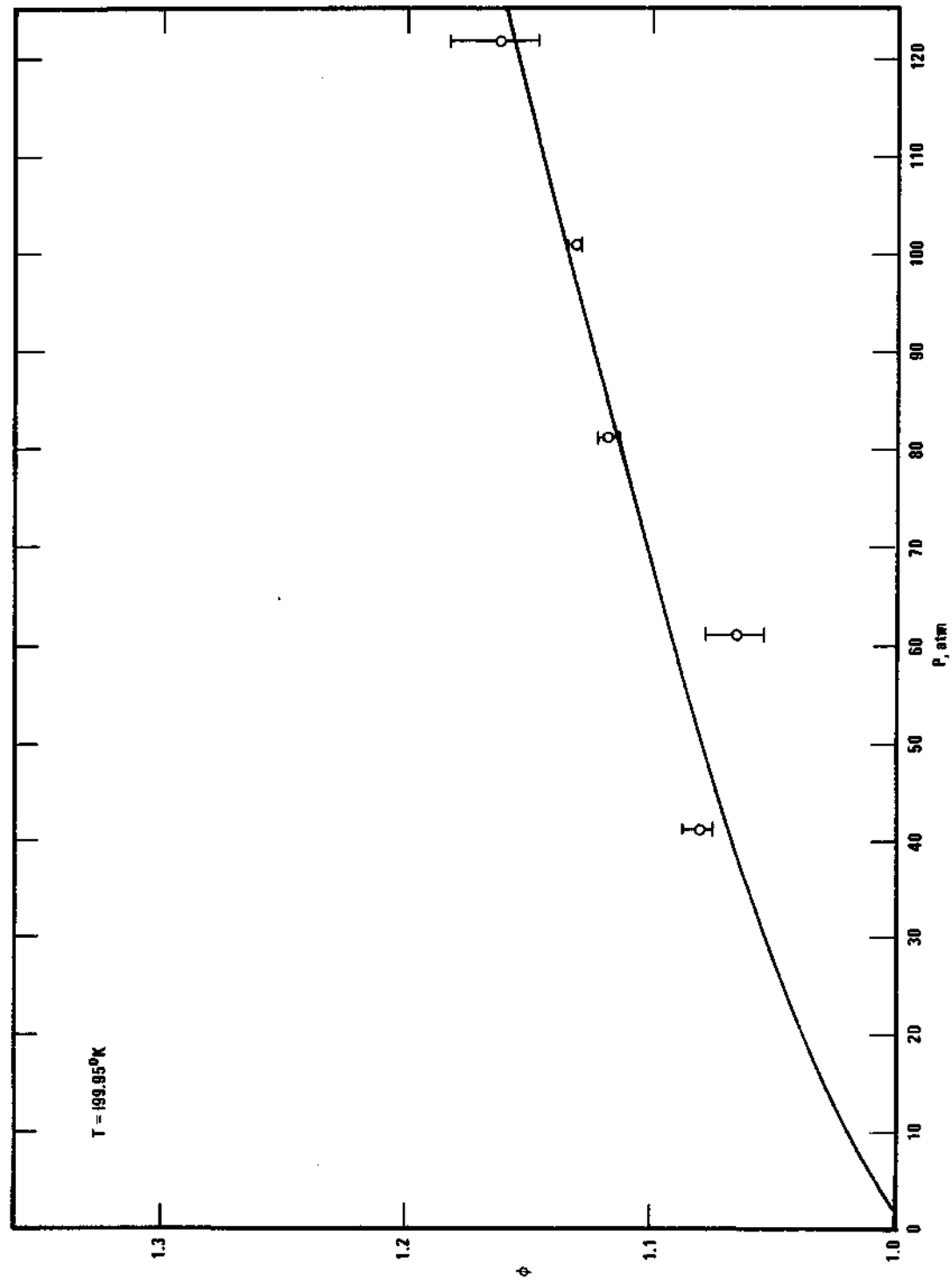

Figure 4. Experimental Enhancement Factor of Carbon Dioxide in Helium at 199.95°K.

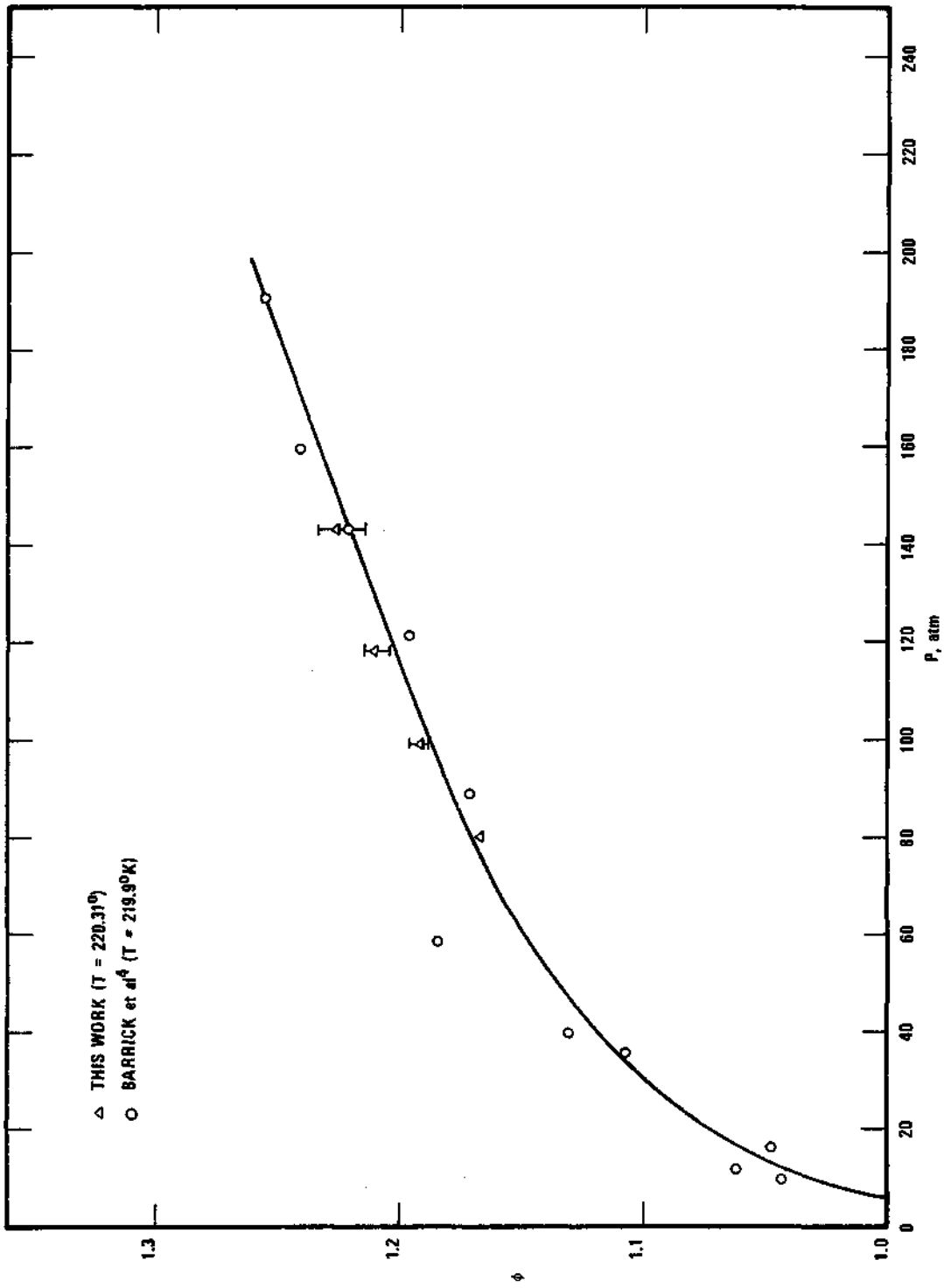

Figure 5. Experimental Enhancement Factor of Carbon Dioxide in Helium at 220.31°K.

Enhancement Factor is below 1.15. In the vapor-liquid region the Enhancement Factor is no larger than the value of 1.479 at 274.9°K and 200 atmospheres reported by Barrick et al.[4] In this system the trend of the Enhancement Factor against the temperature is the same as that of the vapor pressure, which is opposite to the usual trend.

The points at 60 atmospheres are consistently lower than the rest of the points. In the measurement of the vapor pressure of argon and carbon dioxide (see Appendix A) the highest pressures measured were 43.37 and 29.76 atmospheres, respectively. Thus, these measurements did not provide a check on the performance of the pressure gauges at 60 atmospheres. However, the helium-argon measurement at 60 atmospheres (see Figure 17 in Appendix B) appears to check well with that of Mullins.[64] No good reason has been found to account for the observed results at 60 atmospheres.

The scatter of the Enhancement Factor data is about ±3 per cent on the average. The data for the 181.05°K isotherm have the largest scatter, amounting to about ±5 per cent at 118.02 atmospheres. Part of this may be attributed to the error in the analysis of the low carbon dioxide concentration (about 0.3 mole per cent) at this temperature. Ewald[23] used a static equilibrium apparatus to measure the solid-vapor equilibrium of the helium-carbon dioxide system at 190°K. His data are presented in Figure 3 with the 190.03°K data obtained in this work. Below 80 atmospheres the agreement between the two sets of data is close. Above 80 atmospheres Ewald's data are higher than the present results. Thus, at 100.5 atmospheres his result is about 5 per cent above that obtained here. Considering the scatter of Ewald's data and that of the

present data, the agreement between the two sets of data is considered satisfactory. The 199.95°K isotherm (Figure 4) shows less scatter than the others. However, as noted above, the 60 atmosphere point is low. Figure 5 shows the data at 220.31°K in the liquid-vapor region. The data of Barrick et al.[4] at 219.9°K are also shown. Barrick et al. used a vapor-recirculation equilibrium apparatus. The agreement between the two sets of data is very good.

Thus, the results obtained in this work appear to be valid equilibrium data within the estimated average error of ±3 per cent in the Enhancement Factor. Previous experience with the present apparatus by Kirk,[45] and Mullins[64] indicated that an average accuracy of ±2 per cent was attainable. The analysis for carbon dioxide in this work was not as sensitive as the analysis for methane, argon, and hydrogen, with which they were concerned. The column used in the chromatograph to analyze for carbon dioxide was a silica gel column, as was recommended by the instrument manufacturer. Kirk, and Mullins used a molecular sieve column, which irreversibly absorbs carbon dioxide and hence is inapplicable for carbon dioxide. The calibration curves for the molecular sieve column show that Kirk, and Mullins could analyze lower concentrations of their substances than could be obtained for carbon dioxide using a silica gel column. This difference in the sensitivity of the analysis probably accounts at least in part for the difference in the accuracy between the previous data and the present data obtained with this apparatus.

In a single-pass flow-apparatus such as the one used here it is necessary to be sure that equilibrium rather than steady-state results

are obtained. To observe the effect of flow rate on the operation of the apparatus the flow-rate was varied at the 98.08 atmosphere point on the 181.05°K isotherm (Figure 2). The top point corresponds to a residence time in the cell of 14.8 minutes, the middle point to 29 minutes, and the bottom point to 57.5 minutes. The effect of flow rate is as expected: the higher flow rate results in a higher concentration of carbon dioxide, since the entering helium-carbon dioxide mixture contains an excess of carbon dioxide. But the range of the points does overlap each other. A residence time of 30 minutes was considered satisfactory for the attainment of equilibrium. This value of the residence time was thus used in all the runs. Actually, it would have been better to observe the effect of flow rate at each point. The operation requirements of the apparatus made this impractical.

The procedure followed in this work was to start from the highest pressure on an isotherm and work to the lower pressures. Thus, equilibrium was only approached from the high pressure side. The approach to equilibrium from the low pressure side was not investigated. Past experience with the apparatus by Kirk, and Mullins indicated that this was not a problem.

CHAPTER IV

THEORETICAL CALCULATION OF THE ENHANCEMENT FACTOR

Introduction

For a system at equilibrium thermodynamics requires that the chemical potential of each component in each of the phases be equal. This requirement is the basis for phase equilibria calculation. Consider the case of a binary system in vapor-liquid equilibrium at temperature T and pressure P. The chemical potential of component 1 in the liquid phase, $\mu_1^L (P,T,x_1)$, must be equal to its chemical potential in the vapor phase, $\mu_1^V(P,T,y_1)$. The same equality holds for component 2. The condition for equilibrium can thus be expressed by Equation (IV-1).

$$\mu_1^L(P,T,x_1) = \mu_1^V(P,T,y_1) \qquad \text{(IV-1)}$$

Equation (IV-1) as it stands is not useful for making calculations. One needs to know how to calculate μ_1^L and μ_1^V. The reference state on which μ_1^L and μ_1^V is based is the free energy of one mole of component 1 in the ideal gas state at temperature T and one atmosphere pressure. This reference state, g_1^o, is the one usually used. Basing $\mu_1^L (T,P)$ on g_1^o as the reference state, it is expressed by Equation (IV-2). The derivation of the equations used in this section can be found in Mullins.[64]

$$\mu_1^L(P,T,x_1) - g_1^o = \int_{p_{01}}^{P} v_1 dP + \int_{v_{01}}^{\infty} (P-\frac{RT}{V_1})dV_1 + p_{01}V_{01} \qquad \text{(IV-2) (con't.)}$$

$$- RT - RT \ln \frac{V_{01}}{RT} + RT \ln \gamma_1' x_1 \quad \text{(IV-2, con't)}$$

In Equation (IV-2) the activity coefficient $\gamma_1' \rightarrow 1$ as $x_1 \rightarrow 1$ and is based on the chemical potential of pure liquid component 1 at T and P. After correction to the same reference state, μ_1^V is given by Equation (IV-3).

$$\mu_1^V(P,T,y_1) - g_1^o = \int_{V_m}^{\infty} \left[\left(\frac{\partial P}{\partial n_1}\right)_{T,V,n_2} - \frac{RT}{V_m}\right] dV_m - RT \ln \frac{V_m}{RT} + RT \ln y_1 \quad \text{(IV-3)}$$

To satisfy the condition of Equation (IV-1), the right-hand sides of Equations (IV-2) and (IV-3) are set equal. After some algebraic manipulations and rearrangement the resultant equation is given by Equation (IV-4).

$$\ln \frac{Py_1}{p_{01}} = Z_{01} - 1 - \ln Z_{01} + \frac{1}{RT}\int_{p_{01}}^{P} v_1 dP + \frac{1}{RT}\int_{V_{01}}^{\infty} \left(P - \frac{RT}{V_1}\right) dV_1 \quad \text{(IV-4)}$$

$$+ \ln Z_m - \frac{1}{RT}\int_{V_m}^{\infty} \left[\left(\frac{\partial P}{\partial n_1}\right)_{T,V_m,n_2} - \frac{RT}{V_m}\right] dV_m + \ln \gamma_1' x_1$$

The quantity (Py_1/p_{01}) on the left-hand side of Equation (IV-4) is by definition the Enhancement Factor ϕ. Thus Equation (IV-4) is referred to as the Enhancement Factor equation. A similar equation applies to component 2 when the temperature T is less than the critical temperature of both components.

The use of Equation (IV-4) to calculate the Enhancement Factor requires the following information:

1. The molal volume v_1 of pure liquid component 1
2. An equation of state for the vapor phase of pure component 1 and the gas mixture
3. Experimental data or an assumption about γ_1'.

Requirement 1 above is met by expressing v_1 at each temperature as a function of pressure in the form of Equation (IV-5)

$$v_1 = a + b(P-p_{01}) + c(P-p_{01})^2 \qquad \text{(IV-5)}$$

Requirement 2 is met by the selection of the virial equation of state. The choice of this equation has been discussed in Chapter I. Specifically, the virial equation truncated after third virial coefficient is used. It is expressed as Equation (IV-6)

$$\frac{PV}{RT} = 1 + \frac{B}{V} + \frac{C}{V^2} \qquad \text{(IV-6)}$$

In the application of Equation (IV-6) to a mixture the virial coefficients for the mixture are expressed by Equations (IV-7) and (IV-8)

$$B_m = y_1^2 B_{11} + 2y_1y_2B_{12} + y_2^2 B_{22} \qquad \text{(IV-7)}$$

$$C_m = y_1^3 C_{111} + 3y_1^2 y_2 C_{112} + 3y_1 y_2^2 C_{122} + y_2^2 C_{222} \qquad \text{(IV-8)}$$

Requirement 3 is met by the assumption that the solutions encountered in the systems considered here are ideal, that is γ_1' is one. This assumption is based on the following considerations. In the helium systems at temperatures under consideration, and at pressures below 140 atmospheres the solubility of helium in the liquids is about 10 mole

per cent or less. Thus the liquid phase is essentially the pure condensed component 1, whose activity coefficient γ_1' would be expected to be very close to one. Mullins[64] (by computing the activity coefficient of argon along the locus of the three-phase line) showed that in the helium-argon and hydrogen-argon systems the value of γ_1' was indeed essentially one. Thus the assumption that γ_1' is one appears to be reasonable.

Incorporating the preceding information into Equation (IV-4) results in Equation (IV-9):

$$\ell n \frac{Py_1}{p_{01}} = \frac{1}{RT}\left[a(P-p_{01}) + \frac{b}{2}(P-p_{01})^2 + \frac{c}{3}(P-p_{01})^3\right] + \frac{2B_{11}}{V_{01}} + \frac{3}{2}\frac{C_{111}}{V_{01}^2} \qquad \text{(IV-9)}$$

$$- \ell n\, Z_{01} - \frac{2}{V_m}(y_1B_{11}+y_2B_{12}) - \frac{3}{2V_m^2}(y_1^2C_{111}+2y_1y_2C_{112}+y_2^2C_{122})$$

$$+ \ell n\, Z_m + \ell n\, x_1$$

Equation (IV-9) is the working equation used in this work for the calculation of the Enhancement Factor in the vapor-liquid region. The quantity x_1 is assumed to be known experimentally.

In the application of (IV-9) in the vapor-solid region two more assumptions are made. The first is that the solid phase is pure solid component 1. This assumption is reasonable in view of the low solubility of helium in the liquid phase. Mullins,[64] by studying the freezing point curves in the helium-argon and hydrogen-argon systems, concluded that the solid phase was essentially pure argon. This assumption eliminates the $\ell n\, x_1$ term in Equation (IV-9) in the vapor-solid region. The other

assumption is that the solid phase is incompressible in addition to being pure. This assumption is reasonable since the pressure of 140 atmospheres or less encountered are not too high with respect to the solid phase. This assumption eliminates the terms involving b and c in Equation (IV-9), and the constant a becomes the molal volume of saturated solid component 1 at T.

In the helium systems considered here the helium is above its critical temperature. Since it is not realistic to talk of its vapor pressure under such circumstances, the concept of the Enhancement Factor is not useful for helium. The relevant quantity in this case is the Henry's Law constant. This area of study has not been pursued in this work. Mullins[64] discusses the thermodynamics involving the Henry's Law constant, and obtained values of a modified Henry's Law constant for the helium-argon and hydrogen-argon systems. Pierotti[73] has worked out a procedure for the calculation of the theoretical Henry's Law constant from molecular parameters. An interesting study would be the extraction of the Henry's Law constant from the vapor-liquid equilibria data of these helium systems, and a comparison with the predicted values of Pierotti's method.

Calculation of Virial Coefficients

The theoretical calculation of virial coefficients requires the knowledge of the interaction between the molecules in the vapor phase. This interaction is expressed as a potential energy function. The potential energy function is usually a function of the distance between two molecules and also may be taken into account the size and shape of

the interacting molecules. The Lennard-Jones (6-12) potential function[29] expresses the interaction energy between two molecules as the sum of an attractive energy (inversely proportional to the sixth power of the distance of separation between two molecules) and a repulsive energy (inversely proportional to the twelfth power of the distance of separation between two molecules). The function is given by Equation (IV-10):

$$U(r) = 4e\left[\left(\frac{\sigma}{r}\right)^{12} - \left(\frac{\sigma}{r}\right)^{6}\right] \qquad \text{(IV-10)}$$

It has two adjustable parameters e and σ, which have the dimension of energy and length. The distance of separation between two molecules (which are assumed to be point masses) is r. The value of r at $U(r) = 0$ is designated as σ. The minimum $U(r)$, which occurs at $r = 2^{1/6}\sigma$ is designated as e.

The Kihara core model[43,44] is similar to the Lennard-Jones (6-12) model. Instead of a point mass, the molecule is assumed to have a convex impenetrable core. The shape of the core is determined by the geometry of the model. The potential energy function for the Kihara core model is given by Equation (IV-11):

$$U(\rho) = U_o\left[\left(\frac{\rho_o}{\rho}\right)^{12} - 2\left(\frac{\rho_o}{\rho}\right)^{6}\right] \qquad \text{(IV-11)}$$

The potential energy is a function of ρ, the shortest distance between the molecular cores of two interacting molecules. The parameter ρ_o is the shortest distance between two molecular cores at the minimum value of $U(\rho)$, U_o.

The above potential energy functions are the most commonly used for the theoretical calculation of virial coefficients. Other forms of potential energy functions which are in use can be found in Hirschfelder, Curtiss, and Bird.[29]

The Lennard-Jones (6-12) and the Kihara core models were selected for use in this work to calculate the second virial coefficients. The third virial coefficients were calculated with the Lennard-Jones (6-12) model.

Lennard-Jones (6-12) Model (LJCL)

Hirschfelder et al.[29] present methods for the calculation of the second and third virial coefficients based on Equation (IV-10). The second virial coefficient between molecules i and j is represented by Equation (IV-12):

$$B_{ij} = (b_o)_{ij} B^*_{CL}(T^*_{ij}) \qquad \text{(IV-12)}$$

where

$$(b_o)_{ij} = \frac{2\pi}{3} N_A (\sigma)_{ij}^3 \qquad \text{(IV-13)}$$

$$T^*_{ij} = \frac{T}{(e/k)_{ij}} \qquad \text{(IV-14)}$$

The reduced second virial coefficient, B^*_{CL}, is evaluated from the expression given by Equation (IV-15):

$$B^*_{CL}(T^*) = \sum_{j=0}^{\infty} b^{(j)} (T^*_{ij})^{-(1+2j)/4} \qquad \text{(IV-15)}$$

where

$$b^{(j)} = \left(\frac{2^{j+1/2}}{4j!}\right)\Gamma\left(\frac{2j-1}{4}\right) \qquad \text{(IV-16)}$$

The first forty-one values of $b^{(j)}$ are given by Hirschfelder et al.[29] Kirk[45] has recomputed these values. His values agreed with those of Hirschfelder et al. to about 1 part in 10^7 except for the value of $b^{(16)}$, which was $-0.3386316 \times 10^{-5}$ as compared to $-0.3387440 \times 10^{-5}$ computed by Hirschfelder et al. The values of Kirk for $b^{(j)}$ were selected for use here.

The third virial coefficient among molecules i, j, and k is similarly given by an expression of the form in Equation (IV-17):

$$C_{ijk} = (b_o)^2_{ijk} C^*_{CL}(T^*_{ijk}) \qquad \text{(IV-17)}$$

The reduced third virial coefficient is given by Equation (IV-18):

$$C^*_{CL}(T^*_{ijk}) = \sum_{j=0}^{\infty} c^{(j)} (T^*_{ijk})^{-(j+1)/2} \qquad \text{(IV-18)}$$

The expression for $c^{(j)}$ is more complicated than that for $b^{(j)}$ as given in Equation (IV-16). It is presented by Rowlinson et al.,[81] who also have computed the first twenty-one values for $c^{(j)}$. Their results were used here to compute the third virial coefficient.

For mixtures the mixture rules are given by Equations (IV-19), (IV-20), (IV-21), and (IV-22):

$$\left(\frac{e}{k}\right)_{ij} = \left(\frac{e}{k}\right)_i^{1/2}\left(\frac{e}{k}\right)_j^{1/2} \qquad \text{(Geometric average)} \qquad \text{(IV-19)}$$

$$\left(\frac{e}{k}\right)_{ijk} = \left(\frac{e}{k}\right)_i^{1/3}\left(\frac{e}{k}\right)_j^{1/3}\left(\frac{e}{k}\right)_k^{1/3} \qquad \text{(IV-20)}$$

$$(b_o)_{ij} = \frac{1}{8}\left[(b_o)_i^{1/3} + (b_o)_j^{1/3}\right]^3 \qquad \text{(Lorentz average)} \qquad \text{(IV-21)}$$

$$(b_o)_{ijk} = \frac{1}{27}\left[(b_o)_i^{1/3} + (b_o)_j^{1/3} + (b_o)_k^{1/3}\right]^3 \qquad \text{(IV-22)}$$

The Lennard-Jones (6-12) model used here is the classical form, and does not include quantum corrections.

Kihara Core Model (KIH)

The expression for the second virial coefficient for the Kihara core model has been derived by Kihara.[43] It is given by Equation (IV-23):

$$\frac{(B_k)_{ij}}{N_A} = \frac{2}{3}\pi(\rho_o)_{ij}^3 F_3 + \frac{(M_o)_i + (M_o)_j}{2}(\rho_o)_{ij}^2 F_2 \qquad \text{(IV-23)}$$

$$+\left[\frac{(S_o)_i + (S_o)_j}{2} + \frac{(M_o)_i (M_o)_j}{4\pi}\right](\rho_o)_{ij} F_1 + \frac{(V_o)_i + (V_o)_j}{2}$$

$$+\frac{(M_o)_i (S_o)_j + (M_o)_j (S_o)_i}{8\pi}$$

The functions F_1, F_2, and F_3 are functions of Z, where $Z = U_o/kT$. They are given by Equation (IV-24):

$$F_s = \sum_{j=0}^{\infty} b_s(j)\, Z^{(6j+s)/12} \qquad \text{(IV-24)}$$

where

$$b_s(j) = -\left(\frac{s}{12}\right)\left(\frac{2^j}{j!}\right)\Gamma\left(\frac{6j - s}{12}\right) \qquad \text{(IV-25)}$$

The first forty values of $b_s(j)$ for $s = 1, 2, 3$ have been computed by Mullins[64] and are presented by Kirk.[45] These results were used here to compute F_1, F_2, and F_3.

The parameters M_o, S_o, and V_o are related to the core size and shape. They have dimensions of length, area, and volume, respectively.

Prausnitz and Myers[77] have determined the Kihara core model parameters for a number of gases. Their values for the parameters are used here (see Table 15 for the values of the parameters used). For the light gases, helium, hydrogen, and neon, they introduced the first two translational quantum corrections to the second virial coefficients. The quantum corrections were computed, however, from the Lennard-Jones (6-12) model, which is the same as the Kihara core model in the special case of a vanishing core. The value of σ for the Lennard-Jones (6-12) model is related to the Kihara core model parameter, ρ_o, by Equation (IV-26):

$$\sigma_{ij} = 2^{-1/6}(\rho_o)_{ij} + \frac{(M_o)_i + (M_o)_j}{4\pi} \qquad \text{(IV-26)}$$

Equation (IV-26) is exact for the case of the spherical core but is approximate for other cores. Thus, the second virial coefficient as

calculated here is given by Equation (IV-27):

$$B_{ij} = (B_k)_{ij} + (b_o)_{ij}\left[(\Lambda^*_{ij})^2 B^*_I + (\Lambda^*_{ij})^4 B^*_{II} - (\Lambda^*_{ij})^3 B^*_o\right] \qquad \text{(IV-27)}$$

The reduced quantum mechanical parameter Λ^* is given by Equation (IV-28):

$$(\Lambda^*_{ij})^2 = \frac{h^2}{k\sigma_{ij}^2 m_{ij}(\frac{e}{k})_{ij}} \qquad \text{(IV-28)}$$

The mass of the molecule is denoted by m, where $m = M/N_A$. M and N_A are the molecular weight and Avogadro's number, respectively. (Note that $m_{ij} = M_{ij}/N_A$.) Kihara[44] has derived the first three reduced translational quantum corrections to the second virial coefficient for a (6-12) potential. The first two corrections which are used here are given by Equations (IV-29) and (IV-30):

$$B^*_I = \sum_{j=0}^{\infty} b_I(j)(T^*)^{-(6j+13)/12} \qquad \text{(IV-29)}$$

$$B^*_{II} = \sum_{j=0}^{\infty} b_{II}(j)(T^*)^{-(6j+23)/12} \qquad \text{(IV-30)}$$

where

$$b_I(j) = -\left[\frac{11 - 36j}{768\pi^2}\right]\left[\frac{2^{j+13/6}}{j!}\right]\Gamma\left[\frac{6j - 1}{12}\right] \qquad \text{(IV-31)}$$

$$b_{II}(j) = -\left[\frac{3024j^2 + 4728j + 767}{491520\pi^4}\right]\left[\frac{2^{j+23/6}}{j!}\right]\Gamma\left[\frac{6j + 1}{12}\right] \qquad \text{(IV-32)}$$

The first forty-two values for $b_I^{(j)}$ and $b_{II}^{(j)}$ computed by Kirk[45] were used here to make the quantum correction to the second virial coefficient. The value of B_o^*, the ideal gas quantum correction, is given by Equation (IV-33):

$$B_o^* = \frac{3}{32\pi^{5/2}(T^*)^{3/2}} \qquad \text{(IV-33)}$$

The sign of Equation (IV-33) is that for a Bose-Einstein gas.

Thus, the second virial coefficient computed here with Equation (IV-27) consists of the part $(B_k)_{ij}$ (given by Equation (IV-23)) plus the quantum correction for the first two translational terms.

Kihara Core Model with Quadrupole (KIHQ)

For components such as nitrogen and carbon dioxide, which have significant quadrupole moments, an additional correction is applied. The quadrupole correction derived by Pople[74] is given by Equation (IV-34):

$$B_Q = -\frac{2}{3}\pi N_A \sigma^3 \left(\frac{7}{320}\right)(Q^*)^2 H_{10}(2/\overline{Z}) \qquad \text{(IV-34)}$$

where

$$Q^* = \frac{Q^2}{U_o \sigma^5} \qquad \text{(IV-35)}$$

The parameters Q and Q^* are the molecular and reduced quadrupole moments, respectively. The parameter σ is again given by Equation (IV-26). As in the case of the quantum correction, the quadrupole correction given by Equation (IV-34) is strictly correct only for the Lennard-Jones (6-12)

potential function. It is applied here as recommended by Prausnitz and Myers[77] as an approximation to the Kihara potential function. Equation (IV-36) gives the expression for the function H_{10}:

$$H_{10}(2\sqrt{Z}) = (2\sqrt{Z})^{17/6} \sum_{j=0}^{\infty} \Gamma\left(\frac{6j+7}{12}\right) \frac{(2\sqrt{Z})^j}{j!} \qquad \text{(IV-36)}$$

Kirk[45] has computed the first forty coefficients in Equation (IV-36) which are used in this work to make quadrupole corrections to the second virial coefficient.

The mixing rules used for the Kihara core model are given by Equation (IV-37) through Equation (IV-40):

$$(U_o/k)_{ij} = (U_o/k)_i^{1/2} \, (U_o/k)_j^{1/2} \qquad \text{(IV-37)}$$

$$(\rho_o)_{ij} = \frac{(\rho_o)_i + (\rho_o)_j}{2} \qquad \text{(IV-38)}$$

$$Q^*_{ij} = \left(Q^*_i \, Q^*_j\right)^{1/2} \qquad \text{(IV-39)}$$

$$M_{ij} = \frac{2M_i M_j}{M_i + M_j} \qquad \text{(IV-40)}$$

Lennard-Jones (6-12) Model Adjusted (LJCLA)

This model is the same as the Lennard-Jones (6-12) model with one difference. This difference is that the parameter $(e/k)_{12}$ has been adjusted to fit the second interaction virial coefficient, with $(b_o)_{12}$ given by Equation (IV-21). In the LJCL model $(e/k)_{12}$ is given by

Equation (IV-19). The adjustment of $(e/k)_{12}$ is discussed in Chapter V.

Thus, the four models used for the theoretical calculation of the Enhancement Factor in this work are the Lennard-Jones (6-12) model (LJCL), the Kihara core model (KIH), the Kihara core model with quadrupole (KIHQ), and the adjusted Lennard-Jones (6-12) model (LJCLA).

Calculation of the Third Virial Coefficient

All the third virial coefficients used in this work were calculated with the Lennard-Jones (6-12) model discussed above. The Kihara core model third virial coefficient for different shaped cores other than the spherical does not appear to have been worked out. The Kihara spherical core third virial coefficients have been worked out by Sherwood and Prausnitz.[84,85] A non-addivity correction has also been applied to the third virial coefficients they derived. The Kihara core parameters used here were those obtained by Prausnitz and Myers[77] for spherical and non-spherical cores. Sherwood and Prausnitz calculated Kihara spherical core parameters for, among other substances, argon, nitrogen, methane, and carbon dioxide. The helium and oxygen parameters (the remaining components considered here) are not available. Sherwood and Prausnitz have also derived the Lennard-Jones (6-12) parameters for the above substances. Chueh and Prausnitz[12] correlated the available experimental third virial coefficient data with a generalized expression. They found essentially no data below a reduced temperature (T/T_c) of 0.8. Orentlicher and Prausnitz[70] recently presented an approximate method for calculating the third virial coefficients of gas mixtures.

A comparison of the above methods for calculating the third virial coefficient was made for argon at 108.02°K. The results are presented in Table 1. The Lennard-Jones (6-12) parameters for argon used by Sherwood and Prausnitz were $e/k = 117.7^{\circ}K$, $b_o = 54.26$ cc/gm mole, as compared with $e/k = 119.30^{\circ}K$, $b_o = 50.91$ cc/gm mole used in the present work. The third virial coefficient, computed with the Lennard-Jones parameters used here together with the value of $\alpha^* = 3.79 \times 10^{-2}$ ($\alpha^* = \alpha/\sigma^3$ is the reduced polarizibility) used by Sherwood and Prausnitz, is 2345 $(cc/gm\ mole)^2$. The additive and non-additive contributions are 259 and 2086 $(cc/gm\ mole)^2$, respectively. It can be seen that the third virial coefficient calculated here without taking non-addivity contributions into account is low. The non-addivity contribution is shown by Sherwood and Prausnitz[84] to be always positive and becomes more significant as the temperature decreases. They also show that the third virial coefficient is more sensitive to the shape of the potential function that the second virial coefficient. They point out that the neglect of three-body repulsive forces in their computations tend to raise the value of the calculated third virial coefficient. For the substances considered here, the third virial coefficient data are extensive at low temperatures only for helium. Figure 20 in Appendix E shows that the third virial coefficient of helium calculated in this work tends to be only slightly lower than the experimental values. In the temperature region of this work it is thus not possible to compare the amount of undershoot resulting from the method used here with the amount of overshoot which would have resulted from the method of Sherwood and Prausnitz. The third virial coefficient of argon at 108.02°K

Table 1. Third Virial Coefficient of Argon at 108.02°K

Method	C, $(cc/gm\ mole)^2$
LJCL (6-12) (this work)	88.0
LJCL (6-12) (Sherwood & Prausnitz[85])	2740
C_{add} = 451	
$C_{non\text{-}add}$ = 2289	
Spherical Kihara core (Sherwood & Prausnitz[85])	1650
C_{add} = -1400	
$C_{non\text{-}add}$ = 3050	
Generalized Equation (Chueh & Prausnitz[12])	-503.0
Extrapolated	

predicted by the extrapolation of the generalized equation of Chueh and Prausnitz[12] is -503 $(cc/gm\ mole)^2$. This is lower than the other values computed above and is due to steepness of the equation when extrapolated to a reduced temperature lower than 0.8.

Because of the absence of experimental third virial coefficient data in the temperature region of interest for most of the substances considered here, the problem of the third virial coefficient was not pursued with great emphasis. It is a subject that needs to be studied in conjunction with the problem of the second virial coefficient. Current practice obtains potential function parameters from a fit to the second virial coefficient only. A simultaneous fit to include the third virial coefficient would probably result in parameters which are better. Third virial coefficients, especially in the low temperature regions, are difficult to measure accurately. However, workers[9,33,34,62,63,105] are involved in this kind of measurement and some data are being obtained.

CHAPTER V

INTERACTION SECOND VIRIAL COEFFICIENT

General

The degree to which the properties of a gas mixture can be accurately described is directly related to how well the interactions between the molecules are known. The interaction virial coefficient such as the interaction second virial coefficient (B_{12}) is a direct measure of the interaction between two dissimilar molecules. Thus a model which can accurately predict B_{12} can be expected to be more successful in phase equilibria calculations. The correct prediction of B_{12} is just the first step, and of course, will not account for all the inadequacies of the model. This chapter discusses the extraction of B_{12} values from phase equilibria data.

The three main ways of obtaining virial coefficients directly are:

(1) PVT measurements on the gas and subsequent treatment (fitting a power series or extrapolation to zero pressure) to obtain virial coefficients.

(2) Measurement of the pressure change on mixing two gases at constant volume and temperature.[16]

(3) The Burnett[6] fixed volume expansion method for PVT measurement. Other methods which have been used are the Joule-Thomson expansion and the velocity of sound[98,99,100] techniques. These methods all require accurate values of the virial coefficients of the pure gases if interaction virial coefficients are to be obtained.

Of all the methods, the Burnett method appears to be the choice of most investigators. Its merits have been discussed in detail by Canfield et al.,[9] Hoover et al.,[33,34] and others.[7,14,26,36,50,51,62,63] Its outstanding advantage over the other methods is that it does not require precise volume measurements. Until recently its application has been mainly at room temperatures and above. Investigators[9,14,33,34,62,63] have adopted the method for the lower temperature regions.

The direct measurement of PVT data is difficult because volume is difficult to measure accurately. An example of this procedure is the work of White et al.[106] on the PVT data of helium. Dantzler et al.[16] have obtained the interaction second virial coefficient of hydrocarbon mixtures and argon-hydrocarbon mixtures from the measurement of the pressure change on mixing two gases at constant volume and temperature. The difficulty here is that of accurately measuring small pressure differences. Dantzler et al.[17] and Pecsok and Windsor[71] also describe a recent application of gas-liquid chromatography for obtaining the second interaction virial coefficient.

At cryogenic temperatures such as are encountered in the systems considered here, the direct methods mentioned above present experimental difficulties. Hence, indirect methods have been developed to obtain virial coefficients at low temperatures. For pure substances, the assumption of a particular intermolecular potential function permits extrapolation to low temperatures by means of parameters determined at high temperatures. With assumed combination rules for pure component parameters, this procedure could be applied to the evaluation of interaction virial coefficients of mixtures. However, these combination

rules are empirical and are not always valid.

Another method is to derive the interaction virial coefficients from phase equilibria data. Such a method has been discussed by Reuss and Beenakker,[79] and Dokoupil.[20] Mullins[64] developed a method to obtain B_{12} from phase equilibria data. His is the method used in this work. More recently Chiu and Canfield[11] also developed a method for obtaining B_{12} from phase equilibria data. Dokoupil applied his method to the hydrogen-nitrogen system. Reuss and Beenakker applied their method to the hydrogen-nitrogen and hydrogen-carbon monoxide systems. Mullins used his method for the helium-argon and hydrogen-argon systems. Chiu and Canfield used their method for the hydrogen-methane system. A comparison of the Mullins, and Chiu and Canfield methods is presented in the following section. Hiza and Duncan[30] obtained B_{12} for the helium-ethane, helium-ethylene, and several other systems by a least-squares fit of the Enhancement Factor equation to the experimental Enhancement Factor data.

The following section discusses the method used here to extract B_{12} from phase equilibria data. Following this discussion, the extracted B_{12} for the different systems and the available B_{12} data from other sources are presented. A concluding section discusses the least-squares fitting of the smooth B_{12} values with the Lennard-Jones (6-12) potential function.

Interaction Second Virial Coefficient from Phase Equilibria Data

The Enhancement Factor equation, Equation (IV-9), can be rearranged (Mullins[64]) to give:

$$B_{12} = \frac{V_m}{2y_2}\left\{\frac{2B_{11}}{V_{01}} + \frac{3C_{111}}{2V_{01}^2} - \ell n\, Z_{01}\right. \qquad \text{(V-1)}$$

$$- \frac{3}{2V_m^2}\left(y_1^2 C_{111} + 2y_1 y_2 C_{112} + y_2^2 C_{122}\right)$$

$$+ \frac{1}{RT}\left[a(P - p_{01}) + \frac{b}{2}(P - p_{01})^2 + \frac{c}{3}(P - p_{01})^3\right] - \frac{2y_1 B_{11}}{V_m}$$

$$\left. + \ell n\, Z_m + \ell n\, x_1 - \ell n \frac{Py_1}{p_{01}}\right\}$$

At each experimental point along an isotherm Equation (V-1) is solved for B_{12}. The values of B_{12} thus obtained are plotted against $(P - p_{01})$ and extrapolated to $(P - p_{01}) = 0$. The intercept then is assumed to be the true value of B_{12} at that temperature. This method has been described and used by Mullins to obtain B_{12} for the helium-argon and hydrogen-argon systems. His results are in good agreement with the single value for each system obtained from PVT measurements reported in the literature.[48,77]

The phase equilibria data of Kirk[45] for the hydrogen-methane system have been analyzed by Chiu and Canfield[11] to obtain the values of B_{12}. The lowest and highest isotherms of Kirk at 66.88 and 116.53°K, respectively, were also analyzed in the present work by the method used here. The values of the Lennard-Jones (6-12) parameters used to obtain B_{11}, C_{111}, C_{112}, C_{122} in Equation (V-1) were those of Chiu and Canfield. The resulting B_{12} are compared with those of Chiu and Canfield in Table 2.

Table 2. B_{12} for the Hydrogen-Methane System

	B_{12}, cc/gm mole	
$T^{\circ}K$	This Work	Chiu-Canfield[11]
66.88	-136 ± 6	-138.87
116.53	-55 ± 6	-49.97

As can be seen from Table 2, the B_{12} obtained by the procedure used here and that used by Chiu and Canfield are essentially the same. The estimated accuracy of Kirk's Enhancement Factor data for the hydrogen-methane system was ±2 per cent. This uncertainty was introduced in the value of the Enhancement Factor used in Equation (V-1) and its effect on the B_{12} is reflected in the ±6 cc/gm mole in the value of B_{12}. Thus, the effect of an error in the Enhancement Factor on the value of B_{12} can be significant.

The quoted accuracy of the phase equilibria data used in this work was in most cases about ±3 per cent. This uncertainty was introduced in the Enhancement Factor used for the calculating of B_{12} by Equation (V-1).

For each system the selected phase equilibria data (in the form of the Enhancement Factor and mole fraction of helium in the liquid phase) were first smoothed graphically. The smooth values were read off at regular pressure intervals. These values are presented in Appendix F and were used to calculate B_{12}. The LJCL, KIH, and KIHQ models were used to compute the values for B_{11}, C_{111}, C_{112}, C_{122} in Equation (V-1). In all instances, the parameters selected for use in the several models were those which represented the experimental second virial coefficients of the pure gases with good accuracy.

Figure 6 illustrates some typical results. The 74.05°K isotherm for helium-argon illustrates the symmetric effect of +3 per cent and -3 per cent variation in the experimental Enhancement Factor. The 181.05°K isotherm for helium-carbon dioxide illustrates the dependence on the high-pressure points and also the sensitivity, at lower pressures, of

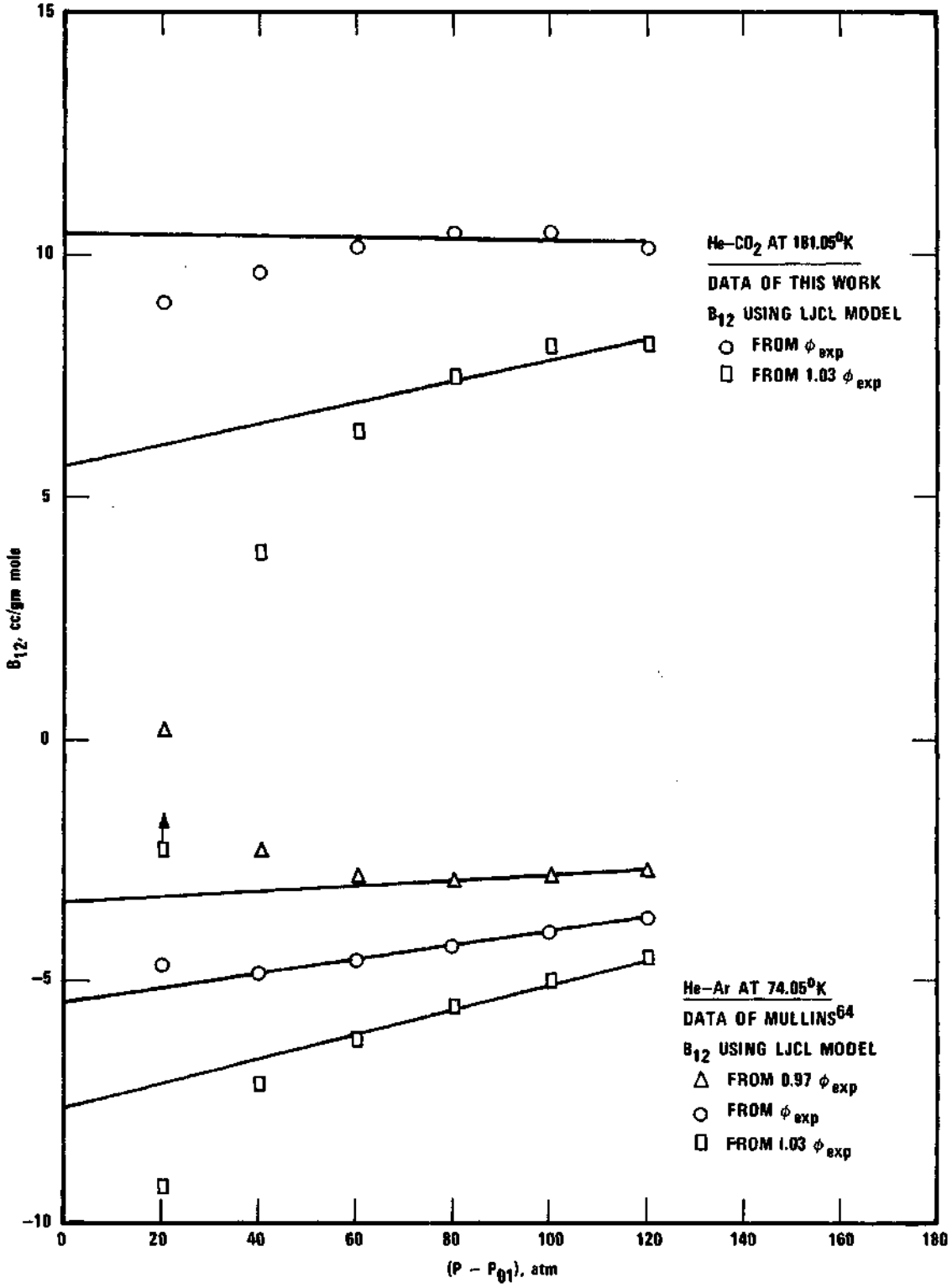

Figure 6. Graphical Determination of Interaction Second Virial Coefficient.

B_{12} to the experimental value of the Enhancement Factor. Where the data resulted in an extremely non-linear B_{12} versus $(P - p_{01})$ relation, no extrapolation was attempted to find the value of B_{12} at $(P - p_{01}) = 0$.

Results of B_{12} Extraction from Phase Equilibrium Data

This section presents the B_{12} values from phase equilibria data for the several systems. Also presented are the B_{12} data available from the literature for the helium-carbon dioxide, -argon, -methane, -nitrogen, and -oxygen systems. The B_{12} data from this work and the B_{12} data from the literature were plotted together and smooth curves were drawn through the data. These smooth curves are presented in Figures 7 to 11 as the unlabeled curves. The curves labeled "LJCL" and "KIH" or "KIHQ" mean that they are the respective theoretical curves for that model. The legends "B_{12} using LJCL model" and "B_{12} using KIH (or KIHQ) model" mean that the LJCL and the KIH (or KIHQ) model, respectively, was used in Equation (V-1) to compute B_{11}, C_{111}, C_{112}, and C_{122}.

It should be noted that the criterion used in the selection of the phase equilibria data for use in the B_{12} extraction is that the experimental Enhancement Factor not show great scatter. Thus, all the discussions of "data" in this section are in the context of the Enhancement Factor.

B_{12} for the Helium-Carbon Dioxide System

The phase equilibria data for the helium-carbon dioxide system consist of those of this work, those of Barrick et al.[4], and the 190°K isotherm of Ewald[23]. The data of Ewald were combined with the 190.03°K isotherm of this work. The smoothed values of the above data are pre-

sented in Table 25 of Appendix F. The physical properties of helium and carbon dioxide presented in Appendix E were used together with the smoothed phase equilibria data to calculate the value of B_{12}. The results are presented in Figure 7 together with the available B_{12} data for this system. The smooth values read from Figure 7 are in Table 3.

The length of the vertical lines indicate the range of error of the B_{12} values. The experimental B_{12} values for helium-carbon dioxide from Cottrell and Hamilton[15], Harper and Miller[26], and Pfefferle, Jr., et al.[72] are also plotted in Figure 7. The drawing of the smooth curve was guided by the data and the curvature of the theoretical curves. The B_{12} obtained in this work show an error of ± 5 cc/gm mole. The single value of Harper and Miller at 303.15°K has a quoted error of ± 1.2 cc. At 303.15°K the value of Pfefferle, et al. is 18.9 cc. The three points of Cottrell and Hamilton have errors of ± 3.4, ± 3.0, and ± 6.8 cc at 303.15, 333.15, and 363.15°K, respectively. The values of B_{12} at 303.15°K by Harper and Miller, and Cottrell and Hamilton agree to within 0.8 cc, lending confidence to this datum point. The single point of Edwards and Roseveare[22] at 298°K for B_{12} is -36.07 cc. This point was not included in the considerations.

It can be seen that the LJCL model computes B_{12} values that are higher, and the KIHQ model computes B_{12} values that are lower than the smooth curve, which passes through the upper limits of the B_{12} obtained here. Thus, great weight was given the literature B_{12} values at the higher temperatures and to the theoretical curvature.

B_{12} for the Helium-Argon System

The phase equilibria data for the helium-argon system consist of

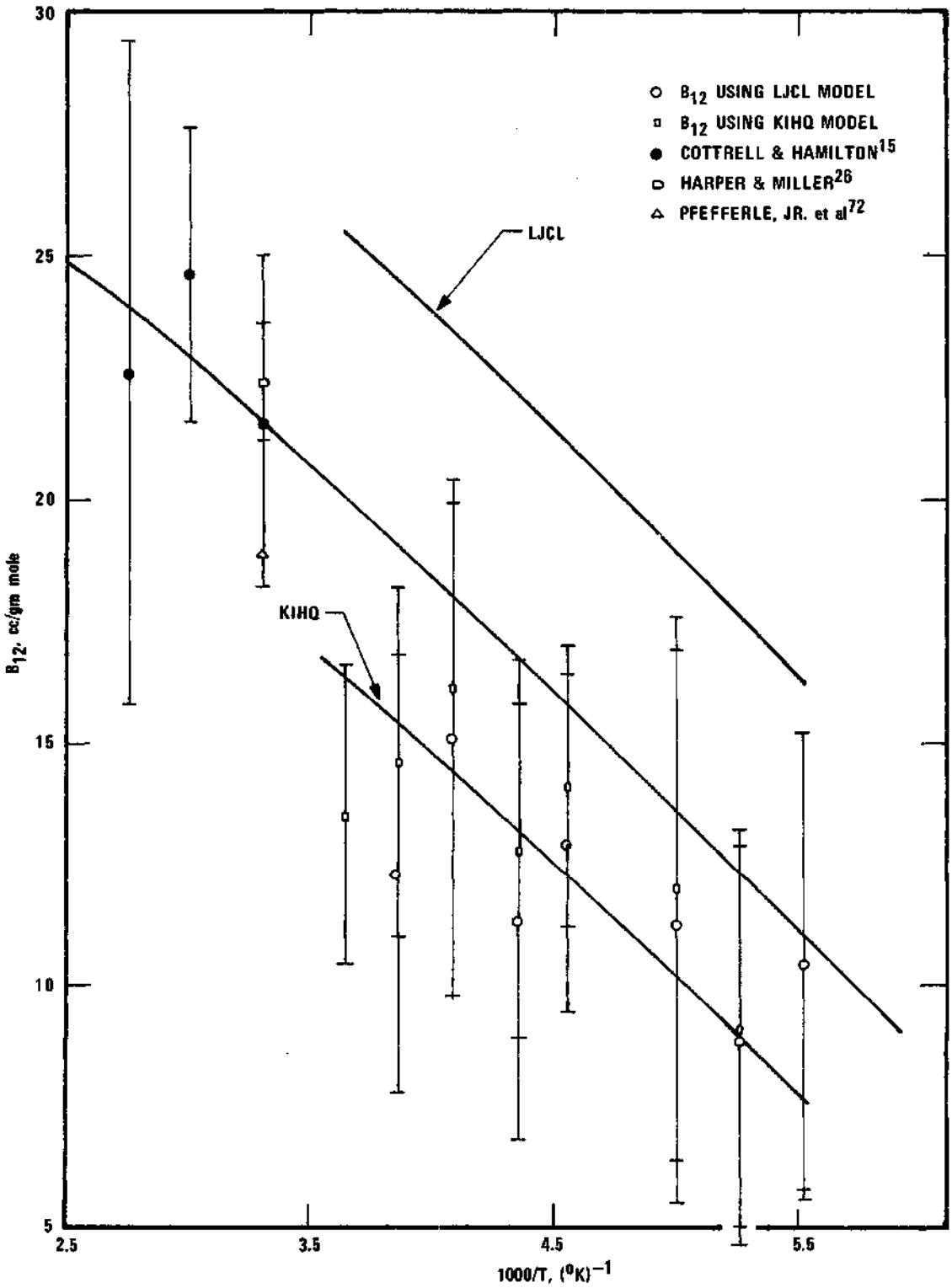

Figure 7. B_{12} for the Helium-Carbon Dioxide System.

Table 3. B_{12} for the Helium-Carbon Dioxide System

$T^{\circ}K$	$1000/T$, $(^{\circ}K)^{-1}$	B_{12}, cc/gm mole
180	5.56	10.9 ± 5
190	5.26	12.3 ± 5
200	5.00	13.5 ± 5
220	4.55	15.7 ± 5
240	4.17	17.6 ± 5
260	3.85	19.1 ± 5
280	3.57	20.4 ± 5
300	3.33	21.5 ± 3.5
350	2.86	23.6 ± 3.5

those of Mulling[64,66], McCain[56], and Sinor and Kurata[86]. McCain measured the dew-points of helium-argon mixtures between 99.74 and 150.62°K. It has been shown[64] that these data appear to be subject to considerable errors, especially at the lower temperatures. Sinor and Kurata measured only the solubility of helium in liquid argon from 93.15 to 148.15°K and from 250 to 2000 psia. Their results are only slightly higher than those of Mullins. The smoothed phase equilibria data of Mullins[64] (Table 26 in Appendix F) were used in this work. He had already computed the B_{12} from his unsmoothed data. The values computed here from the smoothed data are essentially the same as his since the data were quite smooth to begin with. Figure 8 shows the results together with other B_{12} data. The smoothed values from Figure 8 are shown in Table 4.

The other B_{12} data for this system consist of: one point at 90°K by Knobler, et al.[48], which was recomputed by Prausnitz and Myers[77]; six points by Kalfoglou and Miller[36] between 303.15 and 773.15°K. The length of the vertical lines indicates the range of error in the values of B_{12}. No error estimate was quoted for the single point by Knobler, et al. Their value is above that of the present work. But when corrected by Prausnitz and Myers, the point agrees very well with present results. The error in the B_{12} obtained here is ± 2.5 cc. Kalfoglou and Miller quote an error of ± 0.3 cc for their results. The drawing of the smooth curve was guided by the existing data and the theoretical curvature. In the helium-argon system the smooth curve passes through all the points nicely. The smooth curve is higher than the LJCL curve, which is, in turn, higher than the KIH curve.

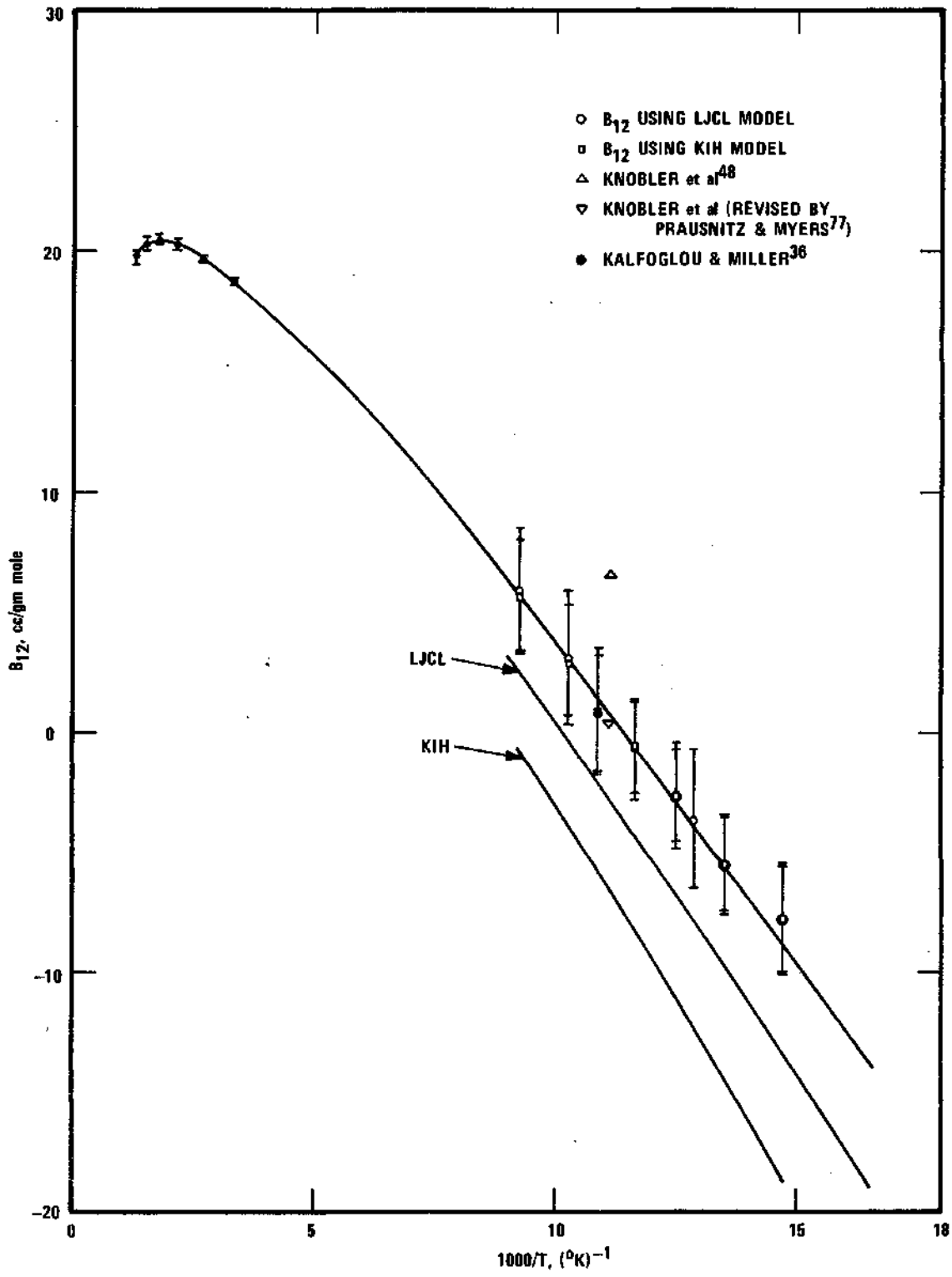

Figure 8. B_{12} for the Helium-Argon System.

Table 4. B_{12} for the Helium-Argon System

T°K	1000/T, $(°K)^{-1}$	B_{12}, cc/gm mole
65	15.39	-10.7 ± 2.5
70	14.29	-7.8 ± 2.5
75	13.33	-5.2 ± 2.5
80	12.50	-2.9 ± 2.5
85	11.77	-1.0 ± 2.5
90	11.11	0.8 ± 2.5
95	10.53	2.4 ± 2.5
100	10.00	3.7 ± 2.5
110	9.09	6.1 ± 2.5
120	8.33	8.0* ± 2.5
130	7.69	9.6* ± 2.5
140	7.14	10.9* ± 2.5
150	6.67	12.1* ± 2.5
160	6.25	13.0* ± 2.5
170	5.88	13.8* ± 2.5
180	5.56	14.5* ± 2.5
190	5.26	15.1* ± 2.5
200	5.00	15.6* ± 2.5
220	4.55	16.4* ± 2.5
240	4.18	17.1* ± 2.5
260	3.85	17.7* ± 2.5
280	3.57	18.2* ± 2.5
300	3.33	18.6 ± 0.3
350	2.86	19.4 ± 0.3
400	2.50	19.9 ± 0.3
450	2.22	20.1 ± 0.3
500	2.00	20.3 ± 0.3
550	1.82	20.4 ± 0.3
600	1.67	20.4 ± 0.3
650	1.54	20.3 ± 0.3
700	1.43	20.1 ± 0.3
750	1.33	19.9 ± 0.3

* Interpolated values

B_{12} for the Helium-Methane System

The phase equilibria data for the helium-methane system consist of the following:

Solid-vapor: Hiza and Kidnay[31] (55 to 87°K up to 140 atm)

Liquid-vapor: Sinor, et al.[87] (93.15 to 188.15°K up to 200 atm)

Heck and Hiza[28] (94.97 to 184.83°K up to 200 atm)

Gonikberg and Fastovskii[25] (90.3 to 106.0°K up to 160 atm)

Kharakhorin[41] (91.1 to 150.3°K up to 170 atm)

The data of Hiza and Kidnay are very smooth, and were selected for use here. The data of Kharakhorin, and Gonikberg and Fastovskii show great scatter. Heck and Hiza have compared these data with their own data with those of Sinor, et al. Below 140°K the gas phase data of Sinor, et al. are consistently higher. Above 140°K the two sets of gas phase data agree well. The liquid phase data of the two groups are in good agreement. The data of both groups were used here. The smoothed data are presented in Table 27 of Appendix F. The results are presented in Figure 9 and the smooth values are in Table 5.

No independently determined values of B_{12} for the helium-methane system are available. Thus, there was no independent guide for the drawing of the smooth curve. The B_{12} obtained from the liquid-vapor data appear to be consistently lower than those from the solid-vapor data. The points in the solid-vapor region follow the curvature of the theoretical curves quite well, and the smooth curve was drawn accordingly. In the higher temperature region the smooth curve was drawn through the points, even though the resultant curvature is at odds with the theoretical curves.

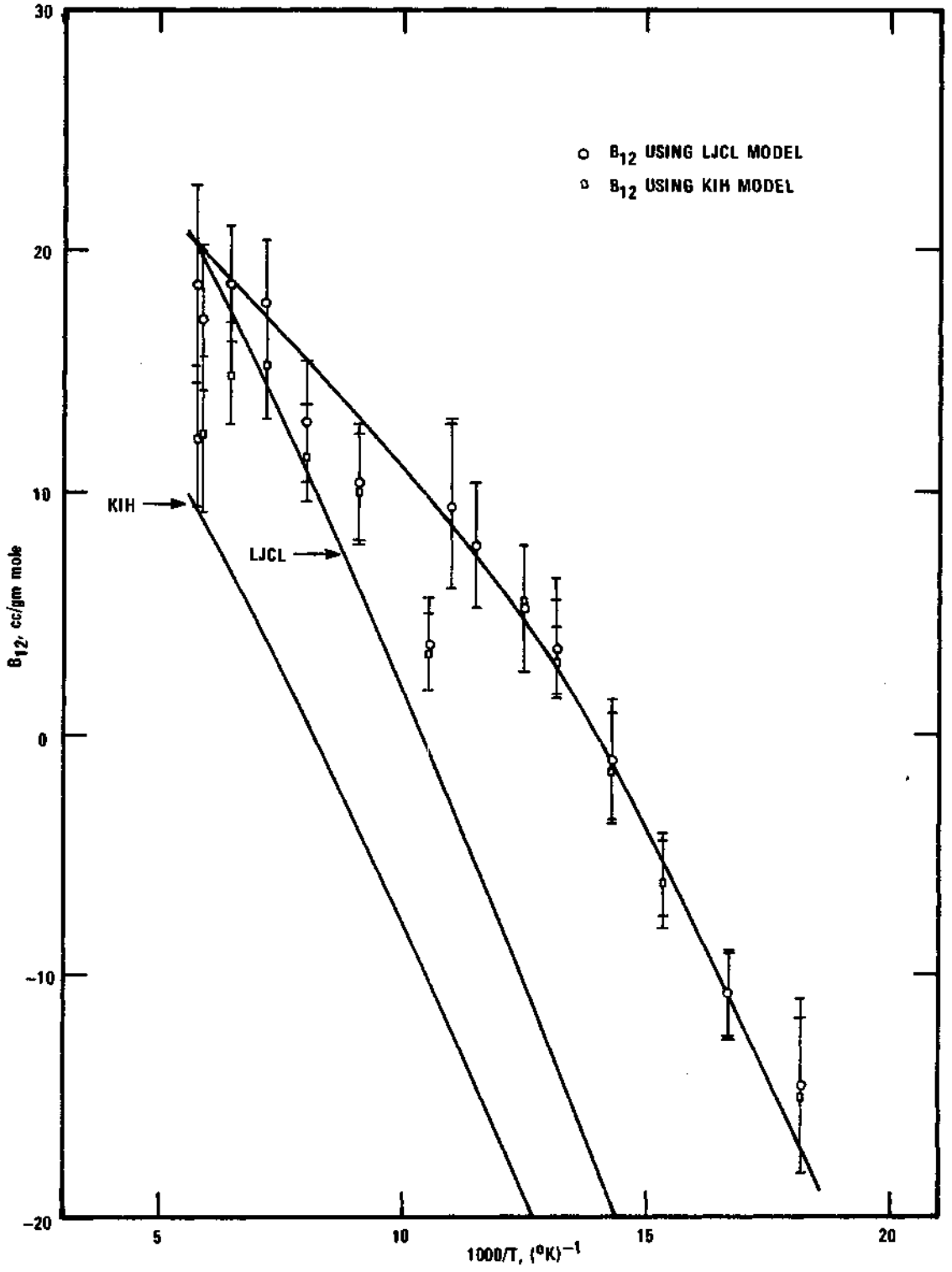

Figure 9. B_{12} for the Helium-Methane System.

Table 5. B_{12} for the Helium-Methane System

$T^{\circ}K$	$1000/T$, $(^{\circ}K)^{-1}$	B_{12}, cc/gm mole
55	18.18	-17.3 ± 3
60	16.67	-11.0 ± 3
65	15.39	-5.5 ± 3
70	14.29	-1.2 ± 3
75	13.33	2.0 ± 3
80	12.50	4.6 ± 3
85	11.77	6.6 ± 3
90	11.11	8.3 ± 3
95	10.53	9.7 ± 3
100	10.00	10.9 ± 3
110	9.09	12.9 ± 3
120	8.33	14.6 ± 3
130	7.69	16.0 ± 3
140	7.14	17.2 ± 3
150	6.67	18.2 ± 3
160	6.25	19.1 ± 3
170	5.88	19.9 ± 3
180	5.56	20.6 ± 3

The average error, as indicated by the length of the vertical lines, is ± 3 cc. The theoretical LJCL and KIH curves are again below the smooth curve, with the LJCL curve higher than the KIH curve.

B_{12} for the Helium-Nitrogen System

The phase equilibria data for the helium-nitrogen system consist of the following in the liquid-vapor region:

Buzyna, et al.[8] (77.23 to 122.82°K up to 67.8 atm)

DeVaney, et al.[18] (77 to 120°K up to 136 atm)

Fedoritenko and Ruhemann[24] (64 to 108°K up to 150 atm)

Kharakhorin[42] (68 to 111.5°K up to 214.5 atm)

Rodewald, et al.[80] (64.9 to 77.2°K up to 68 atm)

In the solid-vapor region there are the data of Dokoupil[20] between 35 and 65°K and from 5 to 10 atmospheres. His data show large scatter and were not used here.

The data of Buzyna, et al. are few and show great scatter. The data of DeVaney, et al. are scattered below 90°K and 50 atm, but are otherwise smooth. Fedoritenko and Ruhemann presented their results graphically, which is inadequate for accurate readings. The helium-nitrogen data of Kharakhorin, as in his data for the helium-methane[41] system, show extreme scatter. The data of Rodewald, et al. are not extensive and are quite smooth. Table 6 shows the Enhancement Factor at 60 atm and a nominal temperature of 77°K from these data sources.

While the results in Table 6 do not show the scatter within the different sets of data, they show the range of agreement of the different sets of data. The data of DeVaney, et al. and Rodewald, et al. were used in this work. The smoothed values of these data are in Table 28 of

Table 6. Enhancement Factor of Nitrogen in Helium at 60 atm and 77°K

Source	Temperature, °K	ϕ
Buzyna et al.[8]	77.23	1.65
DeVaney et al.[18]	77	1.38
Fedoritenko & Ruhemann[24]	78	1.39
Kharakhorin[42]	77.3	1.20
Rodewald et al.[80]	77.2	1.43

Appendix F. The B_{12} obtained are shown in Figure 10, together with other B_{12} data. The smoothed values are shown in Table 7.

The one point at 90°K byKnobler, et al.[48] is higher than the results obtained here. When it is corrected by Prausnitz and Myers[77] it falls below the present results by about the same amount. Canfield, et al.[9] have measured the B_{12} of helium-nitrogen from 133.15 to 273.15°K. Witonsky and Miller[107] measured the B_{12} from 448.15 to 748.15°K, with a quoted accuracy of ± 0.19 to 0.42 cc. The results of Ku and Dodge[51] are at 311.7 and 373.2°K. Kramer and Miller[50] give one value at 303.15°K.

The one B_{12} value of Pfefferle, Jr., et al.[72] at 303.15°K is slightly lower than the other data. At 298°K Edwards and Roseveare[22] report a B_{12} of 12.55 cc, much lower than the other data. Van Itterbeek and Van Doninck[99] have measured the second virial coefficients of helium, nitrogen, and helium-nitrogen with the velocity of sound technique. Their pure virial coefficients were much in error and so were the interaction virial coefficients.

Again, the length of the vertical lines indicates the range of error. The error in this work is ± 2.5 cc. The smooth curve was drawn with more weight given to the data of Canfield, et al., and the theoretical curvature. The smooth curve lies below the B_{12} obtained in the higher temperature region of the phase equilibria data, but passes through the low temperature region nicely.

K. R. Hull[35] has recently measured the B_{12} of helium-nitrogen at -160 and -170°C. His values are 11.26 and 10.90 cc, respectively. The first point almost falls exactly on the smooth curve while the second point is about 1.6 cc above the smooth curve.

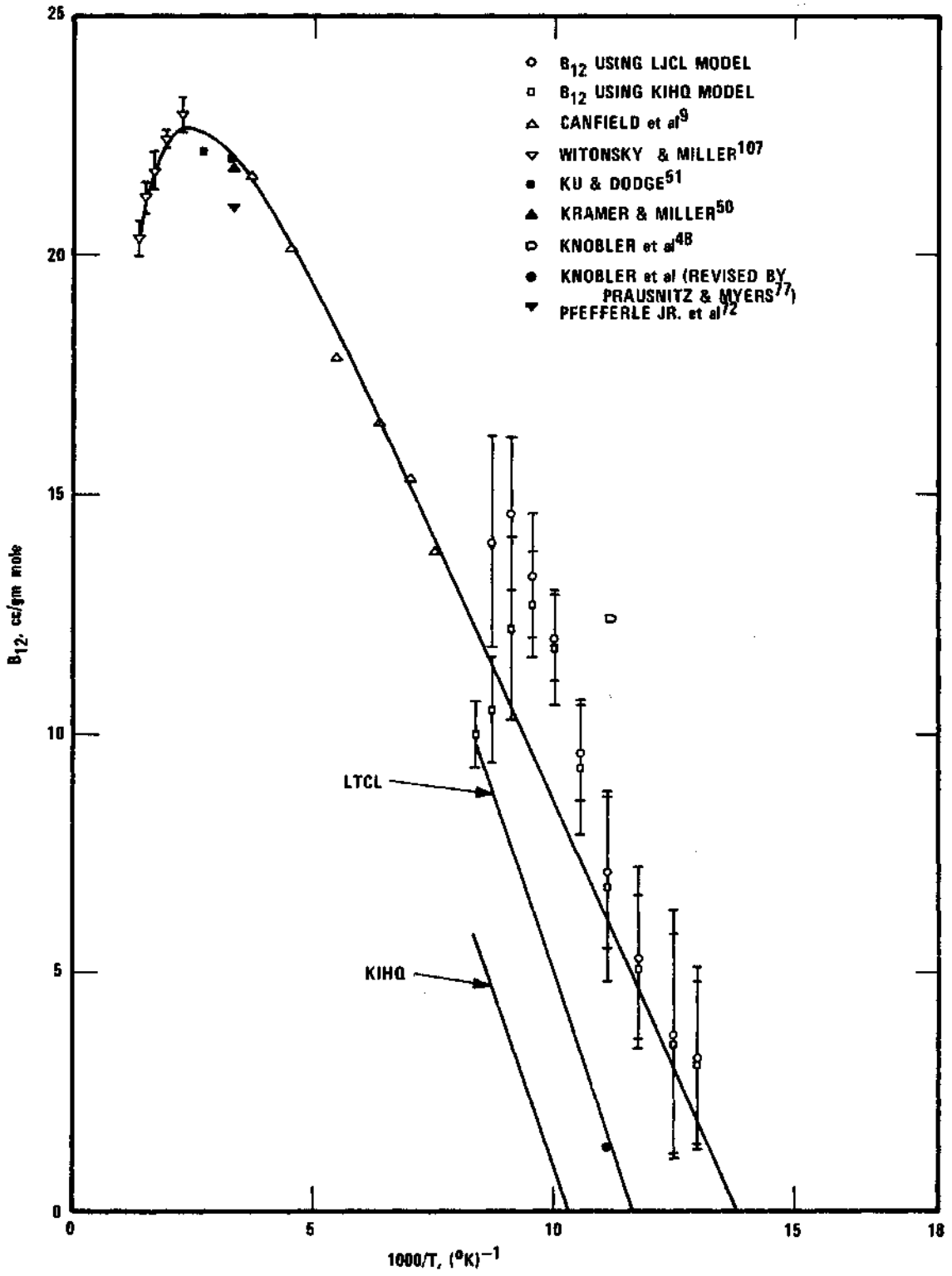

Figure 10. B_{12} for the Helium-Nitrogen System.

Table 7. B_{12} for the Helium-Nitrogen System

$T^{\circ}K$	$1000/T$, $(^{\circ}K)^{-1}$	B_{12}, cc/gm mole
75	13.33	1.2 ± 2.5
80	12.50	3.0 ± 2.5
85	11.77	4.6 ± 2.5
90	11.11	6.1 ± 2.5
95	10.53	7.4 ± 2.5
100	10.00	8.5 ± 2.5
110	9.09	10.6 ± 2.5
120	8.33	12.3 ± 2.5
130	7.69	13.7 ± 2.5
140	7.14	14.9 ± 2.5
150	6.67	15.9 ± 2.5
160	6.25	16.8 ± 2.5
170	5.88	17.5 ± 2.5
180	5.56	18.2 ± 2.5
190	5.26	18.8 ± 2.5
200	5.00	19.3 ± 2.5
220	4.55	20.1 ± 2.5
240	4.17	20.7 ± 2.5
260	3.85	21.3 ± 2.5
280	3.57	21.8 ± 2.5
300	3.33	22.1 ± 2.5
350	2.86	22.5 ± 2.5
400	2.50	22.7 ± 2.5
450	2.22	22.7 ± 0.4
500	2.00	22.5 ± 0.4
550	1.82	22.2 ± 0.4
600	1.67	21.8 ± 0.4
650	1.54	21.4 ± 0.4
700	1.43	20.9 ± 0.4
750	1.33	20.3 ± 0.4

Again, the smooth curve is above the LJCL curve which is in turn above the KIHQ curve.

B_{12} for the Helium-Oxygen System

Barrick and Herring[5] have measured the liquid-vapor equilibrium of the helium-oxygen system from 69.9 to 149.91°K and up to 200 atm. Sinor and Kurata[86] have measured the solubility of helium in liquid oxygen from 77.35 to 143.15°K and up to 2000 psia. The data of these groups agree very well. No other phase equilibria data are available for this system. The data of Barrick and Herring were used here. The smoothed values are presented in Table 29 of Appendix F.

Figure 11 shows the results, and the smooth values are shown in Table 8. Also shown in Figure 11 is the only other B_{12} data point available. It is the point at 90°K of Knobler, et al.[48] It is lower than the smooth curve by 2.4 cc. When corrected by Prausnitz and Myers[77] it becomes even lower, by about 17.2 cc. Van Itterbeek and Van Doninck[99] have measured the second virial coefficients of helium, oxygen, and helium-oxygen mixture with the velocity of sound technique. Their pure virial coefficients were much in error, as also were their interaction virial coefficients. The LJCL curve is in excellent agreement with the results; hence, it is chosen to represent the smooth curve. As in all the other systems, the KIH curve is below that computed by the LJCL model.

Since the LJCL curve is used to represent the smooth curve, the least-squares fitting of the smooth values in Table 8 to the Lennard-Jones (6-12) parameters yields the same values as given by the LJCL model.

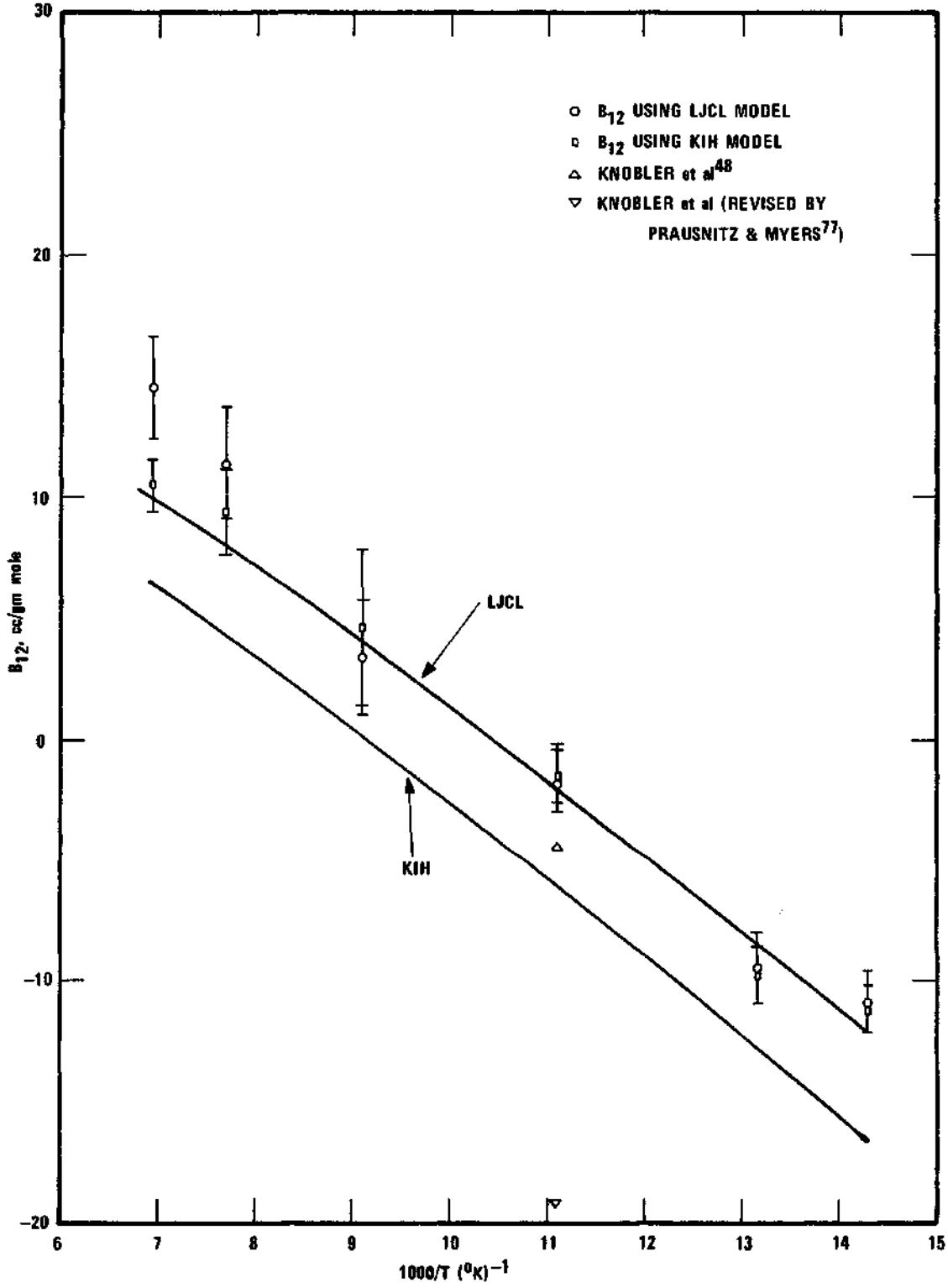

Figure 11. B_{12} for the Helium-Oxygen System.

Table 8. B_{12} for the Helium-Oxygen System

$T^{\circ}K$	$1000/T$, $(^{\circ}K)^{-1}$	B_{12}, cc/gm mole
70	14.29	-12.1 ± 2.5
75	13.33	-8.9 ± 2.5
80	12.50	-6.3 ± 2.5
85	11.77	-4.0 ± 2.5
90	11.11	-2.0 ± 2.5
95	10.53	-0.2 ± 2.5
100	10.00	1.3 ± 2.5
110	9.09	4.1 ± 2.5
120	8.33	6.3 ± 2.5
130	7.69	8.0 ± 2.5
140	7.14	9.5 ± 2.5
150	6.67	10.7 ± 2.5

Least-Squares Fitting of B_{12} to Lennard-Jones (6-12) Parameters

The B_{12} data for the helium-carbon dioxide, -argon, -methane, -nitrogen, and -oxygen systems in Tables 3, 4, 5, 7, and 8, were least-squares fitted (by a procedure worked out by Ziegler and Mullins[108]) to the Lennard-Jones (6-12) parameters for the classical potential function. Three cases were considered:

(i) Both $(e/k)_{12}$ and $(b_o)_{12}$ allowed to vary to fit the B_{12} data

(ii) With $(e/k)_{12}$ fixed at the geometric average, $(b_o)_{12}$ allowed to vary to fit the B_{12} data

(iii) With $(b_o)_{12}$ fixed at the Lorentz average, $(e/k)_{12}$ allowed to vary to fit the B_{12} data.

The data were divided into two groups. One group consisted of only data below 300°K. The other consisted of all the data. The parameters which resulted from a fit of the data below 300°K are presented in Table 9. The point by point fit for the systems is given in Tables 31 through 35 in Appendix H. The parameters resulting from a fit of all the B_{12} data are shown in Table 36 in Appendix H.

In order to compare the parameters in Table 9 with those given by the combination rules of Equations (IV-19) and (IV-21), the following relations are defined:

$$\alpha \equiv \frac{(e/k)_{12} \text{ (from } B_{12} \text{ data)}}{\left[(e/k)_1 (e/k)_2\right]^{1/2}} \tag{V-2}$$

$$\beta \equiv \frac{(b_o)_{12} \text{ (from } B_{12} \text{ data)}}{\frac{1}{8}\left[(b_o)_1^{1/3} + (b_o)_2^{1/3}\right]^3} \tag{V-3}$$

Table 9. Least-Squares Fit of B_{12} to LJCL (6-12) Parameters ($T \leq 300^{\circ}K$)

	Case (i)		Case (ii)[a]		Case (iii)[b]	
System	$(e/k)_{12}$ $^{\circ}K$	$(b_o)_{12}$ cc/gm mole	$(e/k)_{12}$ $^{\circ}K$	$(b_o)_{12}$ cc/gm mole	$(e/k)_{12}$ $^{\circ}K$	$(b_o)_{12}$ cc/gm mole
He-CO_2	38.898	52.95	34.960	47.33	42.873	62.31
He-Ar	25.523	38.13	28.815	37.66*	24.287	35.06
He-CH_4	21.595	50.61	28.216	32.40*	21.896*	60.66
He-N_2	21.564	43.08	25.093	47.17*	21.917	44.58
He-O_2	27.959	38.87	27.920	38.92	27.960	38.83

[a] $(e/k)_{12}$ computed from geometric average using e/k parameters from Table 15

[b] $(b_o)_{12}$ computed from Lorentz average using b_o parameters from Table 15

* Fit of some points outside of error of input data

Values for α and β are shown in Table 10.

It can be seen from Table 10 that a better fit for the interaction second virial coefficient is obtained by an adjustment of the energy parameter (e/k) than by an adjustment of the volume parameter, b_o. The values of α in Table 10 for case (i) and case (iii) are quite close. This indicates that the use of the Lorentz average combination rule (Equation(IV-21)) for b_o is a more valid one than the geometric mean combination rule (Equation (IV-19)) for (e/k). The B_{12} data are fitted better in case (iii) than in case (ii). Thus, the parameters obtained for case (iii) were used in the LJCLA model for calculating the Enhancement Factor.

The least-squares fitting of the second virial coefficient to the Kihara core model is more complicated than for the Lennard-Jones (6-12) model. This is because the shape parameters of the convex cores must be determined. Because of this added complication the least-squares fit of the B_{12} data with the Kihara core model was not attempted. In retrospect, rigor could perhaps have been profitably traded for results by adopting the method used by Mullins[64], and Hiza and Duncan[30], of arbitrarily adjusting (U/k) to fit the B_{12} data.

Recently, Hiza and Duncan[30] developed a correction factor k_{12} for the geometric average combination rule of the Kihara core model. Their k_{12} is equivalent in form to $(1-\alpha)$, where α (defined by Equation (V-2)) is the correction factor derived here for the geometric average combination rule for the Lennard-Jones (6-12) model. Hiza and Duncan took a different approach in the determination of their correction factor. They obtained the B_{12} from phase equilibria data directly by a

Table 10. Ratio of Least-Squares Fitted Interaction LJCL (6-12) Parameters to those Given by Combination Rules ($T \leq 300^{\circ}K$)

System	Case (i)		Case (ii)		Case (iii)	
	α**	β**	α	β	α	β
He-CO_2	1.113	0.850	1.0	0.760	1.226	1.0
He-Ar	0.886	1.088	1.0	1.074*	0.878	1.0
He-CH_4	0.765	0.834	1.0	0.534*	0.776*	1.0
He-N_2	0.859	0.966	1.0	1.058*	0.873	1.0
He-O_2	1.000	1.000	1.0	1.000	1.000	1.0

* Fit of some points outside of error of input data. See Tables 31 to 35 in Appendix H

** Defined by Equations (V-2) and (V-3)

least-squares fit of the experimental Enhancement Factor data with the Enhancement Factor equation. They obtained k_{12} by adjusting the energy parameter in the Kihara core model to fit the B_{12}. Their k_{12} values for the helium-methane, -argon, and -nitrogen systems are 0.40, 0.22 (from Mullins[64]), and 0.25, respectively. The equivalent $(1-\alpha)$ values obtained in this work (Table 10, case iii) for the same systems are 0.224, 0.122, and 0.127, respectively. It is interesting to note that the k_{12} values are nearly twice as large as the $(1-\alpha)$ values. This difference in the correction factors are probably due to the difference in the models for which the factors were derived. They were able to correlate their k_{12} values with ionization potentials of the molecules. However, the equivalent $(1-\alpha)$ values derived here did not fit their correlation. It is also interesting that the $(1-\alpha)$ value for helium-carbon dioxide is negative. This is contrary to their assumption that k_{12} should always be positive. Thus, it seems that such correlation factors may not be universally true but tend to be specific to the models for which they were derived. However, the idea of the correlation of the correction factors for a given model becomes more attractive as more systems are analyzed in this manner.

CHAPTER VI

COMPARISON OF EXPERIMENTAL AND PREDICTED ENHANCEMENT FACTORS

Theoretical Enhancement Factors for the helium-carbon dioxide, -argon, -methane, -nitrogen, and -oxygen system have been calculated with the LJCL, KIH, KIHQ, and LJCLA models (see Chapter IV). The detailed results are presented in Tables 25 through 29 in Appendix F. Figures 12 through 16 show the Enhancement Factor at a low and high temperature for each system. They are representative of the overall results. Also shown for comparison are the experimental Enhancement Factors.

For all the systems, the KIH and KIHQ models predict a larger Enhancement Factor than the LJCL model, which in turn predicts a larger Enhancement Factor than the LJCLA model. This follows from the way the interaction second virial coefficient compares for the four models. Since the models predict the pure second virial coefficients well, it is the B_{12} which is not being predicted correctly. In Chapter V it was shown that the LJCL model calculated a B_{12} that was greater than that calculated by the KIH and KIHQ models. Since B_{12} contributes negatively to the Enhancement Factor, the KIH and KIHQ model Enhancement Factors are greater than the LJCL value. For the same reason, the LJCLA model Enhancement Factor is smaller than that of the LJCL model. However, the helium-carbon dioxide system (Figure 12) is an exception to the preceding considerations. In this system, the LJCLA model Enhance-

ment Factor lies between the KIHQ and LJCL model results. But this is consistent with the fact that the LJCLA model B_{12} lies between the values predicted by the LJCL and KIHQ models, as is shown in Figure 7 of Chapter V.

It is interesting to note that the Enhancement Factor for the helium-carbon dioxide system increases with increasing temperature. This trend is the reverse of the trend for the other helium systems, in which the Enhancement Factor decreases with increasing temperature. Figure 12 shows that the theoretical calculations predict the observed trend of the Enhancement Factor for the helium-carbon dioxide system. The contributions of the various terms in Equation (IV-9) were examined for all the systems for a possible explanation. It was found that no single term by itself could have indicated the unusual behavior of the helium-carbon dioxide system. It is the combination of the relative sizes of the various terms that is important. However, some interesting things are revealed by the detailed examination of the contributions arising from these several terms. One is that the y_2B_{12} term for the helium-carbon dioxide system compared with those for the other systems was relatively insensitive to temperature changes. This observation by itself does not indicate the temperature dependence of the Enhancement Factor. Indeed, y_2 is obtained only after the Enhancement Factor has been calculated. Another interesting feature of the helium-carbon dioxide system is that the B_{12} for this system is positive and greater than the B_{12} for theother systems. This feature would lead one to suspect that the Enhancement Factor for the helium-carbon dioxide system would be smaller than for the other helium systems. But it would not

indicate whether the Enhancement Factor would increase with increasing temperature. Although there does not appear to be an a priori reason for the unusual behavior of the Enhancement Factor for the helium-carbon dioxide system, the theoretical models are able to predict the behavior. This is an encouraging and interesting property of these models.

The isotherms for the helium-carbon dioxide system are shown in Figure 12. The experimental 181.05°K isotherm in the solid-vapor region was measured in this work, while the 274.9°K isotherm in the liquid-vapor region is that of Barrick, et al.[4] At 181.05°K the LJCL model is consistently lower, while the KIHQ model is consistently higher than the experimental results. At 120 atmospheres the LJCL model is low by 9 per cent and the KIH model high by 4 per cent. These are not great disagreements considering the fact that the experimental results are about ± 3 per cent in error. The agreement between the LJCLA model and the experimental results is almost quantitative for the 181.05°K isotherm. At 120 atmospheres the LJCLA model is about 1 per cent high. At 274.9°K all the three models are low with respect to the experimental Enhancement Factor. The LJCL and LJCLA models show a maximum at 110 and 135 atmospheres, respectively. This maximum is absent from the experimental results. The KIHQ model also shows a maximum, but at the higher pressure at 190 atmospheres. At the higher pressures, the influence of the third virial coefficient becomes important and probably accounts in part for the maximum in the theoretical curve. At 274.9°K the agreement between the KIHQ model and experimental results is the best. At 180 atmospheres the KIHQ model is low by 7 per cent,

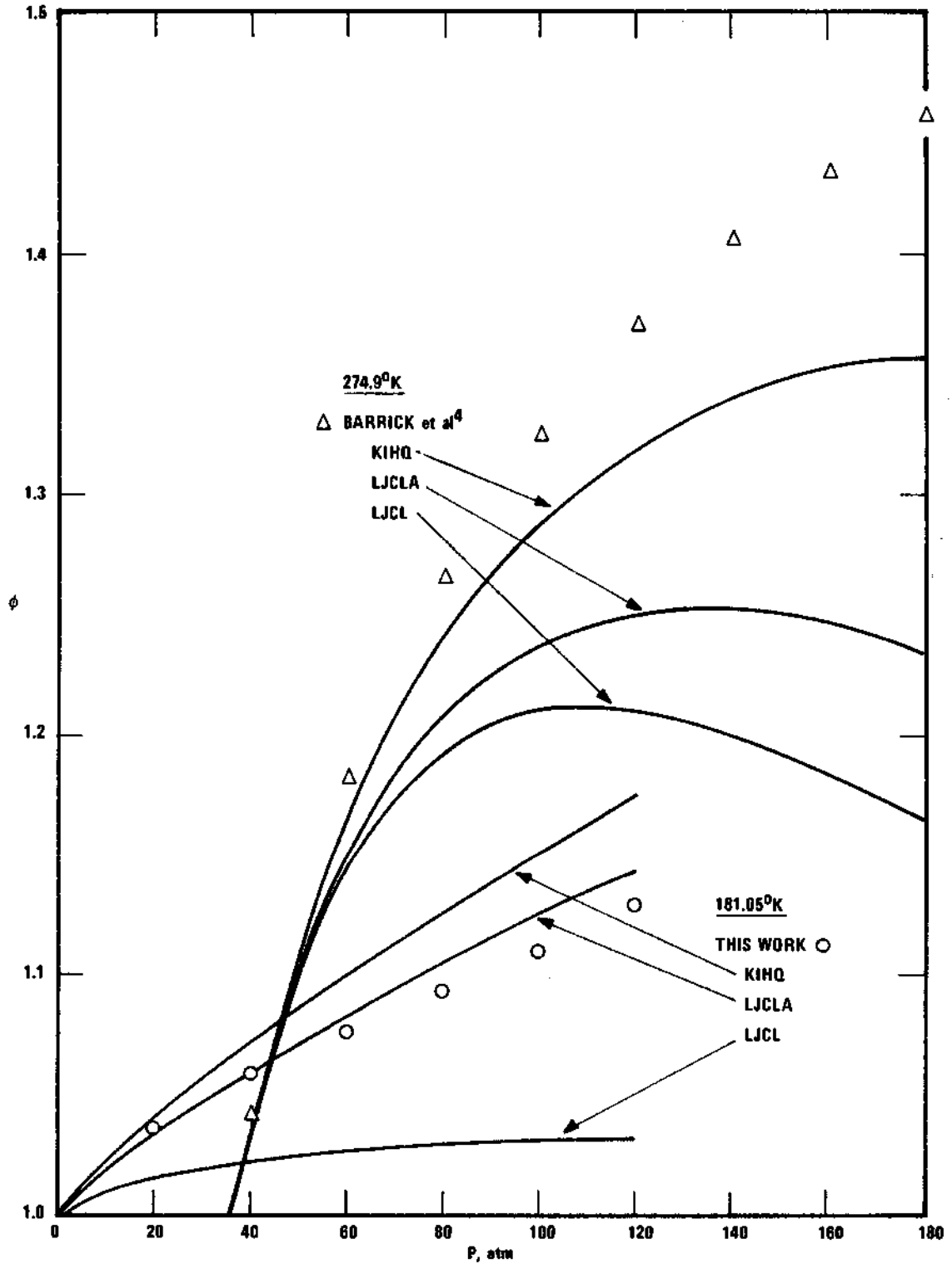

Figure 12. Theoretical and Experimental Enhancement Factors in the Helium-Carbon Dioxide System.

the LJCLA model is low by 15 per cent, and the LJCL model is low by 20 per cent. Thus, in the helium-carbon dioxide system the KIHQ model is better than the LJCL model, especially at the higher temperature. At lower temperatures, the LJCLA model is better, although its improvement over the KIHQ model is slight.

Figure 13 shows the 68.07°K isotherm in the solid-vapor region and the 108.02°K isotherm in the liquid-vapor region for the helium-argon system. The experimental results are those of Mullins[64]. The general order of the theoretical curves with respect to each other and to the experimental results corresponds to the order existing in the interaction second virial coefficient. At 68.07°K and 120 atmospheres the KIH, LJCL, and LJCLA models predict Enhancement Factors which are higher than the experimental value by 55, 31, and 7 per cent, respectively. At 108.02°K and 120 atmospheres, the corresponding figures are 26, 13, and 3 per cent, respectively. In the helium-argon system the LJCLA model is to be recommended for predicting the Enhancement Factor.

The results for the helium-methane system are shown in Figure 14. Also shown are the experimental results at 60°K of Hiza and Kidnay[31] in the solid-vapor region. The 188.15°K experimental isotherm in the liquid-vapor region is that of Sinor, et al.[87] At 60°K and 130 atmospheres, the KIH and LJCL models predict Enhancement Factors which are nearly 3 and 2.25 times the experimental value, while the LJCLA model essentially reproduces the experimental results. At 188.15°K all the three models are inadequate. The KIH, LJCL, and LJCLA models predict Enhancement Factors at 130 atmospheres which are 23, 32, and 37 per cent lowerthan the experimental values, respectively. The LJCLA model does

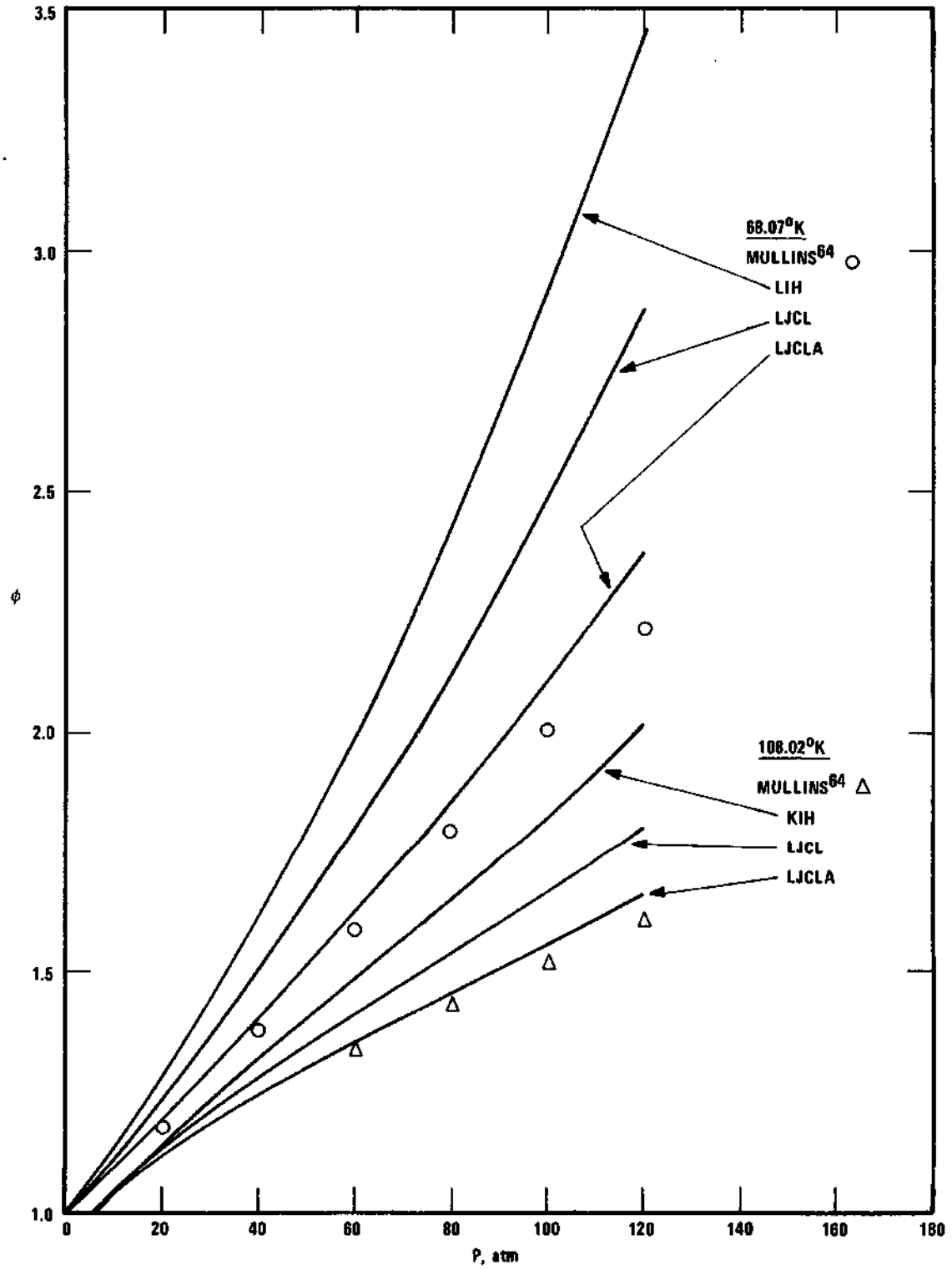

Figure 13. Theoretical and Experimental Enhancement Factors in the Helium-Argon System.

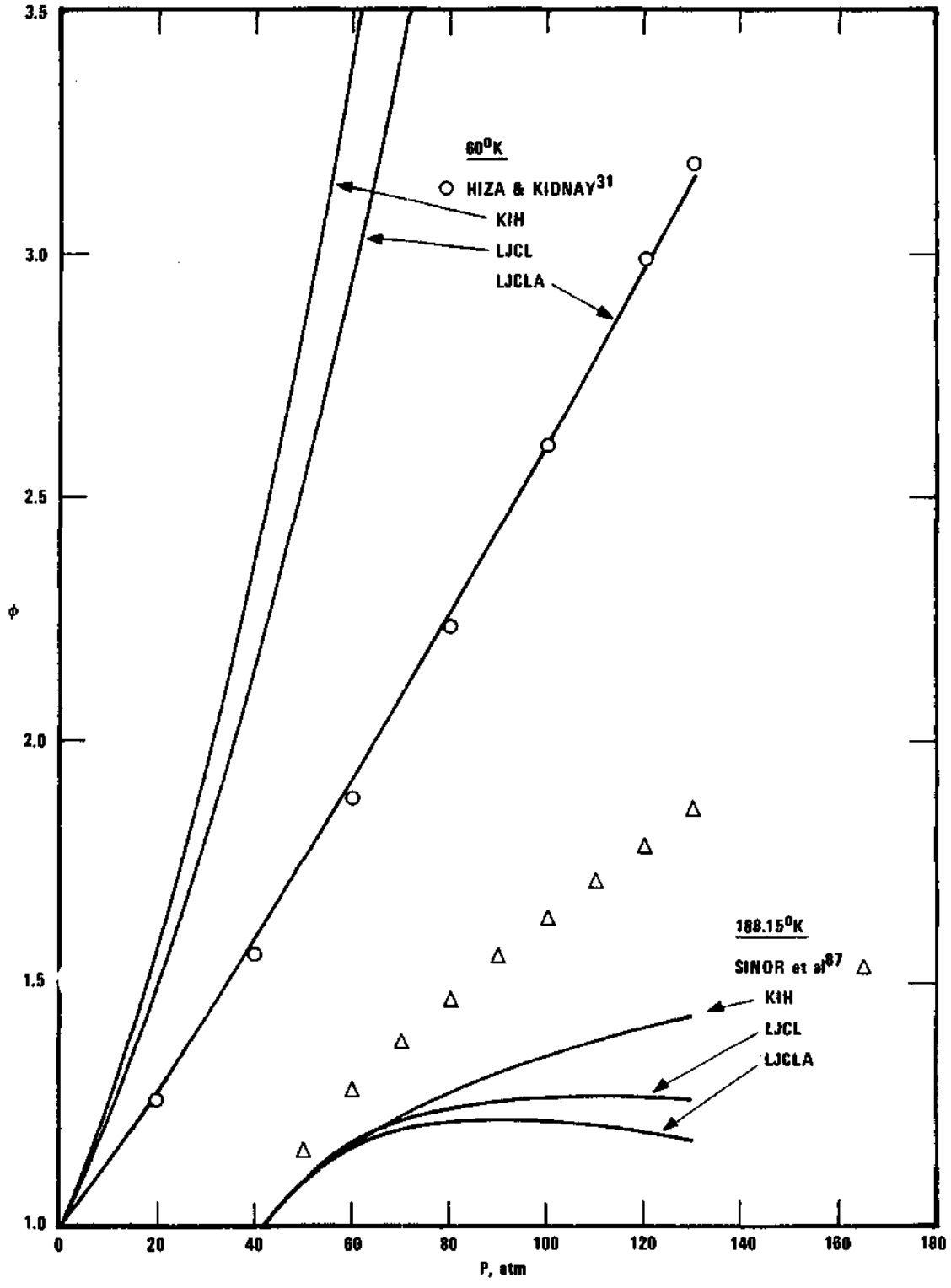

Figure 14. Theoretical and Experimental Enhancement Factors in the Helium-Methane System.

poorly in the liquid-vapor region, but does very well in the solid-vapor region. In the liquid-vapor region up to about 155°K the LJCL model is to be recommended. Above 155°K the KIH model gives slightly better results.

Figure 15 shows the results for the helium-nitrogen system. The experimental isotherms are the 77 and 100°K isotherms of DeVaney, et al.[18] Above 100°K and at the higher pressures, the volumes of the gas phase does not converge and the computations fail. At 77°K and 140 atmospheres, the KIHQ, LJCL, and LJCLA models predict Enhancement Factors which are 63, 35, and 10 per cent higher than the experimental values, respectively. At 100°K and 140 atmospheres, the corresponding figures are 52, 22, and 4 per cent, respectively. However, the LJCLA model at 100°K does better at the higher pressures in comparison to its performance at the lower pressures. In the helium-nitrogen system the LJCLA model gives better results than the KIHQ and LJCL models.

Figure 16 shows the results for the helium-oxygen system. Experimental isotherms in the liquid-vapor region at 69.9 and 129.95°K shown are those of Barrick and Herring[5]. Above 129.95°K and at higher pressures the models calculate non-convergent gas phase volumes. In this system the LJCL and LJCLA models were assumed to be identical. At 69.9°K and 200 atmospheres the KIH and LJCL models predict Enhancement Factors which are 41 and 12 per cent higher, respectively, than the experimental values. At 129.95°K the LJCL model predicts almost exactly the experimental results. The Enhancement Factor predicted by the KIH model at this temperature is consistently higher than the observed values, and at 180 atmospheres is higher by 16 per cent. In the helium-oxygen

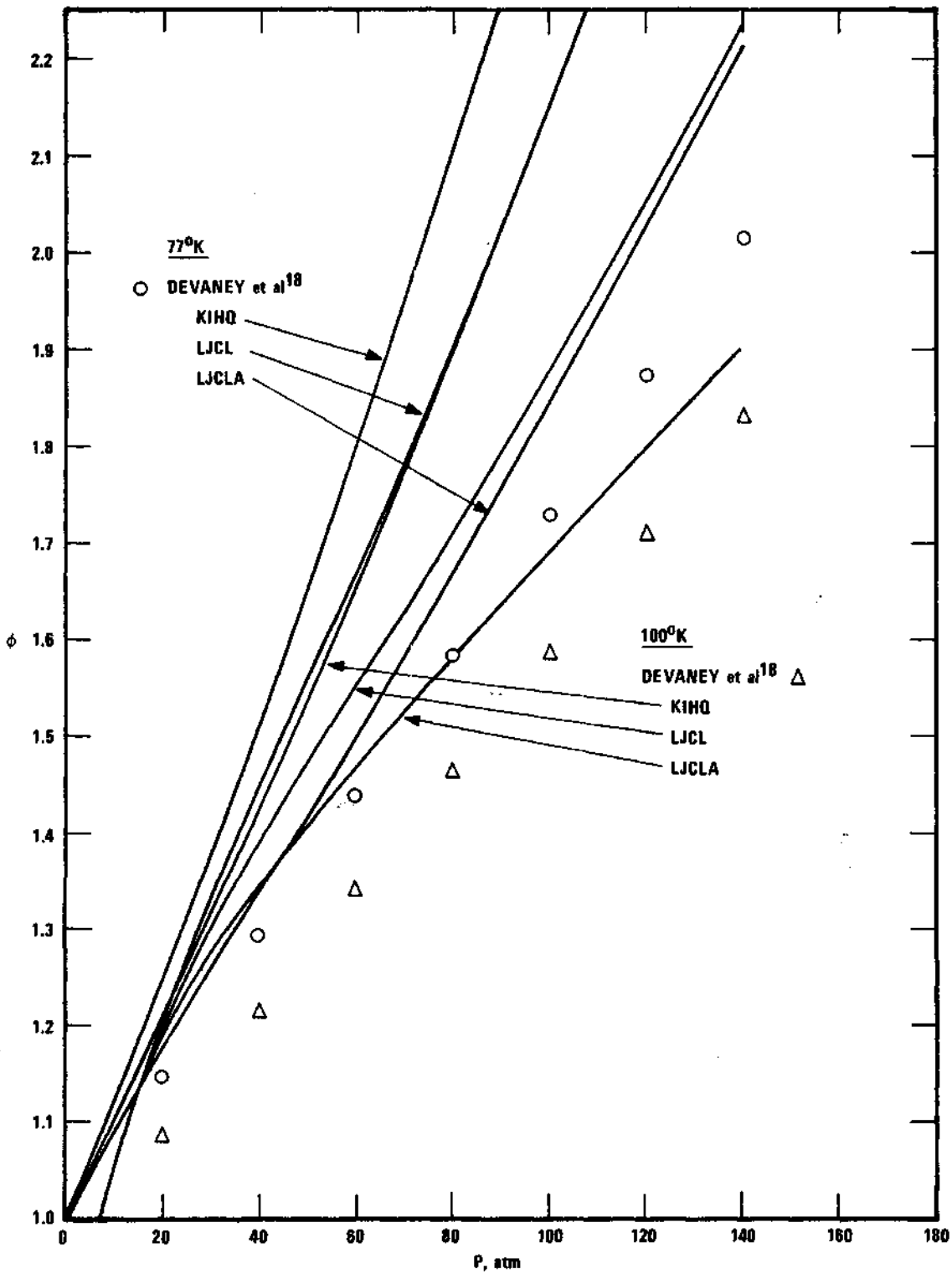

Figure 15. Theoretical and Experimental Enhancement Factors in the Helium-Nitrogen System.

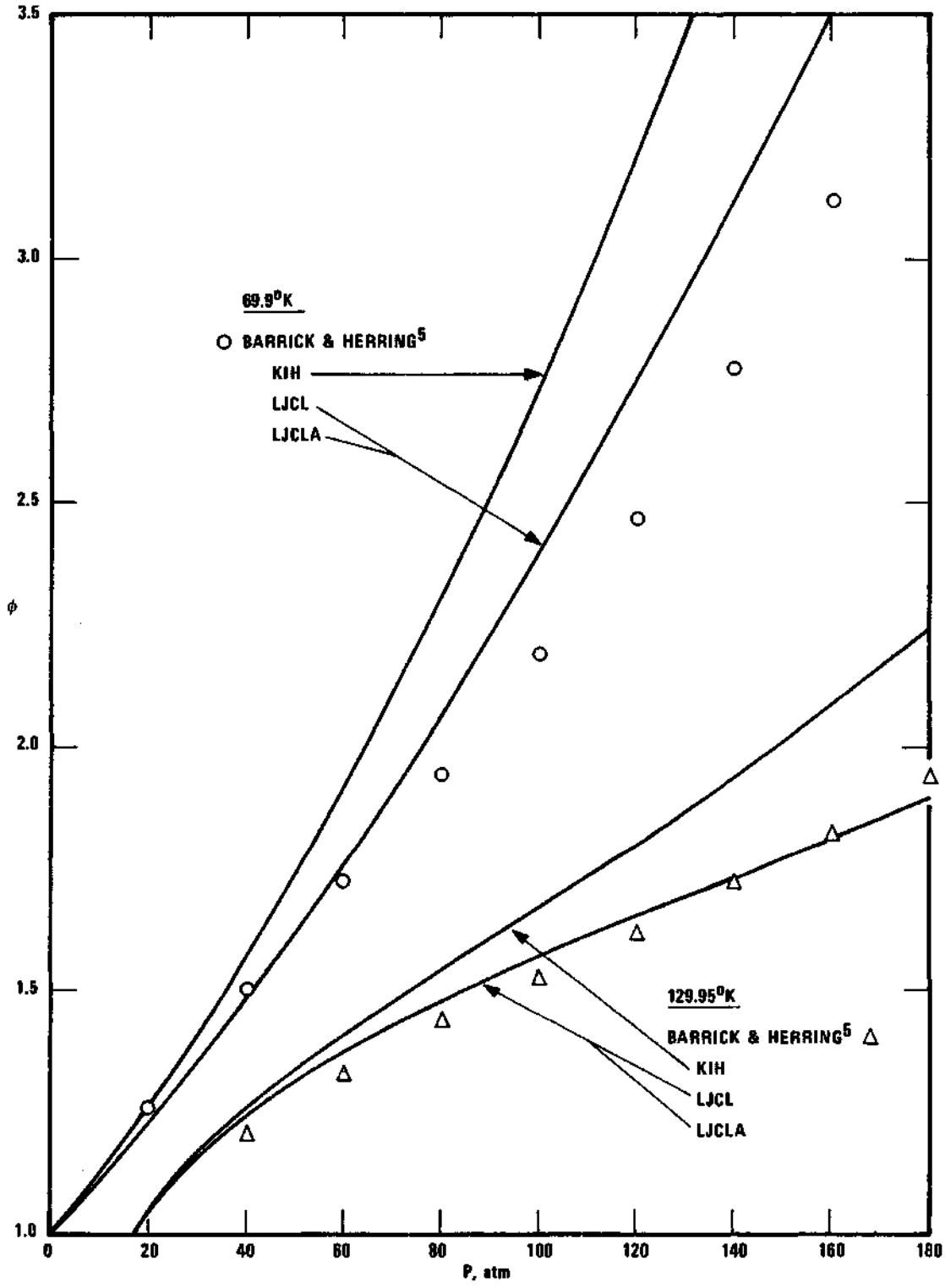

Figure 16. Theoretical and Experimental Enhancement Factors in the Helium-Oxygen System.

system the LJCL and LJCLA models are identical because the B_{12} is adequately represented by the LJCL model. Thus, the LJCL model is recommended for the prediction of the Enhancement Factor in this system. Using the LJCL model, the Enhancement Factor for the helium-oxygen system has been calculated at 5 degrees and 20 atmospheres from 60 to 135^{o}K and up to 200 atmospheres. The results are presented in Table 30 in Appendix G.

It may be concluded from the Enhancement Factor calculations that none of the models examined here are consistently accurate for predicting the Enhancement Factor over all the temperature and pressure ranges. An exception is the LJCL model for the helium-oxygen system, in which the predicted and experimental Enhancement Factors were in close agreement. It can also be concluded that a model which can predict B_{12} accurately is a first step toward the building of improved models. The models presented in this work seems to be of use mainly in semi-quantitative calculations of the Enhancement Factor.

CHAPTER VII

CONCLUSIONS AND RECOMMENDATIONS

Conclusions

The solid-vapor equilibrium for the helium-carbon dioxide system has been studied experimentally at 181.05, 190.03, and 199.95°K and at pressures up to 120 atmospheres. The vapor composition in the liquid-vapor equilibrium region at 220.31°K has been measured from 80 to 140 atmospheres. The Enhancement Factors computed from these data are estimated to be accurate to ± 3 per cent. The gas phase compositions for the 190.03°K isotherm agree well with the 190°K isotherm of Ewald[23], while the 220.31°K results also agree well with the data of Barrick, et al[4] at 219.9°K.

The interaction second virial coefficient, B_{12}, has been extracted from the above phase equilibria data and from other available phase equilibria data for the helium-carbon dioxide, as well as for the helium-argon, helium-methane, helium-nitrogen, and helium-oxygen systems. The virial equation of state up to the third virial coefficient was used to represent the gas phase. The potential functions used to calculate the second virial coefficient were the Lennard-Jones (6-12) and Kihara core models. The third virial coefficient was calculated with the Lennard-Jones (6-12) model. It was assumed that the solid phase was the pure condensed component, and was incompressible; that the liquid phase was an ideal solution. The interaction second virial coefficients

obtained from the phase equilibria data were compared with available B_{12} data for the systems. When compared with the few data available in the temperature region of interest and taken in conjunction with the higher temperature B_{12} data, the B_{12} obtained here appear to be valid values. All the B_{12} data for each system were combined to give a graphically smoothed set of values. The smooth interaction virial coefficients so obtained were least-squares fitted to the Lennard-Jones (6-12) parameters. The resultant parameters showed that the conventional combination rules (geometric means for the energy parameter e/k, Lorentz average for the volume parameter b_o) for the pure component parameters are in general not valid. The exception is the helium-oxygen system in which the conventional combination rules for the Lennard-Jones (6-12) model work very well. Also demonstrated was that the correct representation of the interaction second virial coefficient is more sensitive to the energy parameter, $(e/k)_{12}$, than to the volume parameter, $(b_o)_{12}$. With $(b_o)_{12}$ given by the Lorentz average, the interaction second virial coefficient could be satisfactorily least-squares fitted to $(e/k)_{12}$. The effect on the calculated Enhancement Factor of this modified Lennard-Jones (6-12) model was studied. As is to be expected, correctly calculating B_{12} generally improves the predicted Enhancement Factor over that predicted with conventional combination rules.

The Lennard-Jones (6-12) model (which represented the experimental Enhancement Factor for the helium-oxygen system accurately) was used to calculate the Enhancement Factor for the helium-oxygen system in the liquid-vapor region at regular temperature and pressure intervals.

For the systems studied here, there is no conclusive evidence

that either the Lennard-Jones (6-12) or the Kihara core model is superior. Both represent the second virial coefficients of the pure components equally well. However, the Kihara core model was not as good in predicting the interaction second virial coefficient as the Lennard-Jones (6-12) model, although neither in general predicted the correct B_{12}. Thus, the main usefulness of these models appear to be for making semi-quantitative calculations.

Recommendations

Several suggestions for future study in this area of phase equilibria appeared during the course of this work. They are summarized below.

1. The Kihara core model parameters used here are for cores of different shapes. The procedure for computing the third virial coefficient for this model has been worked out only for spherical cores[84,85]. It is recommended that in future work with this model the assumption of spherical cores be made for all molecules.

2. The contribution of non-additive terms to the third virial coefficient has been shown[84] to be significant, especially at lower temperatures. Such corrections should be taken into account in future calculations of the third virial coefficient.

3. The choice of the potential function parameters in this work was based on their adequacy in representing the second virial coefficient. It is recommended that future work give consideration also to their adequacy in representing the third virial coefficient. The scarcity of third virial coefficient data[12] below a reduced temperature of 0.8 would present some difficulties. Perhaps even a check of the

higher temperature data would be more desirable than no check at all.

4. The method used here to extract the interaction second virial coefficient should be applied to other phase equilibria data. A modification of the present procedure to reduce the sensitivity to the mole fraction at low pressures would be desirable. The method of Chiu and Canfield[11] is somewhat different from the method used here. However, it was shown that in the hydrogen-methane system (see Table 2 in Chapter V), both methods resulted in values of B_{12} which agreed well.

5. The testing of combination rules for potential function parameters should be continued. Chueh and Prausnitz[13] have tested the combination rules for the critical constants and have developed a correction factor for the critical temperature combination rule. Hiza and Duncan[30] have recently developed correction factors for the Kihara core model. Chueh and Prausnitz[13] present their correction factor for an extensive list of substances, mostly hydrocarbon combinations. Eckert, et al[21] and Renon, et al[78] have developed an equation of state for simple liquids. They also use the same notion of a correction factor for the combination of the energy parameter in their equation. Chiu and Canfield[11] have tested the combination rules for the Lennard-Jones (6-12) potential function for the hydrogen-methane system. The development of these correction factors would be very useful in the application of these models in multicomponent systems. An interesting study would be to test whether the correction factors as developed by Chueh and Prausnitz[13] for the critical temperature would be applicable to the energy parameter of the Lennard-Jones (6-12) and Kihara core models.

The correlation scheme for the correction factor developed by Hiza and Duncan[30] warrants further investigation in this regard.

6. An area not investigated in this work is the extraction of the Henry's Law constant from the solubility data of helium in the liquids studied here. Pierotti[73] presents a theoretical method for calculating the Henry's Law constant which could be compared with the experimental results.

7. In the future study of a class of systems, as was done here, it would be advantageous to select systems in which the Enhancement Factor is rather large. A large Enhancement Factor would give better resolution to the various contributions to it. Solid-vapor equilibria data are especially valuable in that the reasonable assumption of a pure condensed phase could be made. For liquid-vapor equilibria data it is not as easy to describe the non-ideality of the liquid phase. Where the solubility of the compressed gas in the liquid is small, the assumption of ideal solution, as made here, could be made.

APPENDICES

APPENDIX A

EXPERIMENTAL VAPOR PRESSURE OF ARGON AND CARBON DIOXIDE

As a check on the temperature and pressure scales being used in the phase equilibrium apparatus, the vapor pressure of liquid argon and carbon dioxide was measured in the apparatus. The vapor pressure of argon was measured before, while that of carbon dioxide was measured after the phase equilibrium measurements on the helium-carbon dioxide system were completed. Tables 11 and 12 present the vapor pressure of argon and carbon dioxide, respectively. The corresponding values computed at the experimental temperatures from published vapor pressure equations are also presented for comparison. The vapor pressure of argon indicates a maximum difference of 0.04 atm between the low pressure gauge readings and the values computed from the equation of McCain and Ziegler.[57] The corresponding maximum difference for the high pressure gauge is 0.4 atm. In the case of carbon dioxide the maximum difference between the low pressure gauge readings and the values computed from Equation 6 of Meyers and Van Dusen[58] is 0.06 atm. For the high pressure gauge the maximum difference is 0.4 atm. While the observed vapor pressure of argon falls both above and below the computed values, the observed vapor pressure of carbon dioxide is consistently higher.

The low pressure gauge readings were corrected by the addition of 1 psi, while the high pressure gauge readings were corrected by the addition of 15 psi. These corrections were determined by Kirk,[45] who calibrated the pressure gauges against a dead-weight gauge. Each scale

Table 11. Experimental Vapor Pressure of Argon

Temperature, °K	Vapor Pressure, atm				
	This Work				
	Low Pressure Gauge	High Pressure Gauge	McCain & Ziegler[57]	Van Itterbeek et al.[97]	Michels et al[61]
95.69	2.29	2.68	2.254	2.254	2.247
100.32	3.29	3.36	3.300	3.300	3.295
105.35	4.79	4.86	4.807	4.807	4.801
110.31	6.76	6.56	6.737	6.737	6.722
115.35	9.21	9.21	9.220	9.219	9.190
120.65	12.45	12.14	12.470	12.469	12.424
125.13	15.75	16.02	15.786	15.785	15.736
132.03	22.07	22.41	22.048	22.047	22.015
135.78	26.12	26.09	26.112	26.110	26.098
140.01	31.33	31.12	31.330	31.328	31.335
144.84	--	38.27	38.203	38.199	38.213
148.09	--	43.37	43.429	43.427	43.430

Table 12. Experimental Vapor Pressure of Carbon Dioxide

Temperature, °K	Vapor Pressure, atm		
	This Work		
	Low Pressure Gauge	High Pressure Gauge	Meyers & Van Dusen[58] (Eq. 6)
229.24	8.60	8.94	8.575
234.65	10.54	10.84	10.486
239.11	12.34	12.61	12.284
247.07	16.08	16.42	16.047
252.48	19.11	19.48	19.053
258.92	23.19	23.43	23.134
267.46	29.52	29.76	29.497

division on the low pressure gauge represented 2 psi. On the high pressure gauge each scale division represented 10 psi. The pressure gauges were readable to the nearest half division, which corresponds to an experimental precision of 1 psi (0.07 atm) and 5 psi (0.34 atm) in the readings of the low and high pressure gauges respectively. Thus the vapor pressure of argon and carbon dioxide measured in this work agrees with the literature values within the range of the experimental accuracy of the pressure measurements of this work. These vapor pressure measurements also provide a check of the temperature scales (NBS 1955 Scale for temperatures below 90.18°K and International Practical Kelvin Scale for temperatures above 90.18°K) and the purity of the argon and carbon dioxide used in this laboratory. The agreement of the Enhancement Factor in the helium-carbon dioxide system measured in this work with those measured by Barrick et al.[4] (see Figure 5) provide an indirect check of the pressure measurements above the range of these vapor pressure measurements.

APPENDIX B

HELIUM-ARGON SYSTEM MEASUREMENTS

Between the measurements made by Mullins[64] using this apparatus and the present measurements the apparatus was relocated at another laboratory. To provide a quick check on the operation of the apparatus after the move and to gain some operating experience, a limited run was made for the helium-argon system. This consisted of three points in the solid-vapor region at 80°K. The results are compared with those of Mullins in Figure 17. It can be seen that while the agreement is not very close, it can be concluded that the apparatus was in operating condition. Part of the disagreement is probably due to inexperience in the operation of the apparatus at that point in the investigations.

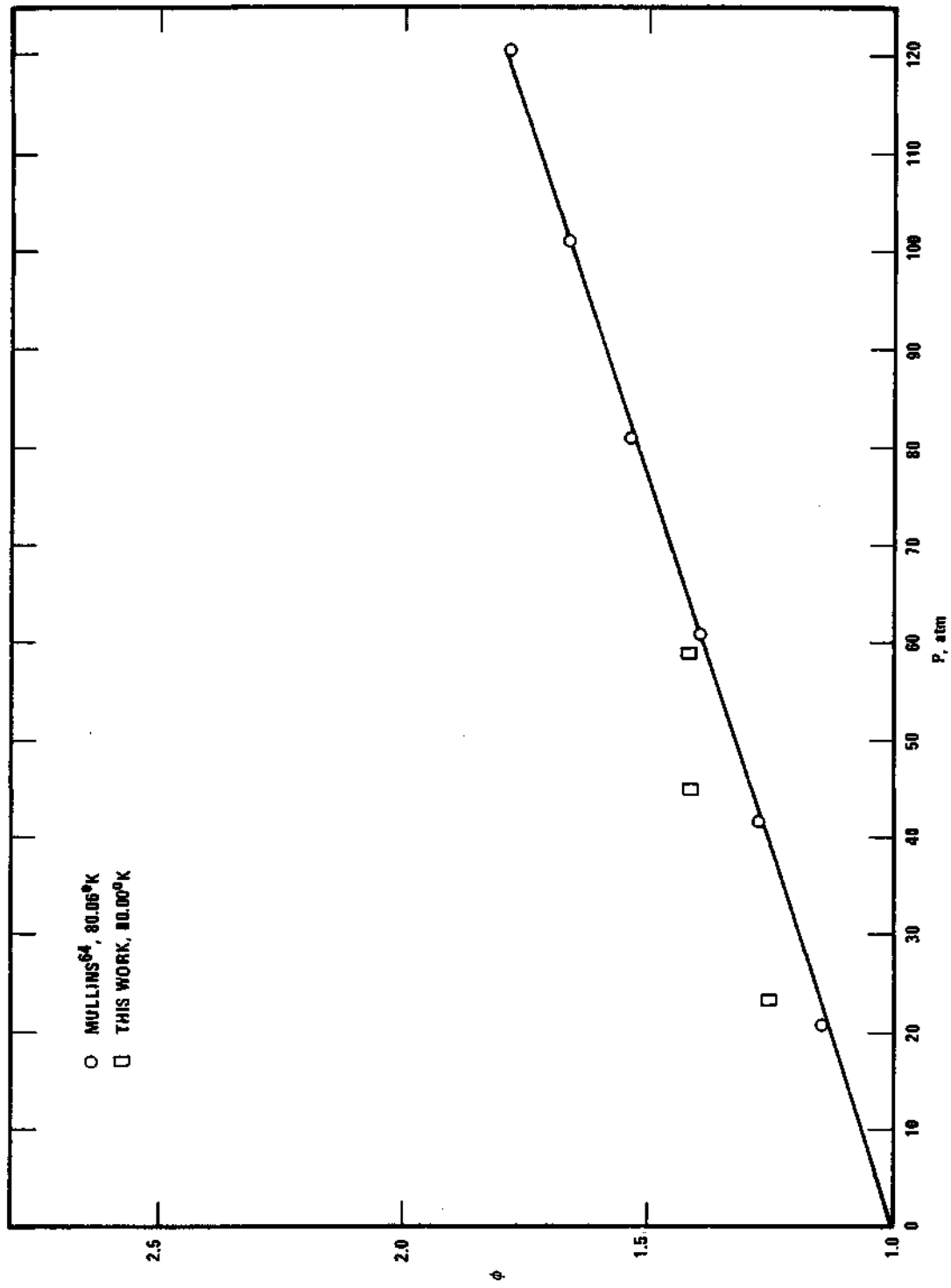

Figure 17. Experimental Enhancement Factor in the Helium-Argon System (Check Run).

APPENDIX C

CALIBRATION OF GAS CHROMATOGRAPH

Gas chromatography was used to analyse for carbon dioxide in the gas phase equilibrium helium-carbon dioxide mixtures. The Perkin-Elmer 154B chromatograph, as modified by Kirk,[45] was calibrated for this purpose. The analyses were made using a one-meter silica gel column.

The calibration was obtained by the following procedure. A helium-carbon dioxide mixture consisting of measured volumes of the two gases is prepared in a gas-mixing burette (see Kirk[45] for description). It is injected into the chromatograph with helium as the carrier gas. Only one peak corresponding to the prepared concentration of carbon dioxide is obtained since helium is the carrier gas. If h is the peak height at an attenuation factor setting of s on the chromatograph, the product then (h.s) is the actual peak height corresponding to the prepared concentration y of carbon dioxide in the helium-carbon dioxide mixture. The peak height is first corrected by the procedure described below for any drift in the chromatograph. The corrected (h.s) is then plotted against (h.s/y) to obtain a point on the calibration curve. Any drift in the chromatograph is corrected by the following procedure. Bottles of helium-carbon dioxide mixtures of approximate composition lying within the planned range of the calibration curve are prepared prior to the calibration. The peak heights corresponding to these bottles are determined. These peak heights, $(h.s)^{o}$, in effect fix the state of the chromatograph at that point in time. Later runs on the chromatograph

are referred back to that state by means of Equation (C-1):

$$\frac{(h.s)' \text{ sample}}{(h.s)'' \text{ sample}} = \frac{(h.s)^{o} \text{ bottle sample}}{(h.s)'' \text{ bottle sample}} \qquad \text{(C-1)}$$

In Equation (C-1) $(h.s)''$ indicates the peak heights measured at a time subsequent to the measurement of $(h.s)^{o}$ of the bottle samples. Since the composition of the bottle samples remains the same, the right hand side measures the drift of the chromatograph. Thus $(h.s)'$ is the peak height of a sample if the sample had been analysed at the time $(h.s)^{o}$ was measured. Equation (C-1) is most sensitive if the peak height of a sample and that of the bottle sample are close together. This is the reason for preparing several helium-carbon dioxide samples.

The calibration curve of carbon dioxide in helium is shown in Figure 18. As can be seen, the accuracy of the curve is about ±2 per cent.

After running a sample of unknown composition through the chromatograph, a bottle sample of nearest composition is injected into the chromatograph. Equation (C-1) is then used to obtain the corrected peak height of the unknown sample, which can be then used to obtain the composition from the calibration curve.

The description and normal operating conditions of the chromatograph are presented below:

Chromatograph: Perkin-Elmer Model 154B, modified by Kirk[45]

Column: Perkin-Elmer Column J; 1 meter silica gel column

Oven setting: 30

Oven temperature: 54°C

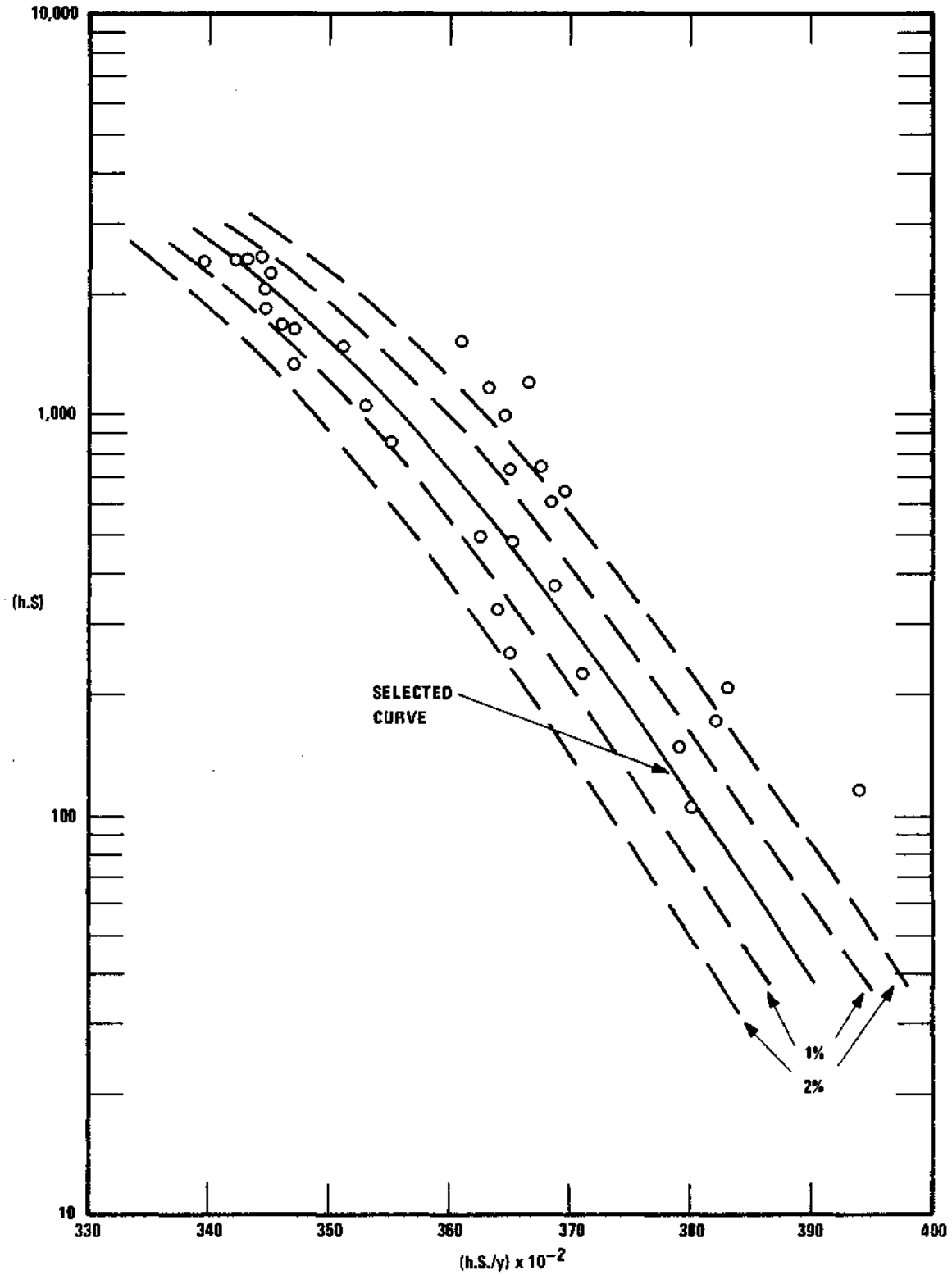

Figure 18. Calibration Curve for Carbon Dioxide in Helium.

Carrier gas: Helium at 15 psig; flow rate at 25°C and 1 atm pressure was about 300 cc/min

Sample size: 25 cc at room temperature (25°C) and atmospheric pressure (745 mm Hg)

Detector voltage: 60 mv at shunt

Recorder standardization voltage: 35 mv at shunt

Chart speed: 1.5 inches per minute

Elution time of carbon dioxide peak: 1 minute

Table 13 gives the reference peak heights and composition of the standard sample.

Table 13. Composition of "Standard" Samples

Bottle No.	$(h.s)^{\circ}$	mole % CO_2
4	64.8 x 2	0.342
5	65.1 x 4	0.701
6	64.4 x 8	1.415
7	61.6 x 16	2.769
8	61.1 x 32	5.656

APPENDIX D

SUMMARY OF EXPERIMENTAL DATA FOR THE HELIUM-CARBON DIOXIDE SYSTEM

The experimental phase-equilibria data measured in this work for the helium-carbon dioxide system are presented in Table 14. Only the vapor phase composition was analyzed. The solid phase was assumed to be pure carbon dioxide. As a check with the 219.9°K isotherm of Barrick et al.,[4] in the liquid-vapor region, the vapor composition of four points was measured for the 220.3°K isotherm. No liquid analysis was performed as no calibration had been prepared for the liquid range compositions.

The data are presented in the order they were measured. The letter G or L refers to whether the sample was taken through the gas or liquid sample line. The numbers preceding and following G or L are the run number and sample number, respectively. When running in the vapor-solid region, the gas line sample is taken from the bottom of the cell while the liquid line sample is taken from a point approximately mid-point in the cell. Thus an agreement between the analysis of these two samples is a check on the equilibrium. When running in the vapor-liquid region the gas line sample is taken from the top of the cell, while the liquid sample is taken through the liquid sample line. As can be seen from Table 14 there is close agreement between the Enhancement Factors for the gas line and liquid line samples. The selected values for the temperature, pressure, and Enhancement Factor are the average values.

The residence time is the time a gas sample spends in the cell if it were in plug flow. The longer the residence time the closer is the

Table 14. Experimental Vapor Phase Equilibrium Compositions in the Helium-Carbon Dioxide System.

Sample	T°K	P, atm	p_{01}, atm	y_1	$\phi = Py_1/p_{01}$
1G1	181.117	118.02	0.30213	0.003035	1.186
1G2	181.076	118.02	0.30096	0.002998	1.176
1L3	181.128	118.02	0.30245	0.002823	1.102
1L4	181.082	118.02	0.30113	0.002770	1.086
1G5	181.028	118.02	0.29959	0.002904	1.146
Selected	181.09	118.02	(Residence Time = 23.5 min)		1.139
1G6	180.997	98.08	0.29871	0.003429	1.126
1L7	181.065	98.08	0.30065	0.003435	1.121
1G8	181.014	98.08	0.29920	0.003440	1.128
1G9	181.020	98.08	0.29937	0.003413	1.118
Selected	181.02	98.08	(Residence Time = 29 min)		1.123
1G10	181.017	98.08	0.29928	0.003397	1.113
1G11	181.016	98.08	0.29925	0.003413	1.119
1G12	181.067	98.08	0.30070	0.003332	1.087
Selected	181.03	98.08	(Residence Time = 57.5 min)		1.106
1G13	181.040	98.08	0.29993	0.003483	1.139
1G14	181.044	98.08	0.30005	0.003473	1.135
1L15	181.102	98.08	0.30170	0.003403	1.106
1G16	181.024	98.08	0.29948	0.003440	1.127
Selected	181.05	98.08	(Residence Time = 14.8 min)		1.127
1G17	181.011	81.27	0.29911	0.004038	1.097
1G18	181.016	81.27	0.29925	0.003979	1.081
1L19	181.068	81.27	0.30073	0.003973	1.074
1G20	181.024	81.27	0.29948	0.003958	1.074
Selected	181.03	81.27	(Residence Time = 25.5 min)		1.081
1G21	181.017	59.98	0.29928	0.005072	1.017
1L22	181.068	59.98	0.30073	0.005212	1.040
1G23	181.024	59.98	0.29948	0.004995	1.000
Selected	181.04	59.98	(Residence Time = 29.6 min)		1.019

Table 14 (continued)

Sample	$T^{\circ}K$	P, atm	p_{01}, atm	y_1	$\phi = Py_1/p_{01}$
1L24	181.078	42.56	0.30102	0.007510	1.062
1G25	181.045	42.56	0.30008	0.007288	1.034
1L26	181.095	42.56	0.30150	0.007547	1.065
1G27	181.061	42.56	0.30053	0.007646	1.083
Selected	181.07	42.56	(Residence Time = 23.6 min)		1.061
1G28	181.063	21.26	0.30059	0.01534	1.085
1G29	181.073	21.26	0.30087	0.01538	1.087
1L30	181.124	21.26	0.30233	0.01498	1.053
1G31	181.078	21.26	0.30102	0.01518	1.072
Selected	181.08	21.26	(Residence Time = 13.3 min)		1.074
2G1	190.025	119.86	0.67541	0.006470	1.148
2G2	190.020	119.86	0.67512	0.006437	1.143
2L3	190.049	119.86	0.67680	0.006414	1.136
2G4	190.020	119.86	0.67512	0.006470	1.149
Selected	190.03	119.86	(Residence Time = 29.4 min)		1.144
2G5	190.005	103.39	0.67424	0.007355	1.129
2G6	190.011	103.39	0.67459	0.007323	1.122
2L7	190.035	103.39	0.67599	0.007245	1.108
2G8	190.009	103.39	0.67448	0.007411	1.136
Selected	190.02	103.39	(Residence Time = 31.1 min)		1.124
2G9	190.011	81.95	0.67459	0.009140	1.110
2L10	190.033	81.95	0.67589	0.009273	1.124
2G11	190.016	81.95	0.67488	0.009218	1.119
2L12	190.039	81.95	0.67622	0.009251	1.121
Selected	190.02	81.95	(Residence Time = 29.2 min)		1.119
2G13	190.006	61.06	0.67430	0.01185	1.073
2L14	190.028	61.06	0.67558	0.01177	1.064
2G15	190.034	61.06	0.67593	0.01188	1.073
Selected	190.02	61.06	(Residence Time = 27.5 min)		1.070

Table 14 (continued)

Sample	T°K	P, atm	p_{01}, atm	y_1	$\phi = Py_1/p_{01}$
2G16	190.022	40.79	0.67523	0.01789	1.081
2L17	190.047	40.79	0.67669	0.01789	1.078
2G18	190.036	40.79	0.67605	0.01812	1.093
Selected	190.04	40.79	(Residence Time = 29.3 min)		1.084
3G1	199.934	121.76	1.52738	0.01484	1.183
3L2	199.966	121.76	1.53120	0.01448	1.151
3G3	199.929	121.76	1.52679	0.01464	1.168
3L4	199.959	121.76	1.53036	0.01442	1.147
Selected	199.95	121.76	(Residence Time = 30.7 min)		1.162
3G5	199.931	101.01	1.52703	0.01714	1.134
3L6	199.973	101.01	1.53203	0.01712	1.129
3G7	199.942	101.01	1.52834	0.01710	1.130
Selected	199.95	101.01	(Residence Time = 29.4 min)		1.131
3G8	199.938	81.27	1.52786	0.02094	1.114
3L9	199.975	81.27	1.53227	0.02106	1.117
3G10	199.950	81.27	1.52929	0.02112	1.122
Selected	199.95	81.27	(Residence Time = 29.5 min)		1.118
3G11	199.931	61.20	1.52703	0.02657	1.065
3L12	199.966	61.20	1.53120	0.02638	1.054
3G13	199.930	61.20	1.52691	0.02689	1.078
Selected	199.94	61.20	(Residence Time = 35.4 min)		1.066
3G14	199.930	41.13	1.52691	0.03992	1.075
3L15	199.962	41.13	1.53072	0.04011	1.078
3G16	199.941	41.13	1.52822	0.04039	1.087
Selected	199.94	41.13	(Residence Time = 23.1 min)		1.080
4G1	220.277	143.74	5.99375	0.05063	1.214
4G2	220.287	143.74	5.99626	0.05129	1.230
4G3	220.305	143.74	6.00077	0.05149	1.233
Selected	220.29	143.74	(Residence Time = 34.0 min)		1.226

Table 14 (continued)

Sample	$T^{\circ}K$	P, atm	p_{01}, atm	y_1	$\phi = Py_1/p_{01}$
4G4	220.317	118.15	6.00378	0.06168	1.214
4G5	220.327	118.15	6.00629	0.06120	1.204
4G6	220.314	118.15	6.00303	0.06168	1.214
Selected	220.32	118.15	(Residence Time = 38.0 min)		1.211
4G7	220.304	99.31	6.00052	0.07186	1.189
4G8	220.325	99.31	6.00579	0.07195	1.190
4G9	220.301	99.31	5.99977	0.07226	1.196
Selected	220.31	99.31	(Residence Time = 35.2 min)		1.192
4G10	220.308	80.46	6.00152	0.08721*	1.169
4G11	220.297	80.46	5.99876	0.08693*	1.166
4G12	220.314	80.46	6.00303	0.08693*	1.165
Selected	220.31	80.46	(Residence Time = 32.0 min)		1.167

* From extrapolated calibration curve.

approach to equilibrium in the exit gas. An experiment to examine the effect of the residence time on the Enhancement Factor was carried out at 181.05°K and 98.08 atmospheres. The experiment (sample numbers 1G6 to 1G16) consisted of three points run at residence times of 29, 57.4, and 14.8 minutes. The average Enhancement Factor at 57.5 minutes residence time is somewhat lower than the average values at the shorter residence times. This is consistent with the method of operating the apparatus by the condensation of the excess carbon dioxide from a super-saturated helium-carbon dioxide mixture. But the range of the individual Enhancement Factors overlap each other. Hence, it was concluded that a residence time of about 30 minutes was sufficient in practice to attain equilibrium for the helium-carbon dioxide system.

The temperature of the equilibrium cell measured with the platinum resistance thermometer was plotted against the time. The temperature gradient between the top and bottom of the equilibrium cell, as measured with a six-junction thermopile, was also plotted against the time. The temperature and temperature gradient of the cell at the time a sample was taken were read from these two plots. The time lag between the time the sample left the cell and the time it was collected was neglected. The temperature of a sample taken through the gas-sample line was obtained by subtracting the temperature difference (between the top and bottom of the cell) from the temperature (on the International Practical Kelvin Scale) of the cell. This was because the top of the cell was warmer than the bottom, and the platinum resistance thermometer was located at the top of the cell. The gas flow was from top to bottom. The liquid-sample line extended to the middle of the cell. Thus the

temperature of a sample taken through this line was obtained by subtracting half of the temperature difference (between the top and bottom of the cell) from the cell temperature.

The observed pressure gauge readings were converted to correct values by means of the calibration curve developed by Kirk.[45] He calibrated the gauges against a dead-weight gauge. The low pressure (0-600 psi) gauge readings were corrected by adding 1 psi to the actual readings. The high pressure (0-3000 psi) gauge readings were similarly corrected by adding 15 psi. An average barometric pressure of 0.98 atmosphere was added to the corrected gauge pressures to give the absolute pressure (P in Table 14). The conversion factor from psia to atmosphere used was 14.696 psia equal to one atmosphere.

The analysis of the samples has already been described in Appendix C.

APPENDIX E

SELECTION OF DATA FOR CALCULATIONS

The physical properties and other data needed for the calculation of the Enhancement Factor are:

(1) The Lennard-Jones (6-12) classical and the Kihara core model potential parameters

(2) Vapor pressure of the condensed component

(3) Molal volumes of the liquid and solid condensed component as a function of temperature and pressure.

The criterion for the selection of the potential function parameters was that the second virial coefficient calculated with the parameters agree with the experimental data. The third virial coefficient, the highest coefficient considered in this work, was calculated in all cases with the Lennard-Jones (6-12) model. The agreement of the calculated third virial coefficients with experimental data could not be tested because essentially no third virial coefficient data exist in the temperature range of this work. Indeed, Chueh and Prausnitz[12] found negligible amounts of third virial coefficient data below a reduced temperature of 0.8. However, Keesom's[38] values for the third virial coefficient of helium are available and are compared with the calculated values in Figure 20. A discussion of the general problem of the third virial coefficient was presented in Chapter IV. Table 15 summarizes the molecular parameters selected. The second virial coefficients calculated with the selected parameters are compared with the experimental

Table 15. Lennard-Jones (6-12) and Kihara Core Parameters

Parameter	He	CO_2	Ar	CH_4	N_2	O_2
LJCL (6-12)						
e/k, °K	6.96[64]	175.6[7]	119.30[109]	114.39[45]	90.467[108]	112.0[68]
b_o, cc/gm mole	22.9	131.8	50.91	126.40	76.869	60.84
KIHARA[77]						
U_o/k, °K	9.927	380.20	146.10	194.00	136.67	168.00
ρ_o, Å	2.921	2.790	3.328	3.535	3.148	2.958
M_o, Å	0.0	9.173	2.199	3.405	4.694	4.420
S_o, $Å^2$	0.0	2.469	0.3848	0.6111	0.8130	0.4106
V_o, $Å^3$	0.0	0.1781	0.02245	0.02470	0.03856	0.01000
Q*	0.0	0.1793	0.0	0.0	0.2110	0.0
Mol. Wt.	4.0026	44.00995	39.948	16.04303	28.0134	31.9988

data in the following sections dealing with each component individually.

Equations which best represented the experimental vapor pressure data were selected for calculating the vapor pressures. The equations are presented in the sections discussing individual components.

The density or specific volume data of the solid condensed components were plotted against the temperature. The data were the saturation values, and the smooth values were obtained from smooth curves drawn through the points. The solid molal volume was assumed to be incompressible. The liquid molal volume was expressed as a function of temperature and pressure. The volume data were least-squares fitted with orthogonal polynomials in temperature (up to the third degree) and pressure (up to the second degree). This least-squares fitting procedure is described by Mullins and Ziegler,[67] and also by Mullins.[64] The pressure polynomial for an isotherm was obtained by substituting the temperature of the isotherm into the polynomial containing both temperature and pressure obtained by the fitting procedure. Again, the selection of the molal volume data is discussed in the following sections.

Helium

The Lennard-Jones (6-12) classical parameters for helium selected are those determined by Mullins[64] by fitting the second virial coefficient data of White et al.[106] The Kihara core model parameters are those determined by Prausnitz and Myers[77] and includes the first two translational quantum corrections. Figure 19 shows a comparison of the calculated second virial coefficients of helium and the experimental data. It can be seen that over the temperature range considered in

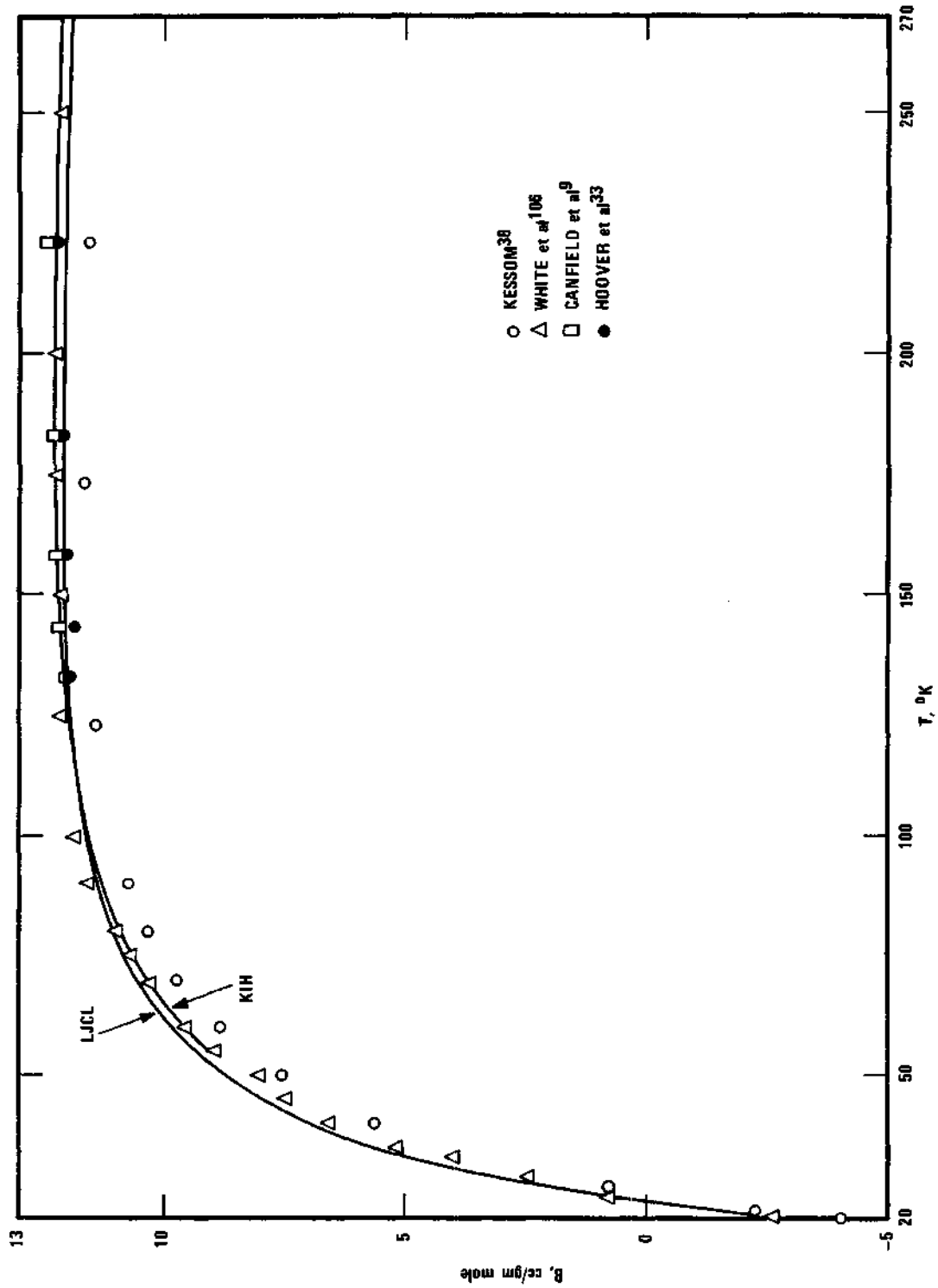

Figure 19. Second Virial Coefficient of Helium.

this work (77 - 275°K) the calculated second virial coefficients of helium agree very well with the experimental data of Keesom,[38] White et al.,[106] Canfield et al.,[9] and Hoover et al.[33] Figure 20 shows the third virial coefficient calculated with the Lennard-Jones (6-12) parameters given in Table 15, together with the experimental data of Keesom,[38] White et al.,[106] Canfield et al.,[9] and Hoover et al.[33] The data of Keesom are higher than those of White et al., Canfield et al., and Hoover et al. The latter three sets of data agree very well. The calculated results are somewhat smaller than the data of White et al., Canfield et al., and Hoover et al.

Carbon Dioxide

The selected Lennard-Jones (6-12) parameters for carbon dioxide (Table 15) are those of Butcher and Dodson.[7] The Kihara core model parameters are from Prausnitz and Myers,[77] and includes an additional quadrupole correction to the second virial coefficient. Other Lennard-Jones (6-12) parameters (such as those of McCormack and Schneider,[54] Hirschfelder et al.[29]) were also considered. The parameters of Butcher and Dodson represented the second virial coefficient data best. Mullins et al.,[65] adjusted the Kihara core model parameters of Prausnitz and Myers to give better agreement between the calculated and experimental vapor pressure (below 1 atmosphere) of carbon dioxide. The parameters which they adjusted were U_o/k to 381.97°K and ρ_o to 2.925Å. The second virial coefficient calculated from the above parameters and the experimental data are shown in Figure 21. No experimental data exist below 200°K, which is in the region of solid-vapor equilibria. The

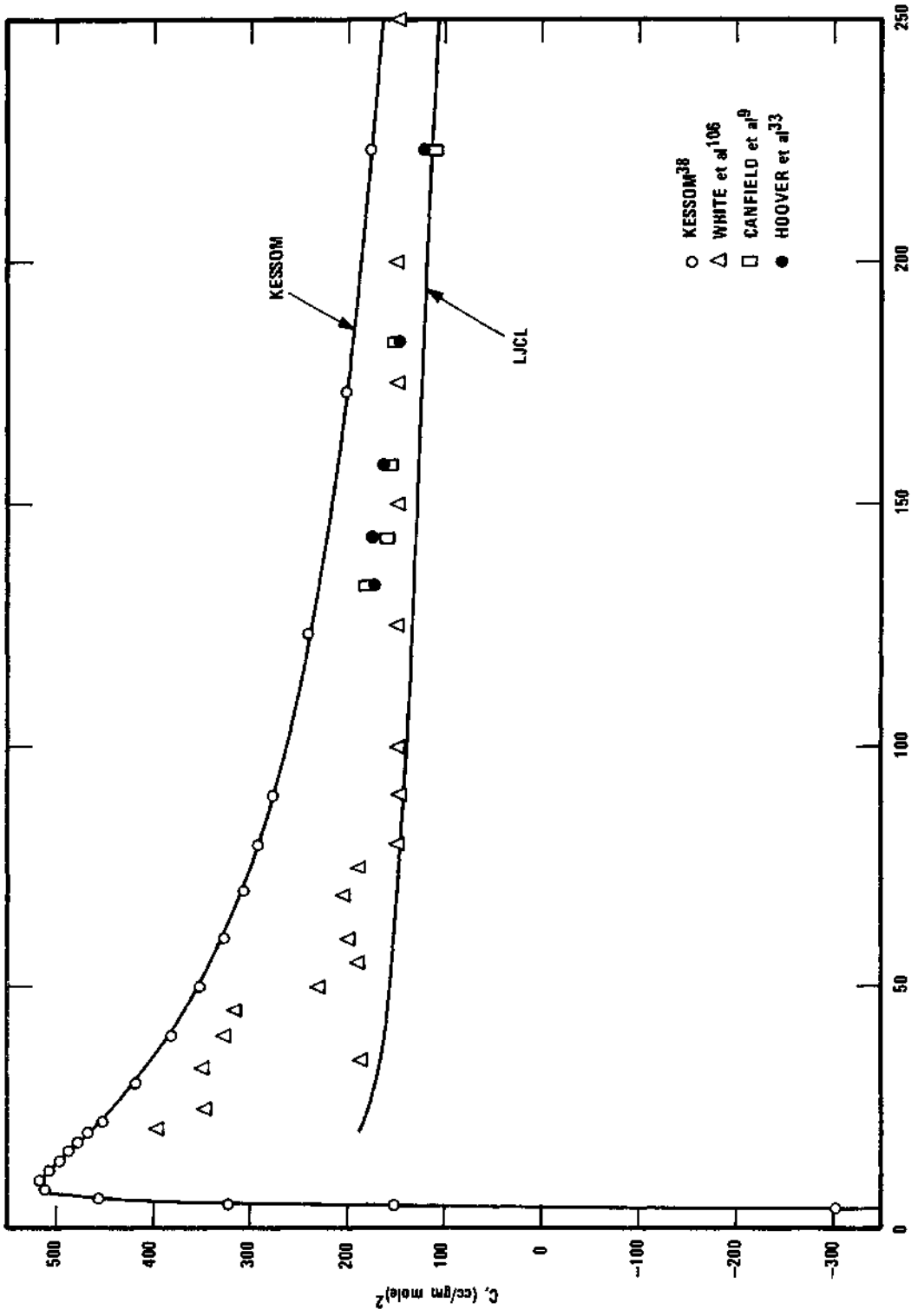

Figure 20. Third Virial Coefficient of Helium.

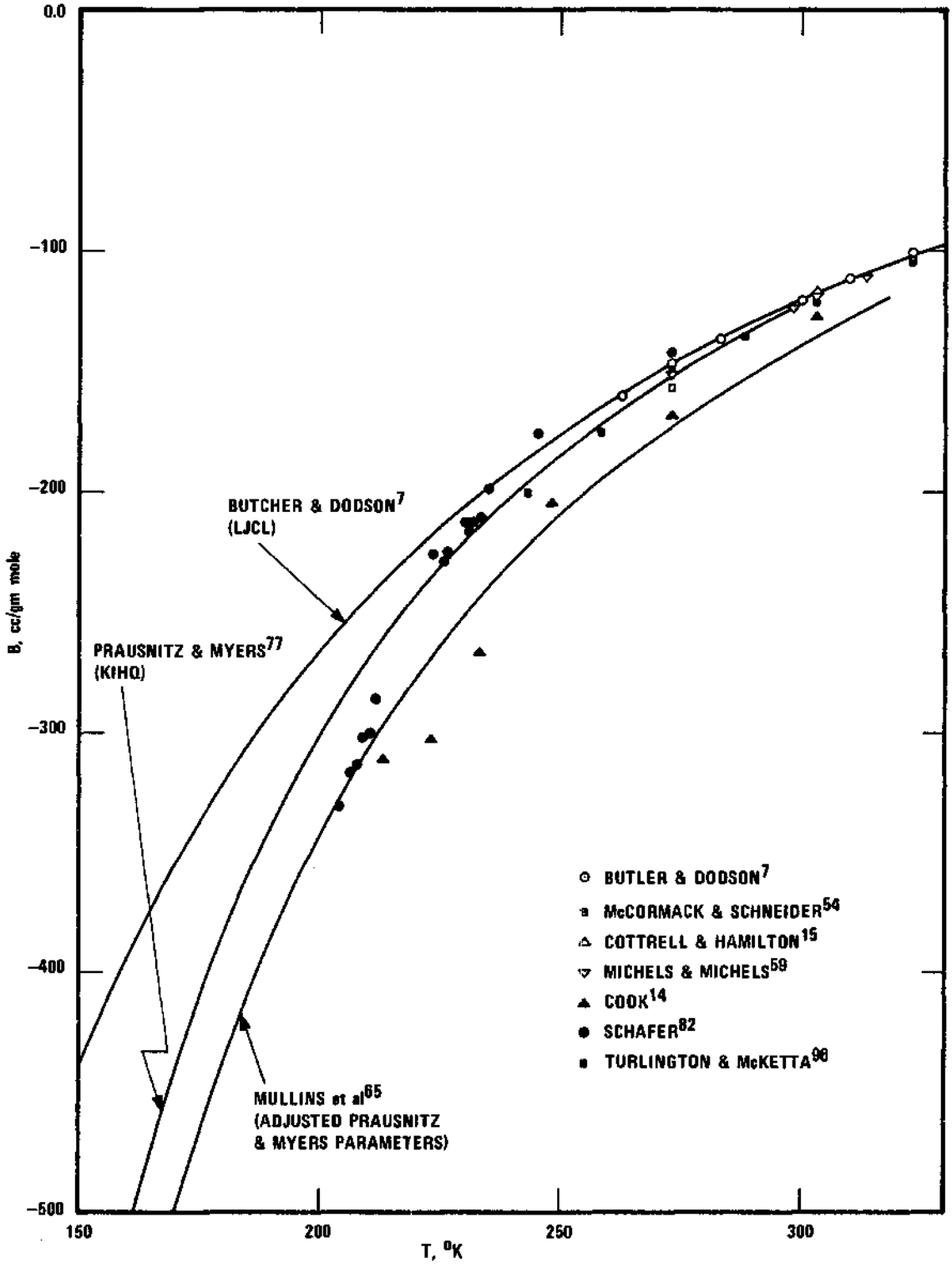

Figure 21. Second Virial Coefficient of Carbon Dioxide.

Lennard-Jones (6-12) second virial coefficients agree well with the experimental data at the higher temperatures, as do those calculated with the Kihara parameters of Prausnitz and Myers. The former model computes a higher second virial coefficient than the latter model. The adjusted Kihara parameters of Mullins et al. predict second virial coefficients which tend to be low at higher temperatures, but do better at the lower temperatures. In view of the scatter of the experimental data at the lower temperatures, the Kihara parameters of Prausnitz and Myers were selected. Enhancement Factors were also calculated with the Kihara parameters of Mullins et al. They did not differ greatly from those calculated with the Prausnitz and Myers' Kihara parameters.

Mullins et al.[65] have calculated the vapor pressure of carbon dioxide below one atmosphere. Their results agree very well with the experimental vapor pressure. Their calculated values from 140 to 194.694°K (vapor pressure equal to one atmosphere) were selected to represent the vapor pressure of carbon dioxide over this temperature range. Twelve points, at five-degree intervals were least-squares fitted with polynomials in the temperature. A sixth degree polynomial, Equation (D-1) below fitted the vapor pressure to within 0.001 mm Hg. Equation (D-1) was used to calculate the vapor pressure of carbon dioxide from 140 to 194.694°K.

$$140 \leq T \leq 194.694^{\circ}K$$

$$\ell n\ P\ (mm\ Hg) = -117.523795 + 2.61225166 \times T - 2.65546830 \times 10^{-2} \times T^{2} \quad (D\text{-}1)$$

$$+ 1.62037156 \times 10^{-4} \times T^{3} - 5.87474846 \times 10^{-7} \times T^{4}$$

$$+ 1.13414387 \times 10^{-9} \times T^{5} - 9.91012043 \times 10^{-3} \times T^{6}$$

Above one atmosphere and up to the triple point (216.55°K, 5.112 atmospheres) Equation 9 of Myers and Van Dusen[58] was used to calculate the vapor pressure of carbon dioxide. It is written as Equation (D-2) below.

$$\log P \text{ (bars)} = 6.92804 - \frac{1}{T}\left[1347.00 - 1.167(T^2 - 35450)^3 \times 10^{-12}\right] \quad \text{(D-2)}$$

where 1 bar = 0.98692327 atmospheres

$T\ ^{\circ}K = t^{\circ}C$ (Int. Pract. Temp. Scale) + 273.10

The present work also uses the International Temperature Scale, but uses the ice point of water as 273.15°K. The difference of 0.05°K between the temperature scale of Equation (D-2) and the present work was corrected for in using Equation (D-2). This was done by subtracting 0.05°K from the absolute temperature used in this work when using Equation (D-2).

The vapor pressure of carbon dioxide from the triple point to the critical point (304.15°K, 72.80 atmospheres) was calculated with Equation (D-3) below.

$$\log P \text{ (bars)} = 4.674193 - \frac{1}{T}\left[855.352 - 1.131 \times 10^{-4}(T^2 - 69700)(10^{4.7 \times 10^{-10}(T^2 - 69700)^2} - 1)\right] \quad \text{(D-3)}$$

where bars and T are as defined in Equation (D-2).

Equation (D-3) is Equation 6 of Myers and Van Dusen.[58] As in using Equation (D-2) the 0.05°K difference between their scale and the present temperature scale was corrected.

Table 17 summarizes the vapor pressure of carbon dioxide used in this work. Below 140°K the calculated values of Mullins et al.[65] were used.

The saturated density of solid carbon dioxide has been measured by Keesom and Kohler[39] between 20 and 114°K. Maas and Barnes[53] have measured it between 90 and 193.55°K. In the overlap region the density data of Keesom and Kohler are about one per cent higher. This is probably due to the different experimental techniques used. Keesom and Kohler used x-ray diffraction to determine the lattice constants of solid carbon dioxide as a function of temperature. From the lattice constants the density was calculated. Maas and Barnes measured the volumes of mixtures of liquid propane and solid carbon dioxide as a function of temperature. The density of liquid propane as a function of temperature was previously determined. The density of solid carbon dioxide as a function of temperature was obtained by difference. A smooth curve was drawn through the data of these two groups. The density of solid carbon dioxide at various temperatures was read from this smooth curve. The molal volumes of solid carbon dioxide used in this work are presented in Table 17.

The specific volume of liquid carbon dioxide has been summarized by Din.[19] In addition to the saturation envelope, data are presented up to 200 atmospheres from 0 to -30°C. From -10 to -30°C the data are up to only 60 atmospheres. These data were plotted graphically and reasonable extrapolations drawn into regions of no data. The lowest temperature used was -55°C and the highest pressure was 200 atmospheres. Values of the specific volume of liquid carbon dioxide were read from this graph at regular temperature and pressure intervals. After conversion to the molal volume they were least-squares fitted to orthogonal polynomials in temperature and pressure. The third degree polynomial in temperature and second degree polynomial in pressure fitted the data

Table 16. Least Squares Fit of the Molal Volume of Liquid Carbon Dioxide

Coefficients, α_{ij}

i \ j	1	2	3	4
0	8.43495153(-1)	2.76262510(-1)	7.18534281(-1)	2.29247923(-1)
1		-5.35894152(-1)	1.70517389	-1.59034699(-1)
2			2.18637336(-3)	8.30305675(-1)
3				-5.68531012(-1)

i \ j	5	6	7	8
0	1.63705643(-1)	6.18102014(-1)	1.92248284(-1)	1.34808335(-1)
1	-4.64749595(-1)	2.19435745	1.10521591(-1)	-2.18013715(-1)
2	8.49405750(-1)	5.52867141(-3)	6.96810333(-1)	6.97971811(-1)
3	-5.79472633(-1)	2.56565799	-6.84795055(-1)	-9.50857886(-1)
4	-1.07624143	1.44534203(-3)	1.69268116	-7.87044496(-2)
5		2.42896505(-4)	-2.31221148(-4)	8.10850993(-1)
6			-3.59308633(-1)	-7.64249940(-1)
7				-1.24545446

Weighting Factors, C_j

j	0	1	2	3
	0.59007638	0.89052752	-0.05430610	3.55921616
j	4	5	6	7
	-0.84887211	0.05001154	17.63243866	-6.29631416
j	8			
	1.15199452			

Normalizing Constants

T_{max} = 303.15	$(P-p_{01})_{max}$ = 194.522067	$(V_1^L)_{max}$ = 7.42048694(-2)

Table 17. Vapor Pressure, Molal Volume of Solid and Liquid Carbon Dioxide

		Solid		
T, °K	p_{01}	a**	b	c
60	4.983(-14)*mm Hg	0.02684	0.0	0.0
65	3.318(-12)	0.02588	0.0	0.0
70	1.211(-10)	0.02593	0.0	0.0
75	2.729(-9)	0.02598	0.0	0.0
80	4.155(-8)	0.02603	0.0	0.0
85	4.578(-7)	0.02608	0.0	0.0
90	3.852(-6)	0.02614	0.0	0.0
95	2.582(-5)	0.02621	0.0	0.0
100	1.426(-4)	0.02627	0.0	0.0
105	6.675(-4)	0.02634	0.0	0.0
110	2.707(-3)	0.02641	0.0	0.0
115	9.692(-3)	0.02649	0.0	0.0
120	3.111(-2)	0.02658	0.0	0.0
125	9.074(-2)	0.02666	0.0	0.0
130	2.431(-1)	0.02674	0.0	0.0
135	6.037(-1)	0.02684	0.0	0.0
140	1.402	0.02693	0.0	0.0
145	3.064	0.02703	0.0	0.0
150	6.342	0.02713	0.0	0.0
155	12.500	0.02724	0.0	0.0
160	23.568	0.02734	0.0	0.0
165	42.686	0.02745	0.0	0.0
170	74.542	0.02757	0.0	0.0
175	125.924	0.02768	0.0	0.0
180	206.410	0.02778	0.0	0.0
185	329.207	0.02791	0.0	0.0
190	512.203	0.02802	0.0	0.0
195	783.020	0.02814	0.0	0.0
200	1166.797	0.02825	0.0	0.0
205	1707.677	0.02837	0.0	0.0
210	2459.773	0.02849	0.0	0.0
215	3293.933	0.02860	0.0	0.0
181.05	0.300 atm	0.02780	0.0	0.0
190.03	0.676	0.02802	0.0	0.0
199.95	1.529	0.02825	0.0	0.0

Table 17 (continued)

		Liquid		
T, °K	p_{01}	a**	b	c
219.90	5.900 atm	3.75627298(-2)	1.41646544(-5)	-1.05198220(-7)
229.90	8.793	3.90100240(-2)	5.05740669(-6)	-3.06757066(-8)
244.90	14.949	4.11519505(-2)	-1.61710110(-5)	8.11080636(-8)
259.90	23.810	4.40628871(-2)	-4.64804839(-5)	1.92891834(-7)
274.90	36.016	4.86471399(-2)	-8.58710123(-5)	3.04675604(-7)

* Number in parentheses indicates powers of 10.

** Molal Volume, $v_1 = a + b(P - p_{01}) + c(P - p_{01})^2$, liters/gm mole where P is in atm.

with an average deviation of 1.28 per cent in the molal volume. The pressure parameter used is $(P - p_{01})$, i.e., the total pressure less the vapor pressure of carbon dioxide. This form makes it more convenient for subsequent use in Enhancement Factor calculations. The coefficients, weighting factors, and normalizing constants for the polynomial are presented in Table 16. Insertion of a particular temperature into the polynomial results in the molal volume of liquid carbon dioxide expressed explicitly as a quadratic in $(P - p_{01})$. Table 17 summarizes the coefficients of this quadratic at the various temperatures.

Argon

The potential function parameters for argon have been presented in Table 15. The Lennard-Jones (6-12) parameters were determined by Levelt.[52] Ziegler et al.[109] have made a critical review of the argon second virial coefficient for the purpose of calculating the vapor pressure of argon below one atmosphere. They selected the Levelt parameters as best representing the second virial coefficient of argon. The Kihara core parameters are those of Prausnitz and Myers.[77] The calculated and experimental second virial coefficient of argon are shown in Figure 22. Figure 22 with just the Lennard-Jones (6-12) second virial coefficient curve is Figure 6 of Ziegler et al.[109] The Kihara second virial coefficient and the data of Weir et al.[105] have been added to it for presentation in Figure 22. It can be seen that both the Lennard-Jones (6-12) and Kihara core models represent the second virial coefficient of argon very well. The latter model is lower in the region below 180°K and slightly higher above that temperature.

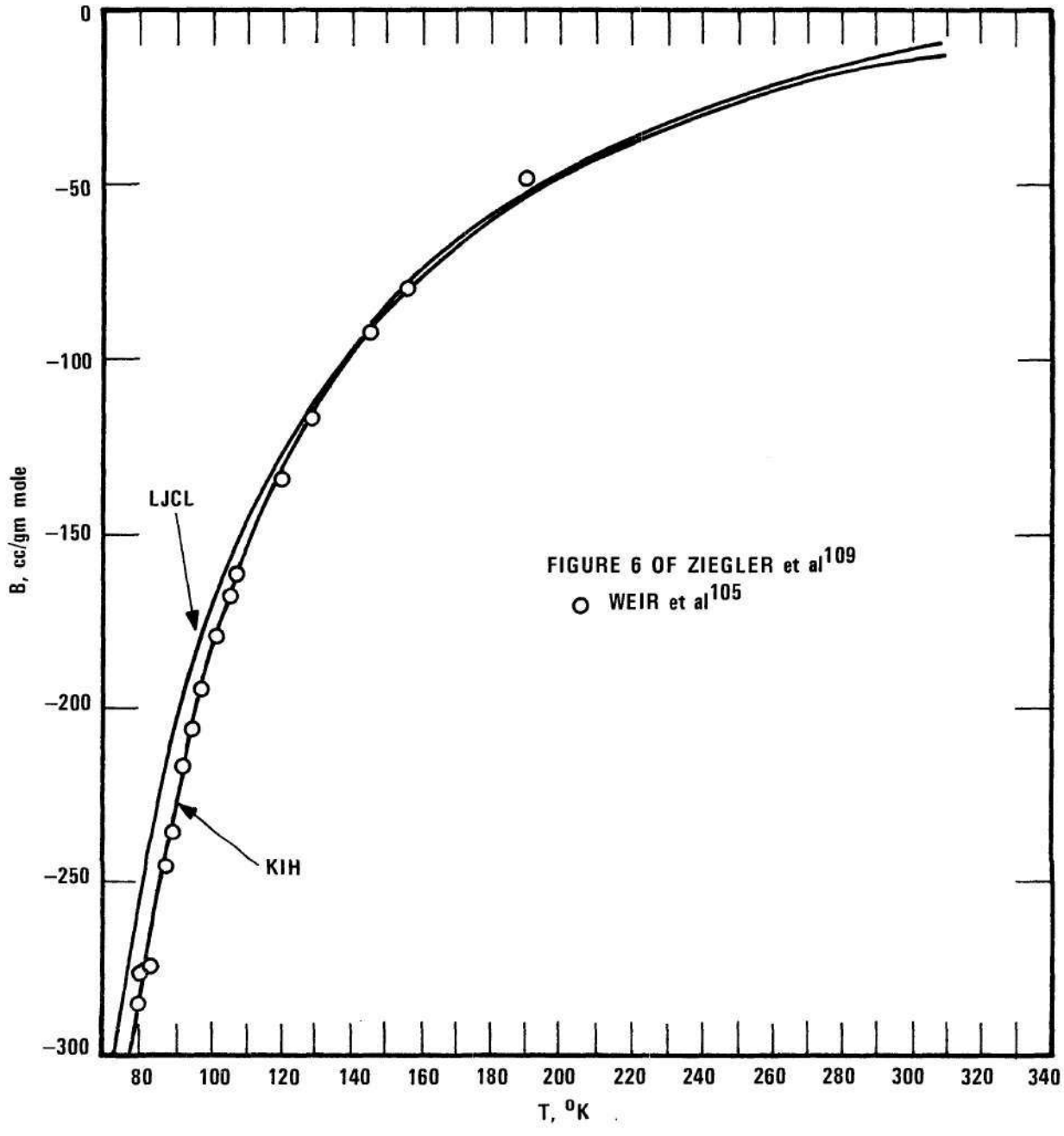

Figure 22. Second Virial Coefficient of Argon.

The equations used to calculate the vapor pressure of argon are the same as were selected by Mullins.[64] Equations (D-4) and (D-5) were obtained by Mullins[64] by a least-squares fit of the calculated vapor pressure of Ziegler et al.[109] Equation (D-6) is that of Michels et al.[61]

$$T < 83.81^{\circ}K$$

$$\log p_{01}(\text{atm}) = 5.9057813 - \frac{740.68409}{T} + \frac{35110.773}{T^2} \qquad \text{(D-4)}$$

$$- \frac{1661065.3}{T^3} + \frac{28979491.0}{T^4}$$

$$83.81 \leq T \leq 88.0^{\circ}K$$

$$\log p_{01}(\text{atm}) = 3.7109859 - \frac{298.12324}{T} - \frac{2257.2649}{T^2} \qquad \text{(D-5)}$$

$$T > 88.0^{\circ}K$$

$$\log p_{01}(\text{atm}) = \frac{-550.8211}{T} - 8.7849395 \log(T) \qquad \text{(D-6)}$$

$$+ 0.0174713 \times T + 21.83790$$

Values of the vapor pressure of argon used in this work are presented in Table 18. The values between 20 and 80°K were taken directly from Ziegler et al.[109]

The molal volume data of solid argon are from Ziegler et al.[109] A smooth curve was drawn through the values recommended by them. The molal volumes of solid argon used in this work are presented in Table 18.

Table 18. Vapor Pressure, Molal Volume of Solid and Liquid Argon

T, °K	p_{01}	a**	b	c
		Solid		
20	4.54(-14)*mm Hg	0.02235	0.0	0.0
24	1.48(-10)	0.02248	0.0	0.0
30	4.95(-7)	0.02265	0.0	0.0
34	2.27(-5)	0.02279	0.0	0.0
40	1.68(-3)	0.02299	0.0	0.0
44	1.54(-2)	0.02312	0.0	0.0
50	2.18(-1)	0.02331	0.0	0.0
55	1.273	0.02348	0.0	0.0
60	5.508	0.02365	0.0	0.0
65	18.946	0.02382	0.0	0.0
70	54.437	0.02401	0.0	0.0
75	135.53	0.02421	0.0	0.0
80	300.64	0.02443	0.0	0.0
68.07	0.048 atm	0.02393	0.0	0.0
74.05	0.151	0.02417	0.0	0.0
77.90	0.286	0.02433	0.0	0.0
80.06	0.398	0.02443	0.0	0.0
		Liquid		
86.02	0.871 atm	0.028511832	-0.79350390(-5)	0.27430468(-7)
91.98	1.605	0.029357910	-0.10644109(-4)	0.27430468(-7)
97.51	2.624	0.030227803	-0.13157875(-4)	0.27431250(-7)
108.02	5.777	0.032106262	-0.17935171(-4)	0.27431250(-7)

* Number in parentheses indicates powers of 10.

** Molal Volume, $v_l = a + b(P - p_{01}) + c(P - p_{01})^2$, liter/gm mole where P is in atm.

The molal volume data for liquid argon over the region of interest here have been least-squares fitted with orthogonal polynomials in temperature and pressure by Mullins.[64] The data were from van Itterbeek and Verbeke,[102] and van Itterbeek et al.[104] The data covered 86.6 to 148°K and up to 290 atmospheres. Mullins[64] fitted the data up to 130°K and 150 atmospheres. The average deviation of his fit (a quadratic both in temperature and pressure) was 0.1926 per cent in the molal volume. His values of the orthogonal coefficients, weighting factors, and normalizing constants were used in this work. However, they are not reproduced here. The coefficients of the quadratic in pressure of the molal volumes at various temperatures are presented in Table 18.

Methane

The Lennard-Jones (6-12) and Kihara core parameters for methane are presented in Table 15. The Lennard-Jones (6-12) parameters are those of Ziegler et al.[110] They plotted the available second virial coefficient of methane and drew a smooth curve through the data. They selected eight points between 108.45 and 280°K and least-squares fitted them to obtain the Lennard-Jones parameters. The Kihara core parameters are from Prausnitz and Myers.[77] The calculated and experimental second virial coefficient for methane are shown in Figure 23. Below 95°K the Lennard-Jones model predicts a second virial coefficient that is higher than that of the Kihara core model. Above 95°K the Kihara core model second virial coefficient is slightly higher than that of the Lennard-Jones model. But both models represent the second virial coefficient data equally well.

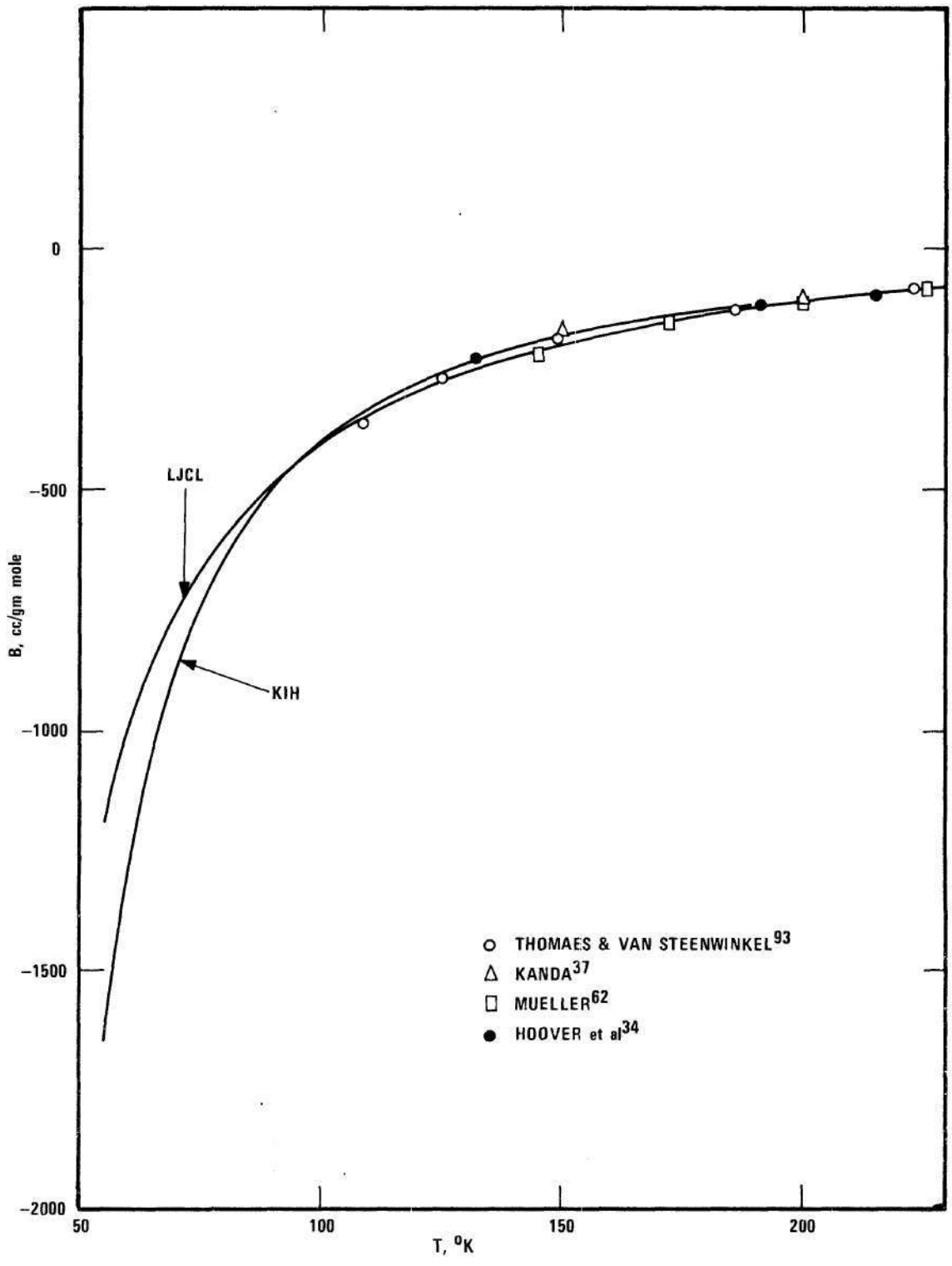

Figure 23. Second Virial Coefficient of Methane.

The calculated vapor pressure of methane by Ziegler et al[110] has been least-squares fitted by Kirk[45] to give Equations (D-7) and (D-8)

$$35.0^{\circ}K \leq T \leq 90.652^{\circ}K \text{ (triple point)}$$

$$\log P(\text{mm Hg}) = 7.3058842 - \frac{453.92414}{T} - \frac{4055.6016}{T^2} + \frac{115352.19}{T^3} - \frac{1165560.7}{T^4} \qquad \text{(D-7)}$$

$$90.652^{\circ}K < T \leq 111.648^{\circ}K \text{ (normal boiling point)}$$

$$\log P(\text{mm Hg}) = 6.7822220 - \frac{437.54809}{T} + \frac{1598.8512}{T^2} - \frac{154567.02}{T^3} \qquad \text{(D-8)}$$

Equations (D-7) and (D-8) were used in this work to calculate the vapor pressure of methane below $111.648^{\circ}K$. Above $111.648^{\circ}K$ the vapor pressure of methane was calculated with Equation (D-9).

$$\log P(\text{mm Hg}) = 10.685962 - \frac{595.546}{(T + 0.01)} - 0.0348039 \times T + 1.33375 \times 10^{-4} \times T^2 - 1.7869 \times 10^{-7} \times T^3 \qquad \text{(D-9)}$$

Equation (D-9) is from Armstrong et al.,[2] and has been modified by Kirk[45] to correct for the fact that Armstrong et al. used a temperature scale $0.01^{\circ}K$ higher than that used by Kirk, and also used in this work. The temperature scale of Ziegler et al.[110] was also corrected before being used to obtain Equations (D-7) and (D-8). Ziegler et al.[110] used a temperature scale based on the defined oxygen point of $90.168^{\circ}K$ and

assigned an ice point of 273.15°K. The temperature scale is used by Kirk[45] and here is based on an oxygen and ice point of 90.18°K and 273.15°K, respectively. The method of the temperature scale correction is discussed by Ziegler et al.[110] The choice of Equation (D-9) was based on its agreement with the normal boiling point at 111.648°K.

The vapor pressures of methane used in this work are presented in Table 20. The values between 20 and 90°K at five-degree intervals were taken directly from Ziegler et al.[110]

The data for the molal volume of solid methane have been reviewed and presented by Kirk et al.[47] Their values were selected for use in this work. The molal volumes of solid methane used are presented in Table 20.

Keyes et al.[40] have measured the saturated liquid density of methane between 100.9 and 190.38°K. Van Itterbeek et al.[104] have measured the density of liquid methane between 114.53 and 188.19°K and up to 290 atmospheres. The smoothed data of Keyes et al.[40] and those of van Itterbeek et al.[104] up to 210 atmospheres were least-squares fitted to orthogonal polynomials in temperature and pressure. For a third degree in temperature and second degree in pressure, the polynomial fitted the data with an average deviation of 1.04 per cent in the molal volume. Table 19 presents the orthogonal coefficients, weighting factors, and normalizing constants for the least-squares fit. The coefficients for the quadratic in pressure for the molal volume of liquid methane at various temperatures are presented in Table 20.

Table 19. Least-Squares Fit of the Molal Volume of Liquid Methane

Coefficients, α_{ij}				
i j	1	2	3	4
0	0.82671445	0.34518192	0.69976554	0.28370685
1		-0.10178893	0.16064943	0.22226583
2			-0.76153455(-2)	0.80348330
3				0.17727656
j	5	6	7	8
0	0.21257731	0.60470523	0.23816931	0.17249224
1	-0.19919307	0.19656845(1)	0.42433569	0.20050473(-1)
2	0.85420598	-0.17714681(-1)	0.65862331	0.68380305
3	-0.71128660(-3)	0.23838295(1)	0.55457929	-0.54828783(-2)
4	-0.22247567	-0.11788144(-1)	0.15915306(1)	0.62892507
5		-0.16751171(-2)	-0.11502536(-1)	0.79963456
6			0.49906314	0.16072368
7				-0.9826047(-1)

Weighting Factors, C_j				
j	0	1	2	3
	0.67273726	0.63452694	-0.10470382	0.10218289(1)
j	4	5	6	7
	-0.62564709	0.10664774	0.21131322(1)	-0.25542888(1)
j	8			
	0.99375548			

Normalizing Constants		
T_{max} = 188.19	$(P - p_{01})_{max}$ = 212.54427	$(V_1^L)_{max}$ = 0.67547708(-1)

Table 20. Vapor Pressure, Molal Volume of Solid and Liquid Methane

T, °K	p_{01}	a**	b	c
		Solid		
20	3.810(-18)*mm Hg	0.03004	0.0	0.0
25	1.345(-13)	0.03024	0.0	0.0
30	3.248(-10)	0.03043	0.0	0.0
35	8.742(-8)	0.03063	0.0	0.0
40	5.912(-6)	0.03083	0.0	0.0
45	1.582(-4)	0.03102	0.0	0.0
50	2.202(-3)	0.03122	0.0	0.0
55	1.902(-2)	0.03142	0.0	0.0
60	1.146(-1)	0.03162	0.0	0.0
65	5.228(-1)	0.03182	0.0	0.0
70	1.916	0.03202	0.0	0.0
75	5.890	0.03221	0.0	0.0
80	15.698	0.03241	0.0	0.0
85	37.200	0.03261	0.0	0.0
90	79.946	0.03280	0.0	0.0
55	0.2495(-4)atm	0.03142	0.0	0.0
60	0.1503(-3)	0.03162	0.0	0.0
65	0.6862(-3)	0.03182	0.0	0.0
70	0.2514(-2)	0.03202	0.0	0.0
76	0.9507(-2)	0.03225	0.0	0.0
80	0.2061(-1)	0.03241	0.0	0.0
87	0.6707(-1)	0.03268	0.0	0.0
		Liquid		
91.0	0.121 atm	0.03560	-0.76923(-5)	0.0
94.97	0.195	0.03597	-0.76923(-5)	0.0
109.90	0.863	0.03760	-0.76923(-5)	0.0
113.15	1.130	0.03805	-0.76923(-5)	0.0
124.85	2.639	0.039506863	0.56022187(-5)	-0.77219531(-7)
133.15	4.379	0.040858625	-0.60242578(-5)	-0.11682031(-7)
139.83	6.295	0.042152876	-0.17586960(-4)	0.41060156(-7)
153.15	11.829	0.045525928	-0.46516234(-4)	0.14623203(-6)
154.80	12.699	0.046034460	-0.50644492(-4)	0.15926171(-6)
169.81	22.863	0.051820267	-0.93710351(-4)	0.27777500(-6)
173.15	25.743	0.053431440	-0.10464435(-3)	0.30414687(-6)
184.83	37.886	0.060162225	-0.14674840(-3)	0.39636963(-6)
188.15	41.980	0.062416110	-0.15981434(-3)	0.42259062(-6)

* Number in parentheses indicates powers of 10.

** Molal Volume, $v_1 = a + b(P - p_{01}) + c(P - p_{01})^2$, liter/gm mole where P is in atm.

Nitrogen

The nitrogen Lennard-Jones (6-12) and Kihara core model parameters are presented in Table 15. The Lennard-Jones parameters are from Ziegler and Mullins.[108] The Kihara parameters are from Prausnitz and Myers,[77] and include a quadrupole correction. Ziegler and Mullins[108] took the second virial coefficient of nitrogen from 69.57 to 373°K and least-squares fitted them to obtain the Lennard-Jones parameters. Figure 24 (reproduced from Figure 8 of Ziegler and Mullins[108]) shows the calculated and experimental second virial coefficients for nitrogen. The data of Canfield et al.[9] and Hoover et al.[33] which are in excellent agreement with each other and also with the other data, have been added to Figure 24. Both the Lennard-Jones and Kihara core models represent the data equally well. Below 100°K the Kihara core model is lower than the Lennard-Jones model, but it is higher above 100°K.

Ziegler and Mullins[108] have calculated the vapor pressure of nitrogen below one atmosphere. In the liquid range their calculated vapor pressure was in excellent agreement with the experimental data. Armstrong's[1] equation for the vapor pressure of liquid nitrogen below one atmosphere gives a normal boiling point of 77.364°K. This equation was modified to calculate a normal boiling point of 77.347°K, which was the value selected by Ziegler and Mullins.[108] The modified equation, Equation (D-10), represented the vapor pressure of nitrogen below 90.90°K well and was selected for use here.

$$64^{\circ}K \leq T \leq 90.90^{\circ}K$$

$$\log p_{01}(\text{mm Hg}) = 6.49594 - \frac{255.821}{(T - 6.583)} \qquad \text{(D-10)}$$

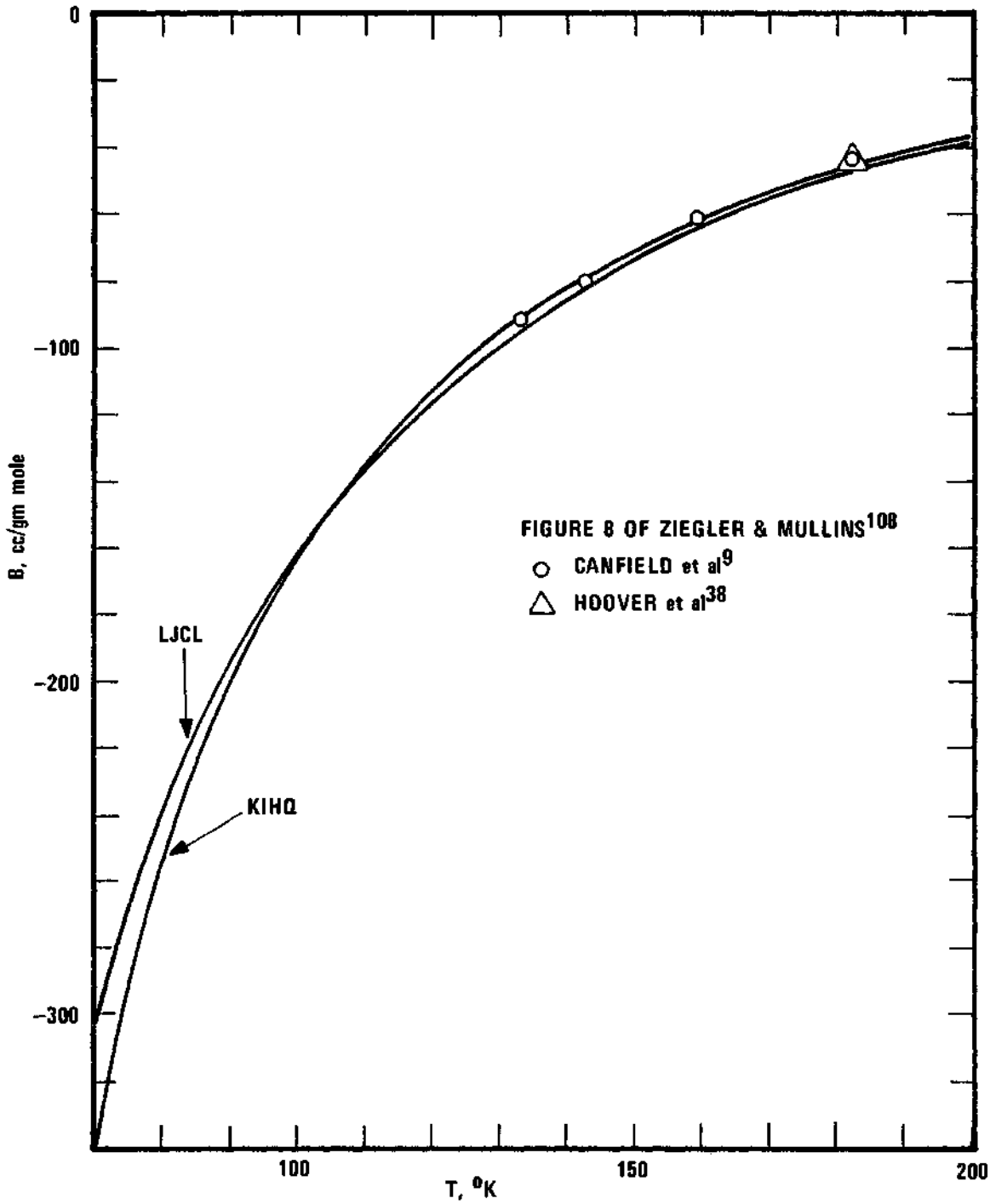

Figure 24. Second Virial Coefficient of Nitrogen.

Above 90.90°K the vapor pressure equation of Michels et al.[60] was selected for use in this work. It is written as Equation (D-11) below.

$$\log p_{01}(\text{atm}) = -\frac{634.3337}{T} - 15.33647 \times \log T + 0.0332183 \times T + 34.58230 \qquad \text{(D-11)}$$

Michels et al.[60] have compared their data (96.853 to 125.238°K) with other available data. They concluded that their critical point data are more consistent with the vapor pressure measurements than those of the other investigators. However, all the vapor pressure data considered by Michels et al. agreed within 0.10 atmospheres. Michel et al. (whose temperature scale is the same as used here) point out that part of the differences between the different data could be attributed to the different temperature scales.

The vapor pressure of liquid nitrogen used here are presented in Table 22. The vapor pressure of solid nitrogen were from Ziegler and Mullins.[108]

Ziegler and Mullins[108] have reviewed the density data for solid nitrogen. Their data were used in this work to calculate the molal volumes of solid nitrogen, which are shown in Table 22.

Van Itterbeek and Verbeke[102] have measured the density of liquid nitrogen from 68.85 to 90.60°K and up to 145 atmospheres. Van Itterbeek and Verbeke[103] measured the density of liquid nitrogen at 77.31°K and 90.26°K and up to 815 atmospheres. The density of saturated liquid nitrogen has also been measured by Baly and Donnan[3] (68.8 to 83.7°K) and by Mattias et al.[55] (64.7 to 125.0°K). More recently, Streett and

Table 21. Least-Squares Fit of the Molal Volume of Liquid Nitrogen

Coefficients, α_{ij}				
i j	1	2	3	4
0	0.75305112	0.41726170	0.58733003	0.31864737
1		0.21873180	0.15235478(1)	0.56624003
2			-0.53721438(-2)	0.78628952
3				0.14357654
j	5	6	7	8
0	0.24872371	0.47313226	0.25142070	0.19337500
1	0.30000591	0.17792260(1)	0.74213675	0.45680163
2	0 88287650	-0.12786905(-1)	0.63375218	0.70113401
3	-0.32502884	0.22808015(1)	0.62321604	-0.57741037(-1)
4	0.41823695	-0.30998698(-2)	0.15456238(1)	0.11329720(1)
5		-0.33261609(-2)	-0.17021830(-1)	0.79221780
6			0.86347339(-1)	-0.20579851
7				0.40969919

Weighting Factors, C_j				
j	0	1	2	3
	0.59155954	0.48344210	-0.93670881(-1)	0.65552763
j	4	5	6	7
	-0.50734181	0.12216734	0.13179400(1)	-0.17290769(1)
j	8			
	0.96624683			

Normalizing Constants		
T_{max} = 125.00	$(P - p_{01})_{max}$ = 194.63531	$(V_1^L)_{max}$ = 0.64120940(-1)

Table 22. Vapor Pressure, Molal Volume of Solid and Liquid Nitrogen

T, °K	p_{01}	a**	b	c
		Solid		
20	1.085(-11)*mm Hg	0.02729	0.0	0.0
25	7.844(-8)	0.02752	0.0	0.0
30	2.965(-5)	0.02775	0.0	0.0
35	2.028(-3)	0.02799	0.0	0.0
40	4.332(-2)	0.02821	0.0	0.0
45	4.569(-1)	0.02845	0.0	0.0
50	2.968	0.02870	0.0	0.0
55	13.544	0.02895	0.0	0.0
60	47.486	0.02921	0.0	0.0
		Liquid		
64.9	0.169 atm	3.20364120(-2)	2.66129748(-5)	-2.91383209(-7)
69.3	0.344	3.26834504(-2)	2.29954132(-5)	-2.33814384(-7)
77.0	0.960	3.40178926(-2)	1.24903914(-5)	-1.33068941(-7)
80.0	1.351	3.46345000(-2)	6.95935164(-6)	-9.38174688(-8)
85.0	2.253	3.58177261(-2)	-4.05116505(-6)	-2.83983497(-8)
90.0	3.535	3.72316689(-2)	-1.73018282(-5)	3.70207687(-8)
95.0	5.365	3.89181934(-2)	-3.27926379(-5)	1.02439888(-7)
100.0	7.724	4.09191644(-2)	-5.05235940(-5)	1.67859007(-7)
105.0	10.741	4.32764470(-2)	-7.04946967(-5)	2.33278126(-7)
110.0	14.517	4.60319061(-2)	-9.27059459(-5)	2.98697245(-7)
115.0	19.170	4.92274065(-2)	-1.17157342(-4)	3.64115365(-7)
120.0	24.836	5.29048133(-2)	-1.43848884(-4)	4.29535483(-7)

* Number in parentheses indicates powers of 10.

** Molal Volume, $v_l = a + b(P - p_{01}) + c(P - p_{01})^2$, liter/gm mole where P is in atm.

Staveley's data became available after this work was well in progress and were therefore not incorporated here. However, the agreement between the values of the molal volume of liquid nitrogen used here and those of Streett and Staveley is within 1.6 per cent at 80°K and within 2.5 per cent at 120°K over the pressure range of up to 150 atmospheres. The remaining source of data for the molal volume of liquid nitrogen was Strobridge,[92] who used a Benedict-Webb-Rubin type of equation of state to compute the thermodynamic properties of nitrogen. The data of van Itterbeek and Verbeke,[102] van Itterbeek and Verbeke[103] (up to 193 atmospheres), and the calculated data of Strobridge[92] (saturation data, and from 65 to 125°K and up to 200 atmospheres) were least-squares fitted. The orthogonal polynomial of third degree in temperature and second degree in pressure fitted the data with an average deviation of 1.18 per cent of the molal volume. The orthogonal coefficients, weighting factors, and normalizing constants of the polynomial are presented in Table 21. The coefficients of the quadratic in pressure for the molal volume of liquid nitrogen at various temperatures are presented in Table 22.

Oxygen

The Lennard-Jones (6-12) and Kihara core parameters for oxygen are shown in Table 15. The Lennard-Jones (6-12) parameters are from Mullins et al.[68] The Kihara parameters are from Prausnitz and Myers.[77] Mullins et al.[68] adjusted (for the method see the reference) the Lennard-Jones parameters from Hirschfelder et al.[29] to give better agreement with the second virial coefficient data of Nijhoff and Keesom[69] and those of

Cath and Kamerlingh-Onnes.[10] They found the adjusted parameters gave better agreement between their calculated and the experimental vapor pressure of oxygen. Figure 25 shows the calculated and experimental second virial coefficient of oxygen. There is large scatter in the experimental data below 100°K. Below 115°K the Lennard-Jones model is higher than the Kihara model. Above 115°K the Kihara model is slightly higher. However, both models represent the data about equally well.

Stewart et al.[90] have made a comprehensive review of the vapor pressure of oxygen. Hoge's[32] measurements of the vapor pressure of oxygen from its triple point (54.353°K) to the critical point (154.770°K) were considered the most complete and accurate. Stewart et al.[90] corrected Hoge's temperature scale to the NBS 1955 scale by subtracting 0.01°K from Hoge's values. They then least-squares fitted Hoge's data to pass through the triple point, the normal boiling point (90.180°K), and the critical point. Equation (D-12) used in this work was the equation they obtained.

$$\ell n\, p_{01}(\text{atm}) = -62.5967185 + 2.47450429 \times T - 4.68973315 \times 10^{-2} \quad \text{(D-12)}$$
$$\times T^2 + 5.48202337 \times 10^{-4} \times T^3 - 4.09349868 \times 10^{-6}$$
$$\times T^4 + 1.91471914 \times 10^{-8} \times T^5 - 5.13113688 \times 10^{-11}$$
$$\times T^6 + 6.02656934 \times 10^{-14} \times T^7$$

Equation (D-12) agrees with Hoge's smoothed data (which differs by less than 4 mm Hg from his observed values) to within 0.02 atmospheres. Below the triple point the calculated vapor pressure of Mullins et al.[68]

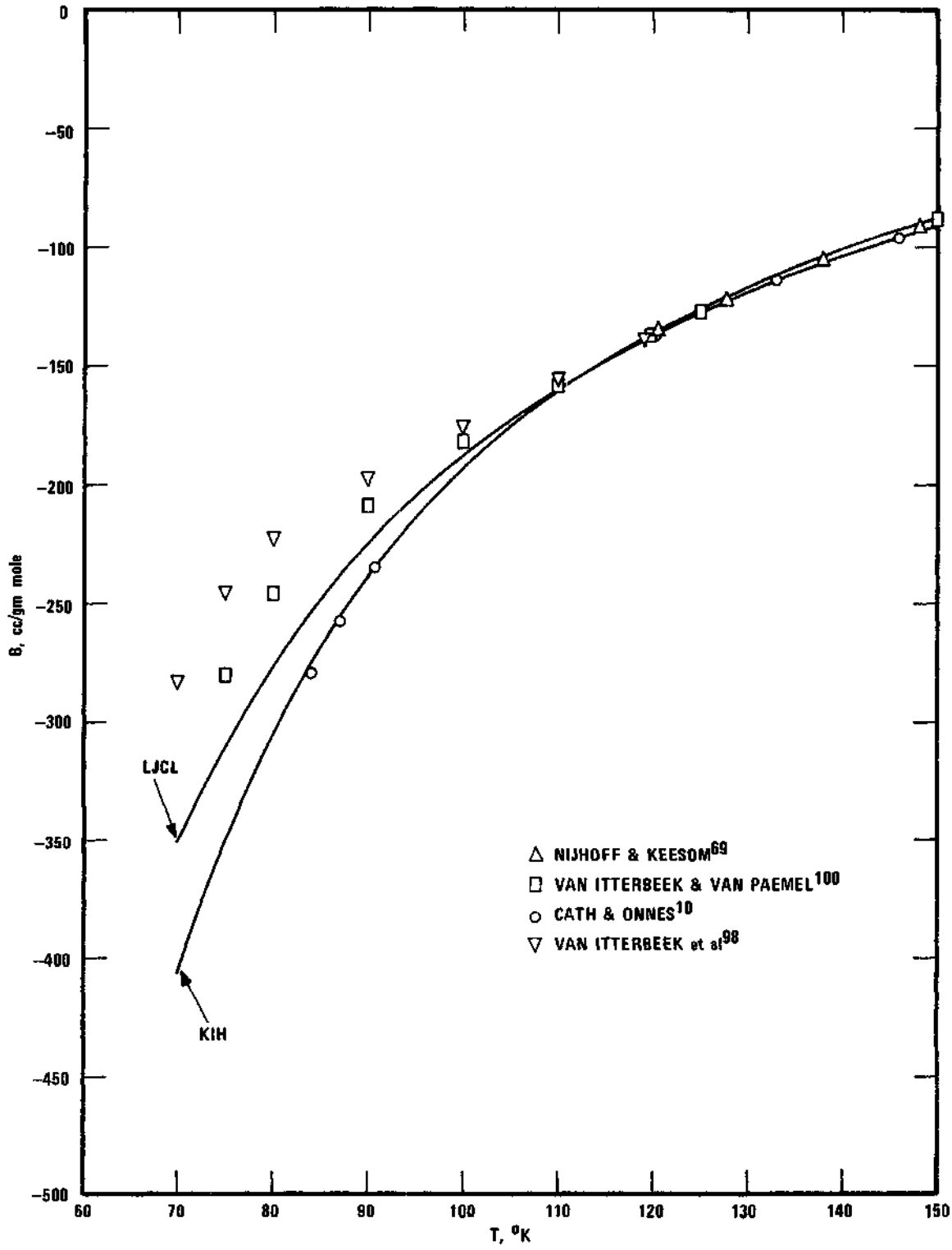

Figure 25. Second Virial Coefficient of Oxygen.

were used. The vapor pressures of oxygen used are presented in Table 24.

The density of liquid oxygen has been measured by van Itterbeek and Verbeke[101] (77.35 and 90.07°K, up to 85 atmospheres), by van Itterbeek and Verbeke[103] (64.66 to 90.29°K, up to 145 atmospheres), and by Timrot and Borisoglebskii[94,95] (83.15 to 153.15°K and up to 195 atmospheres). According to Stewart et al.,[90] Weber (private communication to Stewart et al.) has made extensive measurements of the density of liquid oxygen, which are unpublished. Stewart et al.[90] state that the data of Weber and van Itterbeek and Verbeke[101] agree within the precision of the data sets, while the data of Timrot and Borisoglebskii[94,95] are consistently lower by 0.3 to 0.6 per cent. This last was confirmed by a comparison of the isotherms between 83 and 93°K. The saturated density data and density data between 93.15 and 153.15°K (and up to 195 atmospheres) of Timrot and Borisoglebskii[94,95] together with the data of van Itterbeek and Verbeke[101] were selected for use here. These data were least-squares fitted to an orthogonal polynomial of third degree in temperature and second degree in pressure. The average deviation of the fit was 1.51 per cent of the molal volume. The orthogonal coefficients, weighting factors, and normalizing constants are presented in Table 23. The coefficients of the quadratic in pressure for the molal volume at various temperatures are presented in Table 24.

Table 23. Least-Squares Fit of the Molal Volume of Liquid Oxygen

Coefficients, α_{ij}

i \ j	1	2	3	4
0	0.70012669	0.39147773	0.51927890	0.27201180
1		-0.71201509(-1)	0.14361175	0.31939793
2			-0.68895931(-2)	0.71630024
3				-0.13082163

j	5	6	7	8
0	0.23652100	0.40535373	0.19973753	0.16536251
1	-0.79746871(-2)	0.16018189(1)	0.48966375	0.20027205
2	0.84430531	-0.15356107(-1)	0.53447414	0.60244389
3	-0.54105197	0.21316542(1)	0.18570009	-0.44977560
4	-0.94671606(-1)	-0.68046372(-2)	0.14491451(1)	0.71708621
5		-0.20944893(-2)	-0.20985828(-1)	0.71819266
6			-0.11254049	-0.33883510
7				-0.16060026

Weighting Factors, C_j

j	0	1	2	3
	0.57219662	0.51436793	-0.72539633(-1)	0.81639822
j	4	5	6	7
	-0.46091153	0.10097628	0.17554440(1)	-0.18125896(1)
j	8			
	0.83603657			

Normalizing Constants

T_{max} = 153.15 $(P - p_{01})_{max}$ = 190.33288 $(V_l^L)_{max}$ = 0.54233735(-1)

Table 24. Vapor Pressure, Molal Volume of Solid and Liquid Oxygen

T, °K	p_{01}	a**	b	c
		Solid		
20	1.006(-15)* mm Hg	0.0219	0.0	0.0
24	1.108(-11)	0.0229	0.0	0.0
30	1.156(-7)	0.0229	0.0	0.0
34	9.046(-6)	0.0229	0.0	0.0
40	1.204(-3)	0.0229	0.0	0.0
44	1.457(-2)	0.02462	0.0	0.0
50	2.243(-1)	0.02462	0.0	0.0
		Liquid		
55	0.182(-2) atm	0.02431	-1.55(-6)	0.0
60	0.720(-2)	0.02492	-1.95(-6)	0.0
65	0.229(-1)	2.51701788(-2)	2.51036307(-5)	-2.63445994(-7)
70	0.614(-1)	2.56245477(-2)	2.37512383(-5)	-2.22583944(-7)
75	0.143	2.60771490(-2)	2.13793934(-5)	-1.81721893(-7)
80	0.297	2.65489293(-2)	1.79880961(-5)	-1.40859843(-7)
85	0.561	2.70608352(-2)	1.35773464(-5)	-9.99977925(-8)
90	0.981	2.76338133(-2)	8.14714428(-6)	-5.91357419(-8)
95	1.611	2.82888102(-2)	1.69748975(-6)	-1.82736918(-8)
100	2.509	2.90467726(-2)	-5.77161720(-6)	2.25883583(-8)
105	3.738	2.99286470(-2)	-1.42601766(-5)	6.34504089(-8)
110	5.363	3.09553801(-2)	-2.37681884(-5)	1.04312459(-7)
115	7.454	3.21479184(-2)	-3.42956527(-5)	1.45174510(-7)
120	10.082	3.35272086(-2)	-4.58425693(-5)	1.86036560(-7)
125	13.321	3.51141973(-2)	-5.84089384(-5)	2.26898610(-7)
130	17.249	3.69298311(-2)	-7.19947599(-5)	2.67760661(-7)
135	21.947	3.89950567(-2)	-8.66000338(-5)	3.08622711(-7)
140	27.501	4.13308205(-2)	-1.02224760(-4)	3.49484761(-7)
145	34.018	4.39580693(-2)	-1.18869939(-4)	3.90346812(-7)
150	41.638	4.68977497(-2)	-1.36532570(-4)	4.31208862(-7)
69.60	0.060	2.5615541(-2)	2.3788289(-5)	-2.2340156(-7)
75.90	0.164	2.6160046(-2)	2.0844062(-5)	-1.7436562(-7)
89.98	0.979	2.7631365(-2)	8.1708671(-6)	-5.9300000(-8)
109.96	5.348	3.0946539(-2)	-2.3688195(-5)	1.0398593(-7)
129.95	17.209	3.6910471(-2)	-7.1854085(-5)	2.6735390(-7)
143.93	32.534	4.3370267(-2)	-1.1522142(-4)	3.8160312(-7)
149.91	41.497	4.6841938(-2)	-1.3620567(-4)	4.3047421(-7)

* Number in parentheses indicates powers of 10.

** Molal Volume, $v_l = a + b(P - p_{01}) + c(P - p_{01})^2$, liter/gm mole where P is in atm.

APPENDIX F

SUMMARY OF SMOOTHED EXPERIMENTAL AND THEORETICAL ENHANCEMENT FACTORS, AND SMOOTHED EXPERIMENTAL SOLUBILITY OF HELIUM

This appendix summarizes the smoothed experimental Enhancement Factor and the solubility of helium in the liquid phase for the different systems. Also presented are the theoretical Enhancement Factors for the four models used here to represent the vapor phase. Tables 25 through 29 present these data for the helium-carbon dioxide, -argon, -methane, -nitrogen, and -oxygen systems, respectively. The experimental data were smoothed graphically.

Table 25. Smoothed Experimental, Theoretical Enhancement Factor of Carbon Dioxide in Helium, and the Smoothed Experimental Solubility of Helium in Liquid Carbon Dioxide

P, atm	ϕ (exp)	ϕ (LJCL)	ϕ (LJCLA)	ϕ (KIHQ)	$100x_2$
		181.05°K (This Work)			
20	1.035	1.015	1.034	1.040	0.0[a]
40	1.058	1.022	1.059	1.071	0.0
60	1.076	1.027	1.083	1.099	0.0
80	1.093	1.030	1.105	1.126	0.0
100	1.109	1.032	1.125	1.151	0.0
120	1.129	1.032	1.143	1.175	0.0
		190.03°K (This Work)			
20	1.041	1.018	1.034	1.042	0.0
40	1.069	1.022	1.055	1.069	0.0
60	1.090	1.023	1.073	1.094	0.0
80	1.107	1.023	1.089	1.117	0.0
100	1.124	1.022	1.104	1.138	0.0
120	1.142	1.019	1.117	1.158	0.0
		199.95°K (This Work)			
20	1.038	1.027	1.041	1.051	0.0
40	1.067	1.028	1.057	1.074	0.0
60	1.090	1.026	1.071	1.096	0.0
80	1.112	1.023	1.082	1.115	0.0
100	1.134	1.019	1.093	1.133	0.0
120	1.155	1.014	1.101	1.149	0.0
		219.9°K (Barrick et al.[4])			
20	1.072	1.070	1.077	1.088	0.042
40	1.121	1.088	1.109	1.132	0.150
60	1.150	1.094	1.130	1.165	0.310
80	1.172	1.098	1.147	1.193	0.485
100	1.191	1.097	1.162	1.219	0.660
120	1.207	1.097	1.175	1.244	0.835
140	1.223	1.095	1.186	1.266	1.005
160	1.236	1.092	1.196	1.287	1.170
180	1.251	1.087	1.204	1.306	1.330
200	1.265	1.082	1.211	1.324	1.475

Table 25 (continued)

P, atm	ϕ (exp)	ϕ (LJCL)	ϕ (LJCLA)	ϕ (KIHQ)	$100x_2$
		229.9°K (Barrick et al.[4])			
20	1.052	1.073	1.077	1.086	0.130
40	1.117	1.103	1.120	1.143	0.358
60	1.165	1.112	1.143	1.179	0.585
80	1.202	1.114	1.159	1.207	0.820
100	1.230	1.114	1.172	1.233	1.050
120	1.252	1.112	1.183	1.257	1.270
140	1.268	1.109	1.192	1.279	1.485
160	1.282	1.105	1.201	1.299	1.682
180	1.295	1.100	1.208	1.319	1.855
200	1.306	1.096	1.215	1.338	2.000
		244.9°K (Barrick et al.[4])			
20	1.040	1.047	1.048	1.052	0.090
40	1.127	1.121	1.132	1.150	0.440
60	1.177	1.142	1.165	1.199	0.790
80	1.216	1.147	1.183	1.232	1.130
100	1.248	1.146	1.195	1.259	1.455
120	1.275	1.141	1.203	1.281	1.765
140	1.300	1.135	1.209	1.302	2.065
160	1.322	1.128	1.213	1.320	2.345
180	1.343	1.120	1.217	1.338	2.610
200	1.363	1.113	1.220	1.355	2.850
		259.9°K (Barrick et al.[4])			
40	1.105	1.110	1.114	1.124	0.420
60	1.189	1.161	1.176	1.203	0.925
80	1.248	1.179	1.206	1.250	1.405
100	1.297	1.183	1.222	1.284	1.830
120	1.334	1.179	1.230	1.309	2.220
140	1.366	1.171	1.234	1.329	2.600
160	1.392	1.160	1.235	1.346	2.970
180	1.416	1.148	1.234	1.360	3.330
200	1.438	1.136	1.232	1.373	3.695

Table 25 (continued)

P, atm	ϕ (exp)	ϕ (LJCL)	ϕ (LJCLA)	ϕ (KIHQ)	$100x_2$
		274.9°K (Barrick et al.[4])			
40	1.042	1.035	1.035	1.036	0.160
60	1.182	1.144	1.150	1.165	0.945
80	1.265	1.192	1.208	1.241	1.665
100	1.325	1.210	1.238	1.289	2.370
120	1.371	1.210	1.250	1.320	3.060
140	1.407	1.201	1.252	1.341	3.735
160	1.435	1.185	1.248	1.353	4.425
180	1.458	1.164	1.236	1.358	5.215
200	1.479	1.140	1.221	1.357	6.090

[a]Solid phase assumed to be pure carbon dioxide

Table 26. Smoothed Experimental, Theoretical Enhancement Factor of Argon in Helium, and the Smoothed Experimental Solubility of Helium in Liquid Argon

P, atm	ϕ (exp)	ϕ (LJCL)	ϕ (LJCLA)	ϕ (KIH)	$100x_2$
		68.07°K (Mullins[64])			
20	1.178	1.238	1.192	1.283	0.0[a]
40	1.378	1.504	1.397	1.611	0.0
60	1.585	1.800	1.617	1.990	0.0
80	1.795	2.128	1.853	2.423	0.0
100	2.005	2.488	2.105	2.913	0.0
120	2.214	2.883	2.373	3.464	0.0
		74.05°K (Mullins[64])			
20	1.158	1.197	1.160	1.234	0.0
40	1.322	1.407	1.323	1.493	0.0
60	1.487	1.635	1.495	1.783	0.0
80	1.652	1.881	1.676	2.105	0.0
100	1.817	2.147	1.865	2.462	0.0
120	1.982	2.432	2.064	2.854	0.0
		80.06°K (Mullins[64])			
20	1.137	1.171	1.141	1.204	0.0
40	1.271	1.343	1.276	1.416	0.0
60	1.402	1.527	1.415	1.649	0.0
80	1.531	1.722	1.560	1.903	0.0
100	1.658	1.929	1.710	2.179	0.0
120	1.787	2.148	1.865	2.479	0.0
		77.90°K (Mullins[64])			
80.0	1.570	1.771	1.596	1.965	0.0
60.14	1.430	1.561	1.441	1.692	0.0
		86.02°K (Mullins[64])			
20	1.141	1.168	1.143	1.197	0.146
40	1.270	1.328	1.271	1.393	0.289
60	1.395	1.499	1.403	1.607	0.425
80	1.517	1.680	1.541	1.840	0.552
100	1.637	1.873	1.685	2.094	0.670
120	1.760	2.078	1.835	2.372	0.772

Table 26 (continued)

P, atm	ϕ (exp)	ϕ (LJCL)	ϕ (LJCLA)	ϕ (KIH)	$100x_2$
		91.98°K (Mullins[64])			
20	1.136	1.161	1.141	1.186	0.201
40	1.257	1.303	1.255	1.360	0.393
60	1.368	1.452	1.372	1.548	0.572
80	1.474	1.610	1.492	1.750	0.745
100	1.577	1.775	1.617	1.968	0.910
120	1.677	1.950	1.746	2.204	1.072
		97.51°K (Mullins[64])			
20	1.124	1.159	1.143	1.181	0.240
40	1.240	1.291	1.250	1.342	0.498
60	1.346	1.429	1.357	1.513	0.748
80	1.446	1.569	1.466	1.696	0.982
100	1.542	1.717	1.578	1.892	1.208
120	1.636	1.873	1.694	2.103	1.405
		108.02°K (Mullins[64])			
60	1.336	1.411	1.356	1.484	1.141
80	1.429	1.538	1.455	1.648	1.515
100	1.517	1.669	1.555	1.824	1.880
120	1.602	1.806	1.657	2.013	2.215

[a]Solid phase assumed to be pure argon

Table 27. Smoothed Experimental, Theoretical Enhancement Factor of Methane in Helium, and the Smoothed Experimental Solubility of Helium in Liquid Methane

P, atm	ϕ (exp)	ϕ (LJCL)	ϕ (LJCLA)	ϕ (KIH)	$100x_2$
		55.0°K (Hiza and Kidnay[31])			
10	1.144	1.299	1.181	1.335	0.0[a]
20	1.325	1.661	1.377	1.751	0.0
30	1.524	2.091	1.588	2.260	0.0
40	1.730	2.596	1.812	2.874	0.0
50	1.940	3.181	2.048	3.605	0.0
		60.0°K (Hiza and Kidnay[31])			
20	1.258	1.498	1.285	1.581	0.0
40	1.559	2.142	1.595	2.374	0.0
60	1.884	2.944	1.922	3.417	0.0
80	2.234	3.914	2.263	4.741	0.0
100	2.607	5.062	2.614	6.382	0.0
120	2.987	6.396	2.972	8.370	0.0
130	3.185	7.136	3.152	9.505	0.0
		65.0°K (Hiza and Kidnay[31])			
20	1.191	1.387	1.221	1.463	0.0
40	1.420	1.854	1.449	2.055	0.0
60	1.662	2.402	1.682	2.788	0.0
80	1.930	3.032	1.916	3.674	0.0
100	2.207	3.743	2.149	4.723	0.0
120	2.498	4.536	2.380	5.944	0.0
140	2.795	5.412	2.609	7.348	0.0
		70.0°K (Hiza and Kidnay[31])			
20	1.137	1.308	1.174	1.379	0.0
40	1.306	1.660	1.347	1.838	0.0
60	1.488	2.054	1.518	2.382	0.0
80	1.675	2.490	1.685	3.014	0.0
100	1.863	2.964	1.848	3.736	0.0
120	2.051	3.476	2.005	4.551	0.0
140	2.233	4.024	2.157	5.462	0.0

Table 27 (continued)

P, atm	ϕ (exp)	ϕ (LJCL)	ϕ (LJCLA)	ϕ (KIH)	$100x_2$
		76.0°K (Hiza and Kidnay[31])			
20	1.101	1.239	1.133	1.305	0.0
40	1.220	1.500	1.261	1.658	0.0
60	1.352	1.780	1.383	2.059	0.0
80	1.495	2.077	1.499	2.508	0.0
100	1.640	2.390	1.609	3.005	0.0
120	1.787	2.718	1.713	3.549	0.0
140	1.936	3.059	1.811	4.141	0.0
		80.0°K (Hiza and Kidnay[31])			
20	1.094	1.205	1.113	1.269	0.0
40	1.198	1.422	1.218	1.570	0.0
60	1.308	1.651	1.317	1.906	0.0
80	1.418	1.888	1.410	2.275	0.0
100	1.530	2.134	1.496	2.676	0.0
120	1.642	2.386	1.577	3.108	0.0
140	1.755	2.645	1.652	3.572	0.0
		87.0°K (Hiza and Kidnay[31])			
20	1.071	1.162	1.088	1.221	0.0
40	1.155	1.324	1.164	1.458	0.0
60	1.247	1.490	1.234	1.714	0.0
80	1.344	1.657	1.298	1.988	0.0
100	1.441	1.825	1.356	2.278	0.0
120	1.539	1.994	1.409	2.285	0.0
140	1.638	2.163	1.457	2.907	0.0
		91.0°K (Hiza and Kidnay[31])			
20	1.076	1.153	1.086	1.210	--
40	1.161	1.302	1.159	1.431	--
60	1.251	1.454	1.225	1.669	--
80	1.342	1.606	1.286	1.922	--
100	1.434	1.758	1.341	2.190	--
		94.97°K (Heck and Hiza[28])			
10	1.062	1.074	1.045	1.099	0.034
20	1.120	1.139	1.078	1.193	0.069
40	1.225	1.268	1.140	1.392	0.135
60	1.324	1.398	1.196	1.602	0.200
80	1.415	1.527	1.247	1.823	0.260
100	1.506	1.656	1.292	2.056	0.312
120	1.597	1.782	1.333	2.298	0.362
140	1.686	1.907	1.369	2.548	0.410
160	1.776	2.029	1.401	2.808	0.459
180	1.865	2.150	1.430	3.075	0.503

Table 27 (continued)

P, atm	ϕ (exp)	ϕ (LJCL)	ϕ (LJCLA)	ϕ (KIH)	$100x_2$
		109.90°K (Heck and Hiza[28])			
20	1.080	1.116	1.075	1.162	0.145
40	1.154	1.201	1.111	1.306	0.295
60	1.222	1.282	1.143	1.455	0.428
80	1.286	1.360	1.170	1.608	0.550
100	1.350	1.436	1.193	1.764	0.666
120	1.414	1.508	1.212	1.923	0.773
140	1.476	1.578	1.229	2.086	0.878
160	1.538	1.644	1.243	2.251	0.970
180	1.600	1.709	1.254	2.419	1.048
200	1.664	1.770	1.264	2.589	1.110
		124.85°K (Heck and Hiza[28])			
20	1.107	1.126	1.098	1.160	0.225
40	1.183	1.191	1.125	1.281	0.490
60	1.235	1.250	1.144	1.401	0.750
80	1.277	1.304	1.159	1.523	0.980
100	1.319	1.355	1.171	1.647	1.19
120	1.360	1.404	1.180	1.772	1.39
140	1.400	1.449	1.187	1.898	1.58
160	1.440	1.491	1.191	2.024	1.75
180	1.478	1.529	1.193	2.150	1.92
200	1.518	1.564	1.193	2.275	2.08
		154.80°K (Heck and Hiza[28])			
60	1.288	1.296	1.233	1.390	1.80
80	1.335	1.332	1.237	1.494	2.41
100	1.376	1.357	1.232	1.592	2.96
120	1.416	1.374	1.220	1.683	3.52
140	1.456	1.385	1.206	1.771	4.05
160	1.496	1.395	1.190	1.857	4.55
180	1.535	1.403	1.175	1.943	4.98
200	1.573	1.412	1.161	2.031	5.34
		169.81°K (Heck and Hiza[28])			
60	1.316	1.311	1.272	1.356	2.28
80	1.416	1.363	1.292	1.473	3.40
100	1.497	1.388	1.288	1.572	4.36
120	1.562	1.399	1.272	1.659	5.22
140	1.622	1.400	1.248	1.737	6.04
160	1.677	1.395	1.221	1.807	6.82

Table 27 (continued)

P, atm	ϕ (exp)	ϕ (LJCL)	ϕ (LJCLA)	ϕ (KIH)	$100x_2$
		184.83°K (Heck and Hiza[28])			
60	1.316	1.206	1.195	1.209	2.84
80	1.491	1.300	1.267	1.342	4.81
100	1.637	1.341	1.282	1.440	6.65
120	1.760	1.346	1.263	1.510	8.48
140	1.868	1.333	1.229	1.564	10.17
160	1.971	1.315	1.192	1.611	11.59
180	2.070	1.299	1.159	1.658	12.70
200	2.165	1.285	1.129	1.705	13.60
		113.15°K (Sinor et al.[87])			
40	1.333	1.191	1.107	1.293	0.65
50	1.379	1.227	1.120	1.360	0.84
60	1.425	1.262	1.132	1.429	1.02
80	1.515	1.330	1.153	1.568	1.36
90	1.561	1.363	1.163	1.639	1.51
100	1.606	1.396	1.171	1.711	1.65
110	1.650	1.427	1.179	1.783	1.79
120	1.695	1.458	1.186	1.855	1.94
130	1.741	1.488	1.192	1.928	2.07
		133.15°K (Sinor et al.[87])			
20	1.200	1.137	1.116	1.161	0.29
30	1.250	1.172	1.133	1.221	0.47
40	1.289	1.201	1.144	1.279	0.65
50	1.322	1.227	1.152	1.335	0.84
60	1.350	1.251	1.159	1.390	1.02
70	1.375	1.273	1.163	1.445	1.20
80	1.392	1.295	1.167	1.500	1.35
90	1.418	1.316	1.171	1.556	1.50
100	1.437	1.336	1.173	1.611	1.65
110	1.454	1.355	1.175	1.667	1.80
120	1.470	1.373	1.176	1.722	1.94
130	1.485	1.391	1.177	1.779	2.06
		153.15°K (Sinor et al[87])			
30	1.115	1.192	1.175	1.206	0.67
40	1.144	1.237	1.204	1.275	1.04
50	1.171	1.268	1.219	1.335	1.40
60	1.192	1.291	1.226	1.390	1.76
70	1.222	1.309	1.228	1.441	2.13
80	1.246	1.324	1.227	1.490	2.48
90	1.270	1.336	1.224	1.537	2.82

Table 27 (continued)

P, atm	ϕ (exp)	ϕ (LJCL)	ϕ (LJCLA)	ϕ (KIH)	$100x_2$
100	1.293	1.346	1.219	1.584	3.13
110	1.316	1.356	1.214	1.630	3.41
120	1.339	1.364	1.209	1.676	3.66
130	1.362	1.372	1.203	1.721	3.90
		173.15°K (Sinor et al.[87])			
40	1.183	1.175	1.167	1.171	1.08
50	1.256	1.248	1.230	1.259	1.83
60	1.311	1.297	1.264	1.331	2.59
70	1.357	1.329	1.282	1.392	3.32
80	1.396	1.352	1.290	1.447	3.97
90	1.430	1.368	1.291	1.498	4.56
100	1.461	1.377	1.285	1.543	5.15
110	1.487	1.382	1.277	1.585	5.71
120	1.512	1.383	1.265	1.624	6.25
130	1.535	1.381	1.252	1.659	6.78
		188.15°K (Sinor et al.[87])			
50	1.150	1.085	1.084	1.081	1.33
60	1.275	1.162	1.156	1.162	2.90
70	1.375	1.213	1.198	1.226	4.48
80	1.465	1.242	1.217	1.276	6.05
90	1.550	1.256	1.221	1.315	7.54
100	1.630	1.266	1.219	1.351	8.78
110	1.707	1.267	1.209	1.382	9.96
120	1.784	1.261	1.193	1.405	11.14
130	1.857	1.251	1.173	1.425	12.28
		139.83°K (Heck and Hiza[28])			
40	1.170	1.213	1.164	1.280	0.81
60	1.222	1.261	1.178	1.389	1.21
80	1.264	1.300	1.184	1.494	1.59
100	1.302	1.335	1.185	1.599	1.94
120	1.338	1.365	1.184	1.703	2.26
140	1.375	1.393	1.181	1.806	2.58
160	1.410	1.417	1.176	1.909	2.87
180	1.445	1.440	1.170	2.013	3.15
200	1.480	1.461	1.164	2.116	3.42

[a]Solid phase assumed to be pure methane

Table 28. Smoothed Experimental Theoretical Enhancement Factor of Nitrogen in Helium and the Smoothed Experimental Solubility of Helium in Liquid Nitrogen

P, atm	ϕ (exp)	ϕ (LJCL)	ϕ (LJCLA)	ϕ (KIHQ)	$100x_2$
		64.9°K (Rodewald et al.[80])			
10	1.650	1.140	1.113	1.159	0.140
20	2.235	1.282	1.223	1.323	0.275
30	2.785	1.435	1.338	1.503	0.399
40	3.318	1.598	1.459	1.699	0.505
50	3.830	1.773	1.585	1.912	0.600
60	4.319	1.959	1.715	2.141	0.678
		69.3°K (Rodewald et al.[80])			
10	1.226	1.127	1.105	1.145	0.173
20	1.465	1.248	1.199	1.287	0.345
30	1.698	1.376	1.296	1.440	0.502
40	1.928	1.512	1.397	1.605	0.650
50	2.152	1.656	1.501	1.781	0.778
60	2.382	1.807	1.609	1.971	0.882
70	2.615	1.967	1.720	2.173	0.963
		77.2°K (Rodewald et al.[80])			
10	1.100	1.118	1.102	1.134	0.222
20	1.189	1.215	1.178	1.251	0.455
30	1.260	1.316	1.255	1.373	0.682
40	1.319	1.420	1.333	1.502	0.895
50	1.370	1.529	1.413	1.639	1.094
60	1.418	1.642	1.494	1.784	1.266
70	1.464	1.760	1.578	1.937	1.409
		77.0°K (DeVaney et al.[18])			
20	1.145	1.217	1.180	1.253	0.308
40	1.291	1.426	1.338	1.508	0.628
60	1.437	1.651	1.501	1.794	0.945
80	1.582	1.893	1.671	2.111	1.265
100	1.726	2.154	1.847	2.464	1.580
120	1.872	2.432	2.029	2.853	1.890
140	2.015	2.727	2.215	3.280	2.198

Table 28 (continued)

P, atm	ϕ (exp)	ϕ (LJCL)	ϕ (LJCLA)	ϕ (KIHQ)	$100x_2$
		80.0°K (DeVaney et al.[18])			
20	1.177	1.212	1.179	1.246	0.380
40	1.316	1.404	1.324	1.484	0.787
60	1.450	1.610	1.474	1.747	1.195
80	1.580	1.830	1.629	2.039	1.604
100	1.711	2.066	1.789	2.361	1.982
120	1.842	2.316	1.953	2.716	2.358
140	1.973	2.581	2.121	3.106	2.728
		85.0°K (DeVaney et al.[18])			
20	1.183	1.208	1.181	1.239	0.453
40	1.301	1.383	1.314	1.458	1.026
60	1.416	1.566	1.448	1.696	1.568
80	1.531	1.759	1.583	1.956	2.119
100	1.645	1.963	1.721	2.241	2.652
120	1.758	2.178	1.862	2.555	3.185
140	1.873	2.405	2.006	2.899	3.715
		90.0°K (DeVaney et al.[18])			
20	1.126	1.209	1.187	1.235	0.590
40	1.268	1.375	1.315	1.444	1.305
60	1.407	1.543	1.438	1.666	2.010
80	1.542	1.718	1.560	1.906	2.710
100	1.677	1.900	1.683	2.169	3.395
120	1.810	2.092	1.808	2.457	4.070
140	1.944	2.293	1.934	2.774	4.750
		95.0°K (DeVaney et al.[18])			
20	1.105	1.209	1.192	1.229	0.730
40	1.237	1.379	1.327	1.442	1.650
60	1.358	1.542	1.447	1.660	2.520
80	1.496	1.708	1.562	1.893	3.375
100	1.623	1.879	1.676	2.148	4.235
120	1.748	2.057	1.789	2.429	5.065
140	1.875	2.248	1.907	2.749	5.785
		100.0°K (DeVaney et al.[18])			
20	1.084	1.200	1.189	1.214	0.720
40	1.212	1.388	1.343	1.443	1.890
60	1.338	1.553	1.465	1.663	3.050
80	1.463	1.715	1.577	1.898	4.165
100	1.586	1.881	1.685	2.155	5.215
120	1.708	2.053	1.792	2.444	6.205
140	1.830	2.237	1.900	2.783	7.100

Table 28 (continued)

P, atm	ϕ (exp)	ϕ (LJCL)	ϕ (LJCLA)	ϕ (KIHQ)	$100x_2$
		105.0°K (DeVaney et al.[18])			
40	1.231	1.396	1.358	1.439	2.140
60	1.362	1.575	1.494	1.678	3.57
80	1.490	1.744	1.608	1.927	4.98
100	1.614	1.911	1.713	2.203	6.33
120	1.737	2.085	1.815	--	7.53
140	1.860	2.277	1.921	--	8.53
		110.0°K (DeVaney et al.[18])			
40	1.288	1.394	1.363	1.423	2.40
60	1.434	1.602	1.523	1.693	4.25
80	1.562	--*	1.648	--	6.02
100	1.685	--	1.758	--	7.62
120	1.806	--	1.865	--	8.96
140	1.924	--	--	--	10.03
		115.0°K (DeVaney et al.[18])			
40	1.328	--	--	1.383	2.60
60	1.513	--	--	--	5.00
80	1.659	--	--	--	7.17
100	1.783	--	--	--	9.04
120	1.924	--	--	--	10.73
140	2.053	--	--	--	12.02
		120.0°K (DeVaney et al.[18])			
40	1.275	--	--	--	2.60
60	1.504	--	--	--	5.94
80	1.688	--	--	--	8.84
100	1.866	--	--	--	11.06
120	2.038	--	--	--	12.86
140	2.210	--	--	--	14.26

* The blank spaces indicate lack of convergence of theoretical calculation

Table 29. Smoothed Experimental, Theoretical Enhancement Factor of Oxygen in Helium, and the Smoothed Experimental Solubility of Helium in Liquid Oxygen

P, atm	ϕ (exp)	ϕ (LJCL)	ϕ (LJCLA)	ϕ (KIH)	$100x_2$
		69.9°K (Barrick and Herring[5])			
20	1.260	1.228	1.228	1.266	0.048
40	1.500	1.480	1.480	1.569	0.094
60	1.722	1.759	1.759	1.915	0.140
80	1.947	2.064	2.064	2.304	0.185
100	2.190	2.395	2.395	2.737	0.230
120	2.468	2.750	2.750	3.214	0.272
140	2.777	3.127	1.127	3.732	0.312
160	3.118	3.521	3.521	4.288	0.352
180	3.485	3.929	3.929	4.877	0.386
200	3.878	4.343	4.343	5.492	0.410
		75.9°K (Barrick and Herring[5])			
20	1.211	1.189	1.189	1.223	0.075
40	1.421	1.389	1.389	1.466	0.155
60	1.628	1.605	1.605	1.735	0.229
80	1.842	1.837	1.837	2.032	0.296
100	2.068	2.084	2.084	2.357	0.360
120	2.298	2.346	2.346	2.708	0.425
140	2.531	2.620	2.620	3.085	0.488
160	2.766	2.905	2.905	3.487	0.547
180	3.005	3.199	3.199	3.911	0.598
200	3.242	3.499	3.499	4.353	0.635
		89.98°K (Barrick and Herring[5])			
20	1.145	1.147	1.147	1.173	0.162
40	1.278	1.278	1.278	1.337	0.333
60	1.402	1.415	1.415	1.511	0.500
80	1.520	1.557	1.557	1.697	0.660
100	1.636	1.704	1.704	1.895	0.805
120	1.760	1.857	1.857	2.104	0.952
140	1.890	2.016	2.016	2.326	1.095
160	2.035	2.179	2.179	2.559	1.235
180	2.205	2.345	2.345	2.802	1.461

Table 29 (continued)

P, atm	ϕ (exp)	ϕ (LJCL)	ϕ (LJCLA)	ϕ (KIH)	$100x_2$
		109.96°K (Barrick and Herring[5])			
20	1.105	1.143	1.143	1.157	0.348
40	1.230	1.250	1.250	1.289	0.790
60	1.340	1.346	1.346	1.417	1.215
80	1.441	1.441	1.441	1.546	1.625
100	1.538	1.536	1.536	1.680	2.020
120	1.630	1.633	1.633	1.819	2.400
140	1.718	1.731	1.731	1.964	2.765
160	1.808	1.833	1.833	2.118	3.108
180	1.898	1.938	1.938	2.281	3.443
200	1.985	2.048	2.048	2.455	3.765
		129.95°K (Barrick and Herring[5])			
40	1.200	1.244	1.244	1.255	1.13
60	1.329	1.372	1.372	1.408	2.10
80	1.433	1.475	1.475	1.545	3.06
100	1.521	1.567	1.567	1.677	3.97
120	1.615	1.650	1.650	1.807	4.90
140	1.716	1.732	1.732	1.941	5.72
160	1.825	1.811	1.811	2.079	6.55
180	1.935	1.899	1.899	2.236	7.21
		143.93°K (Barrick and Herring[5])			
60	1.298	--*	--	1.330	2.58
80	1.455	--	--	--	4.33
100	1.582	--	--	--	6.07
120	1.725	--	--	--	7.70
140	1.921	--	--	--	9.24
160	2.165	--	--	--	10.68
180	2.462	--	--	--	12.05
190	2.625	--	--	--	12.70
		149.91°K (Barrick and Herring[5])			
60	1.181	--	--	--	2.50
80	1.408	--	--	--	5.17
100	1.695	--	--	--	7.75
120	2.040	--	--	--	10.25
140	2.429	--	--	--	12.65
150	2.630	--	--	--	13.80

* The blank spaces indicate lack of convergence of theoretical calculations

APPENDIX G

THEORETICAL ENHANCEMENT FACTOR OF OXYGEN IN HELIUM

The LJCL model, with the conventional combination rules defined by Equations (IV-19) and (IV-21), gives good agreement between the calculated and theoretical Enhancement Factors for the helium-oxygen system. This model provides a convenient method for the interpolation or extrapolation of the Enhancement Factor for this system. Thus, the Enhancement Factor of oxygen in helium has been calculated at five-degree intervals from 60 to 135°K, and at 20 atmosphere intervals from 20 to 200 atmospheres. The solubility of helium in oxygen was obtained by graphical interpolation. The results are presented in Table 30. The assumption of ideal liquid solution is made in these calculations.

Table 30. Theoretical Enhancement Factor of Oxygen in Helium Calculated with the LJCL Model

P, atm	20	40	60	80	100	120	140	160	180	200
					60°K					
ϕ	1.336	1.738	2.208	2.750	3.369	4.070	4.857	5.736	6.713	7.794
100 y_1	0.048	0.031	0.027	0.025	0.024	0.024	0.025	0.026	0.027	0.028
100 x_2	0.015	0.025	0.038	0.050	0.060	0.070	0.080	0.090	0.100	0.110
					65°K					
ϕ	1.273	1.586	1.942	2.340	2.779	3.258	3.771	4.313	4.877	5.450
100 y_1	0.146	0.091	0.074	0.067	0.064	0.062	0.062	0.062	0.062	0.063
100 x_2	0.031	0.055	0.085	0.100	0.150	0.160	0.180	0.210	0.230	0.250
					70°K					
ϕ	1.227	1.478	1.756	2.060	2.389	2.742	3.116	3.509	3.914	4.325
100 y_1	0.377	0.227	0.180	0.158	0.147	0.140	0.137	0.135	0.134	0.133
100 x_2	0.050	0.095	0.150	0.180	0.240	0.260	0.320	0.340	0.370	0.420
					75°K					
ϕ	1.194	1.401	1.625	1.866	2.123	2.396	2.682	2.981	3.289	3.600
100 y_1	0.854	0.501	0.387	0.333	0.304	0.285	0.274	0.266	0.261	0.257
100 x_2	0.070	0.145	0.220	0.270	0.350	0.400	0.470	0.500	0.560	0.640
					80°K					
ϕ	1.171	1.345	1.530	1.727	1.935	2.154	2.382	2.619	2.862	3.109
100 y_1	1.737	0.998	0.757	0.641	0.574	0.533	0.505	0.486	0.472	0.461
100 x_2	0.095	0.200	0.310	0.390	0.480	0.560	0.640	0.710	0.800	0.900
					85°K					
ϕ	1.156	1.305	1.462	1.628	1.801	1.982	2.169	2.363	2.561	2.764
100 y_1	3.241	1.830	1.367	1.141	1.010	0.926	0.869	0.828	0.798	0.775
100 x_2	0.125	0.270	0.415	0.520	0.640	0.740	0.850	0.950	1.100	1.240
					90°K					
ϕ	1.147	1.278	1.414	1.556	1.704	1.857	2.015	2.178	2.345	2.516
100 y_1	5.627	3.136	2.313	1.909	1.672	1.519	1.412	1.336	1.278	1.235
100 x_2	0.160	0.340	0.530	0.680	0.820	0.950	1.100	1.250	1.450	1.610

Table 30 (continued)

P, atm	20	40	60	80	100	120	140	160	180	200
					95°K					
ϕ	1.143	1.261	1.381	1.506	1.635	1.767	1.904	2.044	2.187	2.337
100 y_1	9.208	5.080	3.710	3.033	2.634	2.373	2.191	2.058	1.958	1.883
100 x_2	0.200	0.425	0.665	0.860	1.020	1.210	1.400	1.620	1.850	2.040
					100°K					
ϕ	1.143	1.252	1.361	1.472	1.587	1.704	1.824	1.946	2.073	2.205
100 y_1	14.33	7.854	5.690	4.616	3.982	3.562	3.269	3.052	2.889	2.767
100 x_2	0.245	0.510	0.815	1.090	1.260	1.520	1.760	2.050	2.340	2.550
					105°K					
ϕ	1.144	1.249	1.350	1.451	1.556	1.660	1.768	1.878	1.991	2.111
100 y_1	21.37	11.67	8.409	6.778	5.815	5.170	4.719	4.387	4.135	3.946
100 x_2	0.295	0.610	0.990	1.350	1.560	1.930	2.220	2.540	2.880	3.130
					110°K					
ϕ	1.143	1.251	1.347	1.441	1.539	1.633	1.731	1.832	1.935	2.047
100 y_1	30.66	16.77	12.04	9.660	8.252	7.296	6.632	6.140	5.766	5.488
100 x_2	0.350	0.710	1.180	1.640	1.910	2.400	2.750	3.130	3.520	3.800
					115°K					
ϕ	1.138	1.255	1.350	1.440	1.533	1.620	1.712	1.805	1.901	2.005
100 y_1	42.42	23.38	16.78	13.42	11.43	10.06	9.144	8.409	7.874	7.474
100 x_2	0.405	0.820	1.380	1.960	2.330	2.920	3.350	3.800	4.240	4.580
					120°K					
ϕ	1.123	1.258	1.358	1.447	1.537	1.620	1.707	1.795	1.886	1.985
100 y_1	56.60	31.71	22.82	18.24	15.49	13.61	12.29	11.31	10.56	10.01
100 x_2	0.465	0.930	1.590	2.320	2.820	3.510	4.020	4.560	5.070	5.480
					125°K					
ϕ	1.091	1.256	1.367	1.459	1.549	1.630	1.714	1.799	1.886	1.982
100 y_1	72.69	41.83	30.35	24.29	20.63	18.09	16.31	14.97	13.96	13.20
100 x_2	0.525	1.045	1.810	2.720	3.370	4.180	4.820	5.450	6.040	6.530

Table 30 (continued)

P, atm	20	40	60	80	100	120	140	160	180	200
					130°K					
ϕ	1.038	1.243	1.373	1.473	1.566	1.648	1.732	1.812	1.900	1.991
100 y_1	89.53	53.61	39.49	31.76	27.02	23.69	21.34	19.54	18.21	17.17
100 x_2	0.590	1.165	2.035	3.150	4.000	4.970	5.740	6.550	7.200	7.850
					135°K					
ϕ		1.213	1.372	1.487	1.588	1.674	1.756	1.830	1.914	1.996
100 y_1		66.54	50.20	40.78	34.85	30.61	27.52	25.10	23.34	21.90
100 x_2		1.290	2.260	3.600	4.700	5.850	6.870	7.920	8.750	9.650

APPENDIX H

LEAST-SQUARES FIT OF B_{12} TO LENNARD-JONES (6-12) PARAMETERS

The B_{12} data for the helium-carbon dioxide, -argon, -methane, -nitrogen, and -oxygen systems are presented in Tables 3, 4, 5, 7, and 8 in Chapter V. These data were least-squares fitted (by the method developed by Ziegler and Mullins[108]) to the Lennard-Jones (6-12) parameters. The three cases considered were:

(i) Both $(e/k)_{12}$ and $(b_o)_{12}$ allowed to vary to fit the B_{12} data

(ii) With $(e/k)_{12}$ fixed at the geometric average, $(b_o)_{12}$ allowed to vary to fit the B_{12} data

(iii) With $(b_o)_{12}$ fixed at the Lorentz average, $(e/k)_{12}$ allowed to vary to fit the B_{12} data.

Tables 31 through 35 present the results when only B_{12} data below 300°K were used. Table 36 shows the results when all the B_{12} data were used.

Table 31. Least-Square Fit of B_{12} for the Helium-Carbon Dioxide System to LJCL (6-12) Parameters ($T \leq 300^{\circ}K$)

T °K	B_{12}, cc/gm mole	Error, cc/gm mole	Parameter*	B_{12} Calculated from Fitted Parameter		
				Case (i)	Case (ii)	Case (iii)
			$(e/k)_{12}$	38.989	34.960	42.873
			$(b_o)_{12}$	52.95	47.33	62.31
180	10.9	±5.0		10.8	12.2	9.1
190	12.3	±5.0		12.3	13.4	11.1
200	13.5	±5.0		13.6	14.4	12.9
220	15.7	±5.0		15.8	16.1	15.9
240	17.6	±5.0		17.7	17.5	18.4
260	19.1	±5.0		19.1	18.6	20.4
280	20.4	±5.0		20.4	19.6	22.0
300	21.5	±3.5		21.4	20.4	23.4

* $(e/k)_{12}$ in $^{\circ}K$, and $(b_o)_{12}$ in cc/gm mole

Table 32. Least-Squares Fit of B_{12} for the Helium-Argon System to LJCL (6-12) Parameters ($T \leq 300^{\circ}$)

T °K	B_{12}, cc/gm mole	Error, cc/gm mole	Parameter*	B_{12} Calculated from Fitted Parameter		
				Case (i)	Case (ii)	Case (iii)
			$(e/k)_{12}$	25.523	28.815	25.287
			$(b_o)_{12}$	38.13	37.66	35.06
65	-10.7	±2.5		-11.1	-16.8	- 9.8
70	- 7.8	±2.5		- 7.9	-13.1	- 6.9
75	- 5.2	±2.5		- 5.2	-10.0	- 4.4
80	- 2.9	±2.5		- 2.8	- 7.3	- 2.3
85	- 1.0	±2.5		- 0.8	- 5.0	- 0.5
90	0.8	±2.5		0.9	- 2.9	1.1
95	2.4	±2.5		2.5	- 1.1	2.5
100	3.7	±2.5		3.9	0.5	3.8
110	6.1	±2.5		6.2	3.1	5.9
120	8.0	±2.5		8.1	5.3	7.6
130	9.6	±2.5		9.6	7.1	9.0
140	10.9	±2.5		10.9	8.6	10.2
150	12.1	±2.5		12.0	9.9	11.2
160	13.0	±2.5		12.9	11.0	12.0
170	13.8	±2.5		13.7	11.9	12.7
180	14.5	±2.5		14.4	12.7	13.4
190	15.1	±2.5		15.0	13.4	13.9
200	15.6	±2.5		15.6	14.1	14.4
220	16.4	±2.5		16.4	15.1	15.2
240	17.1	±2.5		17.1	15.9	15.8
260	17.7	±2.5		17.7	16.6	16.3
280	18.2	±2.5		18.1	17.2	16.7
300	18.6	±0.3		18.5	17.6	17.1

* $(e/k)_{12}$ in $^{\circ}K$, $(b_o)_{12}$ in cc/gm mole

Table 33. Least-Squares Fit of B_{12} for the Helium-Methane System to LJCL (6-12) Parameter ($T \leq 300^{\circ}K$)

T °K	B_{12}, cc/gm mole	Error, cc/gm mole	Parameter*	B_{12} Calculated from Fitted Parameter		
				Case (i)	Case (ii)	Case (iii)
			$(e/k)_{12}$	21.595	28.216	21.896
			$(b_o)_{12}$	50.61	32.40	60.66
55	-17.3	±3.0		-14.7	-21.7	-18.6
60	-11.0	±3.0		- 9.8	-17.2	-12.6
65	- 5.5	±3.0		- 5.7	-13.5	- 7.6
70	- 1.2	±3.0		- 2.3	-10.4	- 3.4
75	2.0	±3.0		0.7	- 7.8	0.1
80	4.6	±3.0		3.1	- 5.6	3.1
85	6.6	±3.0		5.3	- 3.6	5.8
90	8.3	±3.0		7.2	- 1.9	8.1
95	9.7	±3.0		8.8	- 0.4	10.1
100	10.9	±3.0		10.3	0.9	11.9
110	12.9	±3.0		12.8	3.2	14.9
120	14.6	±3.0		14.8	5.0	17.3
130	16.0	±3.0		16.4	6.5	19.3
140	17.2	±3.0		17.8	7.8	21.0
150	18.2	±3.0		18.9	8.8	22.4
160	19.1	±3.0		19.9	9.7	23.6
170	19.9	±3.0		20.7	10.5	24.6
180	20.6	±3.0		21.4	11.2	25.5

* $(e/k)_{12}$ in $^{\circ}K$, $(b_o)_{12}$ in cc/gm mole

Table 34. Least-Squares Fit of B_{12} for the Helium-Nitrogen System to LJCL (6-12) Parameters ($T \leq 300^{\circ}K$)

T °K	B_{12}, cc/gm mole	Error, cc/gm mole	Parameter*	B_{12} Calculated from Fitted Parameter		
				Case (i)	Case (ii)	Case (iii)
			$(e/k)_{12}$	21.564	25.093	21.917
			$(b_o)_{12}$	43.08	47.17	44.58
75	1.2	±2.5		0.6	- 5.6	0.0
80	3.0	±2.5		2.7	- 2.8	2.3
85	4.6	±2.5		4.6	- 0.3	4.2
90	6.1	±2.5		6.2	1.8	5.9
95	7.4	±2.5		7.6	3.7	7.4
100	8.6	±2.5		8.8	5.3	8.7
110	10.6	±2.5		10.9	8.1	10.9
120	12.3	±2.5		12.6	10.4	12.7
130	13.7	±2.5		14.0	12.3	14.2
140	14.9	±2.5		15.1	13.8	15.4
150	15.9	±2.5		16.1	15.2	16.5
160	16.8	±2.5		16.9	16.3	17.3
170	17.5	±2.5		17.7	17.3	18.1
180	18.2	±2.5		18.3	18.1	18.7
190	18.8	±2.5		18.8	18.8	19.3
200	19.3	±2.5		19.2	19.5	19.8
220	20.1	±2.5		20.0	20.6	20.6
240	20.7	±2.5		20.6	21.4	21.2
260	21.3	±2.5		21.1	22.0	21.7
280	21.8	±2.5		21.4	22.6	22.1
300	22.1	±2.5		21.7	23.0	22.4

* $(e/k)_{12}$ in $^{\circ}K$, $(b_o)_{12}$ in cc/gm mole

Table 35. Least-Squares Fit of B_{12} for the Helium-Oxygen System to LJCL (6-12) Parameter ($T \leq 300^{\circ}K$)

T °K	B_{12}, cc/gm mole	Error, cc/gm mole	Parameter* $(e/k)_{12}$ $(b_o)_{12}$	B_{12} Calculated from Fitted Parameter Case (i) 27.959 38.87	Case (ii) 27.92 38.92	Case (iii) 27.960 38.83
70	-12.1	±2.5		-12.1	-12.0	-12.1
75	- 8.9	±2.5		- 9.0	- 8.9	- 9.0
80	- 6.3	±2.5		- 6.3	- 6.3	- 6.3
85	- 4.0	±2.5		- 4.0	- 3.9	- 4.0
90	- 2.0	±2.5		- 2.0	- 1.9	- 2.0
95	- 0.2	±2.5		- 0.2	- 0.1	- 0.2
100	1.3	±2.5		1.4	1.4	1.4
110	4.1	±2.5		4.1	4.1	4.1
120	6.3	±2.5		6.2	6.3	6.2
130	8.0	±2.5		8.0	8.0	8.0
140	9.5	±2.5		9.5	9.5	9.5
150	10.7	±2.5		10.7	10.8	10.7

* $(e/k)_{12}$ in $^{\circ}K$, $(b_o)_{12}$ in cc/gm mole

Table 36. Least-Squares Fit of B_{12} for the Helium-Carbon Dioxide Argon, - Methane, -Nitrogen, -Oxygen Systems to LJCL (6-12) Parameters

System	Temperature Range, °K	$(e/k)_{12}$ °K	$(b_o)_{12}$ cc/gm mole	Average Deviation of Fit cc/gm mole
Case (i): Fit to both $(e/k)_{12}$ and $(b_o)_{12}$				
He-CO_2	180 - 350	39.044	53.28	±0.1
He-Ar	65 - 750	25.531	38.30	±0.1
He-CH_4	55 - 180	21.595	50.61	±0.9
He-N_2	75 - 750	21.332	42.25	±0.4
He-O_2	70 - 150	27.959	38.87	±0.0
Case (ii):* Fit to $(b_o)_{12}$ with $(e/k)_{12} = [(e/k)_1(e/k)_2]^{1/2}$				
He-CO_2	180 - 350	34.960	48.00	±0.9
He-Ar	65 - 750	28.815	38.25	±2.0
He-CH_4	55 - 180	28.216	32.40	±9.0
He-H_2	75 - 750	25.093	44.35	±2.0
He-O_2	70 - 150	27.920	38.92	±1.0
Case (iii): Fit to $(e/k)_{12}$ with $(b_o)_{12} = 1/8[(b_o)_1^{1/3} + (b_o)_2^{1/3}]^3$				
He-CO_2	180 - 350	43.102	62.31	±1.3
He-Ar	65 - 750	25.250	35.06	±1.1
He-CH_4	55 - 180	21.896	60.66	±2.4
He-N_2	75 - 750	21.903	44.58	±0.8
He-O_2	70 - 150	27.960	38.83	±0.0

* Not recommended

APPENDIX I

EXPERIMENTAL MATERIALS

Helium

The helium used in this work was the high purity grade from the U.S. Bureau of Mines. It was obtained from the Air Reduction Company, which distributes the gas. It had a quoted purity of 99.997 per cent.

Carbon Dioxide

The carbon dioxide used was the Coleman Instrument grade, obtained from the Matheson Company. It had a quoted purity of 99.99 per cent. No extraneous peaks were observed when it was passed through the chromatograph, with helium as the carrier gas.

Argon

The argon used was obtained from the Air Products Company. It had a quoted purity of 99.995 per cent. No extraneous peaks were observed when it was passed through the chromatograph, with helium as the carrier gas.

The results of the vapor pressure measurements on carbon dioxide and argon (Appendix A) tend to substantiate the purity of the materials used in this work.

BIBLIOGRAPHY

1. Armstrong, G. T., "Vapor Pressure of Nitrogen," Journal of Research of the National Bureau of Standards 53, No. 4, 263-266 (1954).

2. Armstrong, G. T., Brickwedde, F. G., and Scott, R. B., "Vapor Pressure of the Methanes," Journal of Research of the National Bureau of Standards 55, 39-52 (1955).

3. Baly, E. C. C. and Donnan, F. G., "The Variation with Temperature of the Surface Energies and Densities of Liquid Oxygen, Nitrogen, Argon, and Carbon Monoxide," Journal of the Chemical Society (London) 81, 907-923 (1902).

4. Barrick, P. L., Heck, C. K., and MacKendrick, R. F., Liquid-Vapor Equilibria of the Helium-Carbon Dioxide System, Quarterly Progress Report No. V, January 15, 1967 to April 15, 1967. Contract No. AF 33(615)-3314. Project No. 7360, Task No. 736001, University of Colorado, Boulder, Colorado.
See also: MacKendrick, R. F., Heck, C. K., and Barrick, P. L., "Liquid-Vapor Equilibria of the Helium-Carbon Dioxide System," Journal of Chemical and Engineering Data 13, 352-353 (1968).

5. Herring, R. N. and Barrick, P. L., Advances in Cryogenic Engineering 10, 151 (1965).
See also: Barrick, P. L. and Herring, R. N., Experimental Program to Determine the Thermodynamic Properties of Solutions of Liquefied Light Gases, Technical Documentary Report No. ML-TDR-64-321 (October, 1964). AF Materials Laboratory, Research and Technology Division, Air Force Systems Command, Wright-Patterson Air Force Base, Ohio.

6. Burnett, E. S., "Compressibility Determination Without Volume Measurements," Journal of Applied Mechanics 3, A136-140 (1936).

7. Butcher, E. G. and Dodson, R. S., "The Virial Coefficients of the Carbon Dioxide-Ethylene System. I. Pure Gases," Proceedings of the Royal Society (London), A277(1371), 448-467 (1964).

8. Buzyna, G., Macriss, R. A., and Ellington, R. T., "Vapor-Liquid Equilibrium in the Helium-Nitrogen System," Chemical Engineering Progress Symposium Series No. 44, 101-111 (1963).

9. Canfield, F. B., Leland, T. W., and Kobayashi, R., "Volumetric Behavior of Gas Mixtures at Low Temperatures by the Burnett Method: Helium-Nitrogen System, 0 to -140°C," Advances in Cryogenic Engineering 8, 146-157 (1963).

10. Cath, P. G. and Kammerlingh Onnes, H., Measurement of Very Low Temperatures XXX. Comparison of the Helium, Argon, Neon, Oxygen, and Nitrogen Thermometers with the Hydrogen Thermometer Corrections Which Will Reduce the Indications of These Thermometers to the International Scale of Kelvin. The Second Coefficient of the Virial for Helium, Argon, Neon, Oxygen, and Nitrogen Below 0°, Leyden Rijksuniversiteit Communications No. 156a (1922). See also: Archives neerlandaises des sciences exactes et naturelles 6, 1-30 (1922).

11. Chiu, C.-h and Canfield, F. B., "Thermodynamic Analysis of Vapor-Liquid and Vapor-Solid Equilibria Data to Obtain Interaction Second Virial Coefficients," Advances in Cryogenic Engineering 12, 741-753 (1967).

12. Chueh, P. L. and Prausnitz, J. M., "Third Virial Coefficients of Non-Polar Gases and Their Mixtures," American Institute of Chemical Engineers Journal 13, No. 5, 896-902 (1967).

13. Chueh, P. L. and Prausnitz, J. M., "Vapor-Liquid Equilibria at High Pressure. Vapor-Phase Fugacity Coefficients in Non-Polar and Quantum-Gas Mixtures," Industrial and Engineering Chemistry. Fundamentals 6, No. 4, 492-498 (1967).

14. Cook, D., "The Second Virial Coefficient of Carbon Dioxide at Low Temperatures," Canadian Journal of Chemistry 35, 268-275 (1957).

15. Cottrell, T. L. and Hamilton, R. A., "The Second Virial Coefficient of Gases and Mixtures. Part I. Carbon Dioxide and Helium Mixtures," Transactions of the Faraday Society 52, 156-160 (1956).

16. Dantzler, E. M., Knobler, C. M., and Windsor, M. L., "Second Virial Coefficients of Some Argon-Hydrocarbon Mixtures and Their Comparison with Chromatographic Values," Journal of Chromatography 32, 433-438 (1968).

17. Dantzler, E. M., Knobler, C. M., and Windsor, M. L., "Interaction Virial Coefficients in Hydrocarbon Mixtures," Journal of Physical Chemistry 72, No. 2, 676-684 (1968).

18. DeVaney, W. E., Dalton, B. J., and Meeks, J. C., Jr., "Vapor-Liquid Equilibria of the Helium-Nitrogen System," Journal of Chemical and Engineering Data 8, No. 4, 473-478 (1963).

19. Din, F., Thermodynamic Functions of Gases, Volumes I, II, III, Butterworths, London (1956-1961).

20. Dokoupil, Z., "Some Solid-Gas Equilibria at Low Temperatures," Progress in Low Temperature Physics, Vol. III, Edited by C. J. Gorter, North-Holland Publishing Company, Amsterdam, Interscience Publishers, Inc., New York, 454 (1961).

21. Eckert, C. A., Renon, H., and Prausnitz, J. M., "Molecular Thermodynamics of Simple Fluids Mixtures," Industrial and Engineering Chemistry. Fundamentals 6, No. 1, 58-67 (1967).

22. Edwards, A. E. and Roseveare, W. E., "The Second Virial Coefficients of Gaseous Mixtures," Journal of the American Chemical Society 64, 2816-2819 (1942).

23. Ewald, A. H., "The Solubility of Solids in Gases. Part 3. The Solubility of Solid Xenon and Solid Carbon Dioxide," Transactions of the Faraday Society 51, 347-356 (1955).

24. Fedoritenko, A. and Ruhemann, M., "Equilibrium Diagrams of Helium-Nitrogen Mixtures," Technical Physics of U.S.S.R. 4, 36-43 (1937).

25. Gonikberg, M. and Fastovskii, V., "The Solubility of Gases in Liquids at Low Temperatures and High Pressures. Fourth Article," Foreign Petroleum Technology 9, No. 6, 214-219 (1941).

26. Harper, R. C., Jr. and Miller, J. G., "Compressibility of Gases. II. Mixtures of Carbon Dioxide and Helium at 30°C," Journal of Chemical Physics 27, 36-39 (1957).

27. Heck, C. K. and Barrick, P. L., "Liquid-Vapor Equilibrium of the Neon-Helium System," Advances in Cryogenic Engineering 12, 714-718 (1967).

28. Heck, C. K. and Hiza, M. J., "Liquid-Vapor Equilibrium in the System Helium-Methane," American Institute of Chemical Engineers Journal 13, 593-599 (1967).

29. Hirschfelder, J. O., Curtiss, C. F., and Bird, R. B., Molecular Theory of Gases and Liquids, John Wiley and Sons, New York (1954).

30. Hiza, M. J. and Duncan, A. G., "Equilibrium Gas-phase Compositions of Ethane and Ethylene in Binary Mixtures with Helium and Neon Below 150°K and a Correlation for Deviations from the Geometric Mean Combination Rule," Preprint of Paper No. B-1, Cryogenic Engineering Conference, Case-Western Reserve University, Cleveland, Ohio, August 19-21 (1968).

31. Hiza, M. J. and Kidnay, A. J., "Solid-Vapor Equilibrium in the System Helium-Methane," Advances in Cryogenic Engineering 11, 338-348 (1965).

32. Hoge, H. J., "Vapor Pressure and Fixed Points of Oxygen and Heat Capacity in the Critical Region," Journal of Research of the National Bureau of Standards 44, 321-345 (1950).

33. Hoover, A. E., Canfield, F. B., Kobayashi, R., and Leland, T. W., Jr., "Determination of Virial Coefficients by the Burnett Method," Journal of Chemical and Engineering Data 9, No. 4, 568-573 (1964).

34. Hoover, A. E., Nagata, I., Leland, T. W., Jr., and Kobayashi, R., "Virial Coefficients of Methane, Ethane, and Their Mixtures at Low Temperatures," Journal of Chemical Physics 48, No. 6, 2633-2647 (1968).

35. Hull, K. R., Private Communication.

36. Kalfoglou, N. K. and Miller, J. C., "Compressibility of Gases. V. Mixtures of Sperially Symmetric Molecules at Higher Temperatures. The Helium-Argon and Helium-Tetrafluotomethane Systems," Journal of Physical Chemistry 71(5), 1256-1264 (1967).

37. Kanda, E., "Determination of the Second Virial Coefficient and the van der Waals' Force of Methane," The Science Reports of the Research Institutes, Tohoku University, Series A 1, 157-160 (1949).

38. Keesom, W. H., Helium, Elsevier, Amsterdam (1942).

39. Keesom, W. H. and Kohler, J. W. L., "The Lattice Constant and Expansion Coefficient of Solid Carbon Dioxide," Physica 1, 655-658 (1934).

40. Keyes, F. G., Taylor, R. S., and Smith, L. B., "The Thermodynamic Properties of Methane," Journal of Mathematics and Physics 1, 211-242 (1922).

41. Kharakhorin, F. F., "Liquid-Vapor Equilibrium in a Helium-Methane System," Inzhenerno-Fizicheskii Zhurnal, Akademiya Nauk Belorusskoi S.S.R. 2, No. 5, 55-59 (1959).

42. Kharakhorin, F. F., "The Phase Relation in Systems of Liquid Gases. First Article, The Binary Mixture Nitrogen-Helium," Foreign Petroleum Technology 9, 397-410 (1941).

43. Kihara, T., "Virial Coefficients and Models of Molecules in Gases," Reviews of Modern Physics 25, No. 4, 831-843 (1953).

44. Kihara, T., "Virial Coefficients and Models of Molecules in Gases. B," Reviews of Modern Physics 27, No. 4, 412-423 (1955).

45. Kirk, B. S., Predicted and Experimental Gas Phase Compositions in Pressurized Binary Systems Containing an Essentially Pure Condensed Phase. Phase Equilibrium Data for the Methane-Hydrogen System from 66.88° to 116.53°K and Up to 125 Atmospheres, Ph.D. Thesis, Georgia Institute of Technology, Atlanta, Georgia (1964).

46. Kirk, B. S. and Ziegler, W. T., "A Phase Equilibrium Apparatus for Gas-Liquid Systems and the Gas Phase of Gas-Solid Systems. Application to Methane-Hydrogen from 66.88° to 116.53°K and Up to 125 Atmospheres," Advances in Cryogenic Engineering 10, 160-170 (1965).

47. Kirk, B. S., Ziegler, W. T., and Mullins, J. C., "A Comparison of Methods of Predicting Equilibrium Phase Composition in Pressurized Binary Systems Containing an Essentially Pure Condensed Phase," Advances in Cryogenic Engineering 6, 413-427 (1961).

48. Knobler, C. M., Beenakker, J. J. M., and Knapp, H. F. P, "The Second Virial Coefficient of Gaseous Mixtures at 90°K," Physica 25, 909-916 (1959).

49. Knorn, M., "Vapor-Liquid Equilibriums of the Neon-Helium System," Cryogenics 7, No. 3, 177 (1967).

50. Kramer, G. M. and Miller, J. G., "Compressibility of Gases. III. The Second and Third Virial Coefficients of Mixtures of Helium and Nitrogen at 30°," Journal of Physical Chemistry 61, 785-788 (1957).

51. Ku, Peh-Sun and Dodge, B. F., "Compressibility of the Binary Systems: Helium-Nitrogen and Carbon Dioxide-Ethylene," Journal of Chemical and Engineering Data 12, No. 2, 158-164 (1967).

52. Levelt, J. M. H., "Reduced Equation of State, Internal Energy, and Entropy of Argon and Xenon," Physica 26, 361-377 (1960).

53. Maass, O. and Barnes, W. H., "Some Thermal Constants of Solid and Liquid Carbon Dioxide," Proceedings of the Royal Society (London) A111, 224-244 (1926).

54. MacCormack, K. E. and Schneider, W. G., "Compressibility of Gases at High Temperatures. IV. Carbon Dioxide in the Temperature Range of 0°-600°C, and Pressures Up to 50 Atmospheres," Journal of Chemical Physics 18, 1269-1272 (1950).

55. Mattias, E., Onnes, H. K., and Crommelin, C. A., "The Rectilinear Diameter of Nitrogen," Leyden Rijksuniversiteit Communications No. 145C (1914).

56. McCain, W. D., Jr., Vapor-Liquid Phase Equilibria of the Binary System Argon-Helium, Ph.D. Thesis, Georgia Institute of Technology, Atlanta, Georgia (1964).

57. McCain, W. D., Jr. and Ziegler, W. T., "The Critical Temperature, Critical Pressure, and Vapor Pressure of Argon," Journal of Chemical and Engineering Data 12(2), 199-202 (1967).

58. Meyers, C. H. and Van Dusen, M. S., "The Vapor Pressure of Liquid and Solid Carbon Dioxide," Journal of Research of the National Bureau of Standards 10, 381-412 (1933).

59. Michels, A. and Michels, C., "Isotherms of Carbon Dioxide Between 0° and 150° and Pressures from 16 to 250 Atmospheres (Amagat Densities 18-206)," Proceedings of the Royal Society (London) A153, 201-214 (1935).

60. Michels, A., Wassenaar, T., Degraaff, W., and Prins, C., "Vapor Pressure of Liquid Nitrogen," Physica 19, 26-28 (1953).

61. Michels, A., Wassenaar, T., and Zwietering, Th., "The Vapor Pressure of Argon," Physica 17, 876-884 (1951).

62. Mueller, W. H., Volumetric Properties of Gases at Low Temperatures by the Burnett Method, Ph.D. Thesis, Rice University, Houston, Texas (1959).

63. Mueller, W. H., Leland, T. W., Jr., and Kobayashi, R., "Volumetric Properties of Gas Mixtures at Low Temperatures and High Pressures by the Burnett Method: The Hydrogen-Methane System," American Institute of Chemical Engineers Journal 7, No. 2, 267-272 (1961).

64. Mullins, J. C., Phase Equilibria in the Argon-Helium and Argon-Hydrogen Systems, Ph.D. Thesis, Georgia Institute of Technology, Atlanta, Georgia (1965).

65. Mullins, J. C., Kirk, B. S., and Ziegler, W. T., Calculation of the Vapor Pressure and Heats of Vaporization and Sublimation of Liquids and Solids, Especially Below One Atmosphere. V. Carbon Monoxide and Carbon Dioxide, Technical Report No. 2, Project A-663, Engineering Experiment Station, Georgia Institute of Technology, Atlanta, Georgia, August 15, 1963 (Contract No. CST-7404, National Bureau of Standards, Boulder, Colorado).

66. Mullins, J. C. and Ziegler, W. T., "Phase Equilibria in the Argon-Helium and Argon-Hydrogen Systems from 68° to 108°K and Pressures Up to 120 Atmospheres," Advances in Cryogenic Engineering 10, 171-181 (1965).

67. Mullins, J. C. and Ziegler, W. T., The System Helium-Argon from 65° to 140°K Up to Pressures of 120 Atmospheres. Correlation of Available Phase Equilibria Data, Technical Report No. 3, Project A-764, Engineering Experiment Station, Georgia Institute of Technology, Atlanta, Georgia, January 10, 1965 (Contract No. CST-1154, National Bureau of Standards, U. S. Department of Commerce, Washington, D.C.)

68. Mullins, J. C., Ziegler, W. T., and Kirk, B. S., The Thermodynamic Properties of Oxygen from 20° to 100°K, Technical Report No. 2, Project A-593, Engineering Experiment Station, Georgia Institute of Technology, Atlanta, Georgia, March 1, 1962 (Contract No. CST-7339, National Bureau of Standards, Boulder, Colorado).

69. Nijhoff, G. P. and Keesom, W. H., Isotherms of Diatomic Gases and Their Binary Mixtures. XXXIII. Isotherms of Oxygen at Temperatures Ranging from -40° to -150° and Pressures from 3 to 9 Atmospheres, Leyden Rijksuniversiteit Communications No. 179b (1925).

70. Orentlicher, M. and Prausnitz, J. M., "Approximate Method for Calculating the Third Virial Coefficient of a Gaseous Mixture," Canadian Journal of Chemistry 45, No. 4, 373-378 (1967).

71. Pecsok, R. L. and Windsor, M. L., "Interaction Second Virial Coefficients of Some Hydrocarbon-Hydrocarbon Gas Mixtures from Gas-Liquid Chromatography," Analytical Chemistry 40, No. 8, 1238-1241 (1968).

72. Pfefferle, W. C., Jr., Goff, J. A., and Miller, J. G., "Compressibility of Gases. I. The Burnett Method. An Improved Method of Treatment of the Data. Extension of the Method to Gas Mixtures," Journal of Chemical Physics 23, No. 3, 509-513 (1955).

73. Pierotti, R. A., "The Solubility of Gases in Liquids," Journal of Physical Chemistry 67, 1840-1845 (1963).

74. Pople, J. A., "The Statistical Mechanics of Assemblies of Axially Symmetric Molecules. II. Second Virial Coefficients," Proceedings of the Royal Society (London), A221, 508-516 (1954).

75. Prausnitz, J. M. and Chueh, P. L., Computer Calculations for High Pressure Vapor-Liquid Equilibria, Prentice-Hall, Inc., Englewood Cliffs, New Jersey (1968).

76. Prausnitz, J. M., Eckert, C. A., Drye, R. V., and O'Connell, J. P., Computer Calculations for Multicomponent Vapor-Liquid Equilibria, Prentice-Hall, Inc., Englewood Cliffs, New Jersey (1968).

77. Prausnitz, J. M. and Myers, A. L., "Kihara Parameters and Second Virial Coefficients for Cryogenic Fluids and Their Mixtures," American Institute of Chemical Engineers Journal 9, No. 1, 5-11 (1963).

78. Renon, H., Eckart, C. A., and Prausnitz, J. M., "Molecular Thermodynamics of Simple Liquids. Pure Components," Industrial and Engineering Chemistry. Fundamentals 6, No. 1, 52-58 (1967).

79. Reuss, J. and Beenakker, J. J. M., "Determination of the Second Virial Coefficient B_{12} of Gas Mixtures," Physica 22, 869-879 (1956).

80. Rodewald, N. C., Davis, J. A., and Kurata, F., "The Heterogeneous Phase Behavior of the Helium-Nitrogen System," American Institute of Chemical Engineers Journal 10, No. 6, 937-943 (1964).

81. Rowlinson, J. S., Sumner, F. H., and Sutton, J. R., "The Virial Coefficients of a Gas Mixture," Transactions of the Faraday Society 50, 1-8 (1954).

82. Schafer, K., "The Second Virial Coefficient of the Different Modifications of Light and Heavy Hydrogen. I. Experimental Determinations," Zeitschrift fuer Physikaliche Chemie B36, 85-104 (1937).

83. Schindler, D. L., Swift, G. W., and Kurata, F., "Phase-Equilibrium Studies in the Nitrogen-Propane, Helium-Propane, and Helium-Nitrogen-Propane Systems," Proceedings of the Annual Convention, Natural Gas Processors Association, Technical Paper 45, 46-51 (1966).

84. Sherwood, A. E. and Prausnitz, J. M., "Third Virial Coefficient for the Kihara, Exp-6, and Square-Well Potentials," Journal of Chemical Physics 41, 413-428 (1964)

85. Sherwood, A. E. and Prausnitz, J. M., "Intermolecular Potential Functions and the Second and Third Virial Coefficients," Journal of Chemical Physics 41, 429-437 (1964).

86. Sinor, J. E. and Kurata, F., "Solubility of Helium in Liquid Argon, Oxygen, and Carbon Monoxide," Journal of Chemical and Engineering Data 11, No. 4, 537-539 (1966).

87. Sinor, J. E., Schindler, D. L., and Kurata, F., "Vapor-Liquid Phase Behavior of the Helium-Methane System," American Institute of Chemical Engineers Journal 12, No. 2, 353-357 (1966).

88. Smith, S. R., Liquid-Vapor Equilibrium for the Helium-Hydrogen System, Ph.D. Thesis, Ohio State University, Columbus, Ohio (1952).

89. Smith, G. E., Sonntag, R. E., and Van Wylen, G. J., "Analysis of the Solid-Vapor Equilibrium System Carbon Dioxide-Nitrogen," Advances in Cryogenic Engineering 8, 162-173 (1963).

90. Stewart, R. B., Hust, J. G., Hanley, H. J. M., McCarty, R. D., Hall, L. A., Childs, G. E., Germann, F. E. E., Gosman, A. L., and Johnson, V. J., "Cryogenic Propellent Fluid Properties." Final Report for Data Evaluation Program on Government Order H-76797, National Bureau of Standards, Report 9198 (1966).

91. Streett, W. B. and Staveley, L. A. K., "The P-V-T Behavior of Liquid Nitrogen at Temperatures from 77 to 120°K and Pressures to 680 Atmospheres," Preprint: Paper G-3, Cryogenic Engineering Conference, Palo Alto, California, August 21-23, 1967.

92. Strobridge, T. R., "The Thermodynamic Properties of Nitrogen from 64 to 300°K Between 0.1 and 200 Atmospheres," National Bureau of Standards, Technical Note 129 (1962).

93. Thomaas, G. and Van Steenwinkle, R., "The Second Virial Coefficient of Methane at Low Temperatures," Nature 187, 229-230 (1960).

94. Timrot, D. L. and Borisoglebskii, V. P., "The Density of Liquid Oxygen on the Saturation Curve," Soviet Physics JETP 11, No. 6, 1248-1250 (1960).

95. Timrot, D. L. and Borisoglebskii, V. P., "Experimental Investigation of the Density of Liquid Oxygen at -190 to -120 Degrees C and Pressures to 200 Kg/cm^2, Including the Saturation Curve," Inzhenerno-Fizicheskii Zhurnal Akademiya Nauk Belorusskoi S.S.R. 4, No. 1, 3-13 (1961).

96. Turlington, B. L. and McKetta, J. J., "The Compressibility of Carbon Dioxide and Nitrous Oxide at Low Pressures," American Institute of Chemical Engineers Journal 7, 336-337 (1961).

97. Van Itterbeek, A., De Boelpep, J., Verbeke, O., Theeuwes, F., and Staes, K., "Vapor Pressure of Liquid Argon," Physica 30, 2119-2122 (1964).

98. Van Itterbeek, A., Nihoul, J., Forrez, G., and Van Gerven, L., "Determination de L'equation de et pour des Mellanges Gazeux H_2-He par la Methode Accoustique," Bulletin de l'Institut International du Froid. Annex II 36, 215-225 (1956).

99. Van Itterbeek, A. and Van Doninck, W., "Measurements on the Velocity of Sound in Mixtures of Hydrogen, Helium, Oxygen, Nitrogen, and Carbon Monoxide at Low Temperatures," Proceedings of the Physical Society (London) 62B, 62-69 (1949).

100. Van Itterbeek, A. and Van Paemel, O., "Measurements of the Velocity of Sound as a Function of Pressure in Oxygen Gas at Liquid Oxygen Temperatures. Calculation of the Second Virial Coefficient and the Specific Heats," Physica 5, 593-604 (1938).

101. Van Itterbeek, A. and Verbeke, O., "Density of Liquid Oxygen as a Function of Pressure and Temperature," Cryogenics 1, No. 2, 77-80 (1960).

102. Van Itterbeek, A. and Verbeke, O., "Density of Liquid Nitrogen and Argon as a Function of Pressure and Temperature," Physica 26, 931-938 (1960).

103. Van Itterbeek, A. and Verbeke, O., "The Variation of the Density of Liquid Nitrogen and Liquid Oxygen as a Function of Pressure," Cryogenics 2(2), 79-80 (1961).

104. Van Itterbeek, A., Verbeke, O., and Staes, K., "Measurements on the Equation of State of Liquid Argon and Methane Up to 300 Kg-cm^{-2} at Low Temperature," Physica 29, 742-754 (1963).

105. Weir, R. D., Jones, I. W., Rowlinson, J. S., and Saville, G., "Equation of State of Gases at Low Temperatures. Part 1. Second Virial Coefficient of Argon and Krypton," Transactions of the Faraday Society 63, No. 6, 1320-1329 (1967).

106. White, D., Rubin, T., Camky, P., and Johnston, H. L., "The Virial Coefficients of Helium from 20 to 300°K," Journal of Physical Chemistry 64, 1607-1612 (1960).

107. Witonsky, R. J. and Miller, J. G., "Compressibility of Gases. IV. The Burnett Method Applied to Gas Mixtures at Higher Temperatures. The Second Virial Coefficients of the Helium-Nitrogen System from 175° to 475°," Journal of the American Chemical Society 85, 282-286 (1963).

108. Ziegler, W. T. and Mullins, J. C., Calculation of the Vapor Pressure and Heats of Vaporization and Sublimation of Liquids and Solids, Especially Below One Atmosphere. IV. Nitrogen and Fluorine, Technical Report No. 1, Project A-663, Engineering Experiment Station, Georgia Institute of Technology, Atlanta, Georgia, April 15, 1963 (Contract No. CST-7404, National Bureau of Standards, Boulder, Colorado).

109. Ziegler, W. T., Mullins, J. C., and Kirk, B. S., Calculation of the Vapor Pressure and Heats of Vaporization and Sublimation of Liquids and Solids, Especially Below One Atmosphere Pressure. II. Argon, Technical Report No. 2, Project A-460, Engineering Experiment Station, Georgia Institute of Technology, Atlanta, Georgia, June 15, 1962 (Contract No. CST-7238, National Bureau of Standards, Boulder, Colorado).

110. Ziegler, W. T., Mullins, J. C., and Kirk, B. S., Calculation of the Vapor Pressure and Heats of Vaporization and Sublimation of Liquids and Solids, Especially Below One Atmosphere Pressure. III. Methane, Technical Report No. 3, Project A-460, Engineering Experiment Station, Georgia Institute of Technology, Atlanta, Georgia, August 31, 1962 (Contract No. CST-7238, National Bureau of Standards, Boulder, Colorado).

VITA

Ker Fah Liu was born on July 16, 1941 in Calcutta, India. He attended Goethals Memorial School in Kurseong, Darjeeling. In 1957 he passed the Cambridge School Leaving Examinations. From 1958 to 1959 he attended Calcutta University at St. Joseph's College in Calcutta, where he received the Intermediate Science Degree. He entered Purdue University in West Lafayette, Indiana in 1959. He received the B.S. degree in Chemical Engineering from Purdue University in 1962. Since 1963 he attended Georgia Institute of Technology in Atlanta, Georgia where he received the M.S. degree in Chemical Engineering in 1965. At present he is employed by the Union Carbide Corporation in South Charleston, West Virginia.

He is a member of the Society of the Sigma Xi.